The Spherical Helical Antenna

by

J. Christopher Cardoso

Thesis submitted to the Faculty of the
Virginia Polytechnic Institute and State University
in partial fulfillment of the requirements for the degree of
Master of Science
in
Electrical Engineering

APPROVED:

A. Safaai-Jazi

Ahmad Safaai-Jazi, Chairman

Warren L. Stutzman

Warren L. Stutzman

William A. Davis

William A. Davis

September 1992

Blacksburg, Virginia

The Spherical Helical Antenna

by

J. Christopher Cardoso

Ahmad Safaai-Jazi, Chairman

Electrical Engineering

(ABSTRACT)

The spherical helical antenna is investigated as a new variation of the conventional helical antenna. The spherical helix is a wire antenna in a helix shape that is wound over a spherical surface instead of the standard cylindrical one. Analysis of this structure requires numerical methods and experimental measurements because its complex geometry makes it very difficult to develop analytic expressions for its radiation characteristics.

The wire antenna code ESP, based on the method of moments, is used to calculate both the gain and phase of the electric-field components, E_θ and E_ϕ, in the far field for spherical helices having between 3 and 10 turns. Several of these antennas were also constructed and tested on the Virginia Tech antenna test range. The numerical analysis and experimental measurements were performed over a wide range of frequencies corresponding to spherical circumferences of between 0.7 and 2.8 wavelengths.

A literature survey of the conventional helical antenna is presented so that comparisons can be made with the spherical helix. The numerical and experimental results of the spherical helical antenna indicate that its behavior is markedly different than the cylindrical helix. It is a broad beam elliptically-polarized radiator, in general, and operates over a relatively wide bandwidth. Under certain conditions, it is circularly polarized over a major portion of the main beam for a narrow bandwidth, a result which has potential applications. The behavior of the spherical helical antenna is not significantly affected by the number of turns and is discussed in this work for a few representative cases.

Abstract

Acknowledgements

I would like to express my sincere appreciation to Dr. Ahmad Safaai-Jazi for serving as my advisor and providing me with a very interesting topic for my thesis. He was a constant source of calm, sound advice during my two and a half years as a graduate student. I would also like to thank the members of my committee, Dr. William A. Davis and Dr. Warren L. Stutzman, for their helpful comments and suggestions. Special thanks go to Dr. Stutzman for supporting me as a graduate research assistant with the OLYMPUS propagation project.

My colleagues in the Satellite Communications Group provided me with indispensable technical advice, especially my two office mates, Fatim Haidara and Ko Takamizawa. Randall Nealy had useful suggestions for antenna construction and Paul Werntz helped with antenna range measurements.

The following group of people made Blacksburg close to home for me over the last six years: C. T. Kong, Jeff Truxel, Larry Andrews, Thomas Ramey, Jeff Seaton, Dave Hundt, Dale Brubaker, Mary Anne Corlett, Doug Bradley, and Lisa Blackburn, who also helped with lots of the editing chores. Back in New Jersey, the support of my family never wavered. I would like to thank my parents, my sister, Suzanne, my brother, Perry, Aunt Dottie and the anchor of it all, Gram.

And once again, I need to thank Chauncey Gardener for *always* "Being There."

Table of Contents

List of Figures

List of Tables

1. Introduction

One problem that has been of considerable interest to antenna designers is how to maintain good circular polarization over a wide bandwidth. This is particularly important in receiving satellite signals which often have wide bandwidths and polarizations that may change due to Faraday rotation. The helical antenna has been used for this and other applications because it is circularly polarized and its radiation characteristics do not significantly vary over a wide range of frequencies.

The *helical antenna* or *helix* was first proposed by J. D. Kraus in 1946 [1]. Much of the initial analysis and early applications of the helix were undertaken by Kraus and his students at the Ohio State University during the late forties and early fifties. In its simplest form the helical antenna is a conductor (tubular or solid wire) wrapped around a non-conducting cylindrical surface. The cylinder is not required if the helix can support its own weight. This type of wire antenna is usually coaxially fed with the center conductor of the cable becoming the helix and the outer conductor becoming a ground plane as shown in Figure 1-1.

Since its conception, researchers have proposed numerous modifications to the original structure of the simple cylindrical helix in the pursuit of increased bandwidth and optimization of other parameters. Some of these modifications will be discussed in Section 2.6. One modified design that has been recently proposed is a helix that is wound over a spherical surface instead of a cylindrical one [2]. This

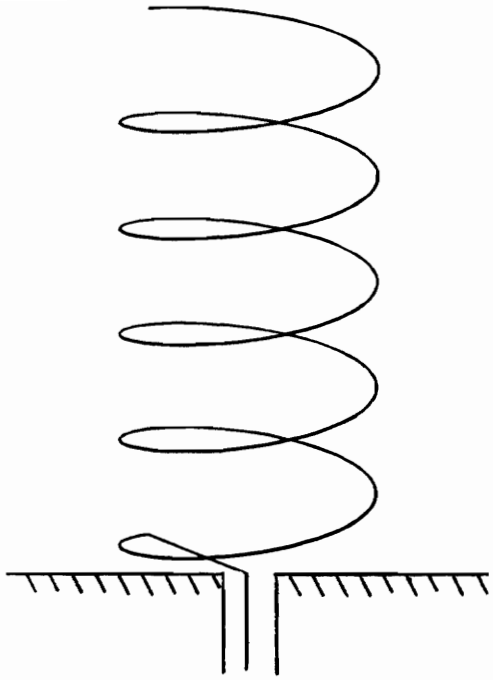

Figure 1-1. The helical antenna over a ground plane fed by a coaxial cable.

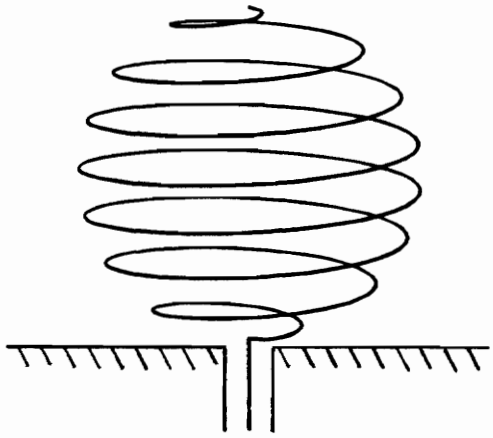

Figure 1-2. The spherical helical antenna over a ground plane fed by a coaxial cable.

so-called "*spherical helical antenna*" is shown in Figure 1-2. It is fed coaxially just like the standard helix.

Powerful numerical electromagnetics codes using the method of moments are now available in the public domain for analyzing wire antennas like the helix. One of these, called *ESP* or *Electromagnetics Surface Patch Code*, will be used to analyze the radiation properties of the spherical helical antenna. The results from ESP will be compared to actual far-field measurements of the spherical helix made on the Virginia Tech antenna test range. The use of computer codes such as ESP has become more prevalent in recent years as personal computers have emerged with increasing computational ability and greater memory. Numerical methods have also become necessary as recent work on the helix has been devoted to precisely optimizing the structure using difficult-to-analyze modifications. Similarly, it is all but impossible to analytically investigate the spherical helix without making some very constraining approximations or using numerical methods.

The results of this study indicate that the radiation properties of the spherical helical antenna are quite different than those of the conventional helical antenna. The cylindrical helix radiates in a directive circularly-polarized beam along its axis while the spherical helix radiates in an elliptically-polarized broad beam along its axis. Both patterns persist over a wide bandwidth but the standard helix has the added advantage of also having its other radiation characteristics (polarization, input impedance, etc.) essentially constant over a wide bandwidth. There are a few narrowband circumstances, however, where the spherical helix exhibits circular polarization over a major portion of the main beam, a result which does not occur for the cylindrical helix and has potential applications. Another advantage the spherical helix has over the cylindrical helix is that it is mechanically a much smaller antenna. Considering these differences, the spherical helical antenna is not presented as an improvement to the cylindrical helical antenna but rather as a variation with its own special properties.

Chapter 2 gives historical background to the work by presenting some of the important findings of the extensively-studied helical antenna. It also includes a comparison of ESP-generated fields to those of an actual helix cited in the literature. This is done to verify the accuracy of ESP. Chapter 3 introduces the

spherical helix by addressing some previous related work on the structure and rigorously defining its geometry. Chapter 4 presents the results of the numerical analysis for a variety of different spherical helical antennas. It also highlights certain cases where the spherical helix is circularly polarized over a major portion of the main beam. Chapter 5 contains the results of antenna test range measurements and compares them with those generated by ESP in Chapter 4. Chapter 6 concludes the work and offers suggestions for further analysis of the spherical helix. The appendices contain the computer codes used to generate the different helical geometries as well as the numerically-generated and measured far-field patterns of a representative spherical helix.

2. The Helical Antenna

The helical antenna is sometimes considered the connecting link between two canonical antenna types, dipoles and loops [1]. In the limiting cases, the helix becomes a linear antenna as its diameter approaches zero and a loop as the spacing between turns approaches zero. As will be seen, elemental dipoles and loops are used under certain circumstances to model the helix to ease an otherwise very difficult analysis.

The cylindrical helical antenna has been used in a wide variety of applications over the last forty years due to its remarkable and unique properties. One drawback already alluded to, however, is that a rigorous solution to wave propagation along a helix has yet to be found since the "Helmholtz equation is not separable in helical coordinates" [3]. For this reason, extensive experimentation, approximation, and numerical analysis have been performed on the structure in order to develop analytic expressions that characterize certain aspects of its behavior (eg., gain, radiation resistance, etc.). The important results of this work are presented in this chapter.

First we define the geometric parameters that describe the general shape of the helix. Referring to Figures 2-1 and 2-2, these parameters are:

$$\begin{aligned} D &= \text{diameter of helix} \\ C &= \text{circumference of helix} = \pi D \end{aligned}$$

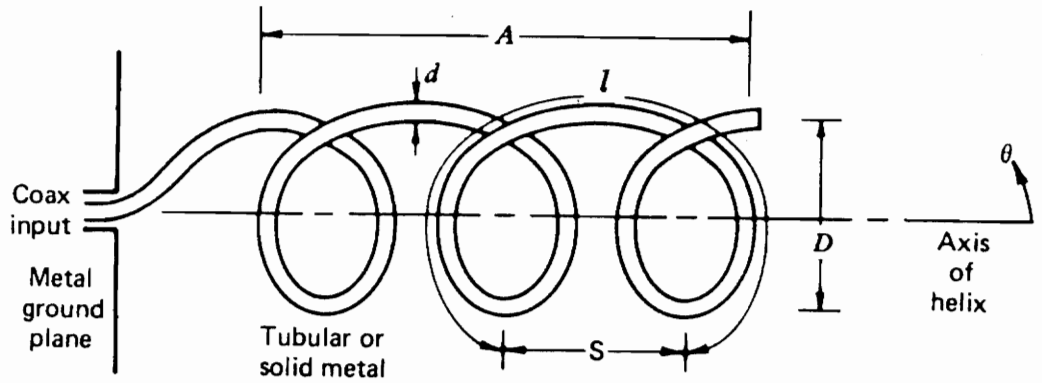

Figure 2-1. Parameters that define the geometry of the helix [4].

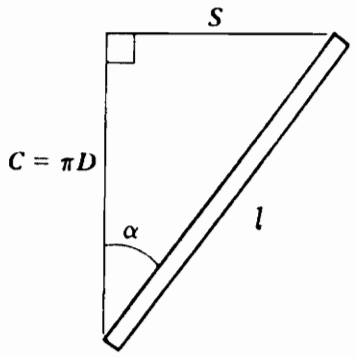

Figure 2-2. Trigonometric relationships between helical dimensions for one uncoiled turn [4].

α = pitch angle
n = number of turns
s = spacing between turns
A = axial length = ns
l = length of one turn
L = total length of conductor = nl
d = diameter of conductor

The diameter and circumference of the helix refer to the cylinder, real or fictitious, over which the helix is wrapped. Figure 2-2 shows the trigonometric relationships between some of the parameters as one of the turns is uncoiled.

2.1 Radiation Modes of the Helix

A long helical coil can operate as a waveguide for the propagation of electromagnetic waves. Like other types of waveguide the helical coil has many *transmission modes* associated with it. When finite helices are used as antennas these transmission modes give rise to different classes of radiated fields which are called "*radiation modes.*" The two lowest radiation modes are the most important to antenna designers and are known as the "*normal mode*" and "*axial mode*," respectively [1]. They are named after the direction in which their radiation is a maximum. In the normal mode, the radiated fields assume a maximum in directions normal to the helix axis and in the axial mode, the radiated fields are a maximum along the axis. The axial mode persists over a wide range of frequencies and is circularly polarized, making the helix one of the most widely used antennas.

2.1.1 Normal Mode

The charge distribution for the lowest-order transmission mode of a long helical coil is shown in Figure 2.1.1-1. This mode dominates when the length of one turn is very small with respect to wavelength ($l \ll \lambda$). If the coil is truncated to make a helical antenna and the total conductor length is very small with respect to wavelength ($L \ll \lambda$), the wave reflected at the end of the helix will be very nearly equal in magnitude to the incident wave. Under this condition, the helix operates as a resonant antenna and the current can be approximated as having uniform magnitude and phase along its entire length. The radiated fields will be a maximum in directions normal to the axis of the helix ($\theta = 90°$) and a minimum along the axis ($\theta = 0°$). In general, the field will vary as $\sin\theta$. This radiation mode has been designated the "normal mode" and is shown in Figure 2.1.1-2. The polarization of this mode is elliptical, in general, but can be made linear and even circular under certain conditions. The normal-mode helix has a low radiation efficiency due to its small electrical size and, like most resonant antennas, it operates over a small bandwidth. Some applications using the normal mode of the helix include mobile whips and the loop-stick antenna [4].

2.1.2 Axial Mode

The charge distribution for the second-order transmission mode (sometimes referred to as the first order mode) of a long helical coil is shown in Figure 2.1.2-1. This mode occurs when the circumference of the helix is on the order of one wavelength and results in regions of positive and negative charges separated by about a half turn. When the coil is truncated to make a helical antenna, as shown in Figure 1-1, it is still electrically large (since $l \approx 1\ \lambda$) and is able to maintain an almost pure traveling wave since reflections from the open end would be very small (unless the helix is very short, $A < \frac{\lambda}{2}$) [4]. Thus, the current distribution on the helical antenna behaves like the charge distribution on a helical coil. Its phase changes by 180° over a half turn but since its direction is also reversed 180° by the

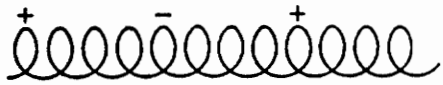

Figure 2.1.1-1. Instantaneous charge distribution for the lowest-order transmission mode on a helix of infinite length [1].

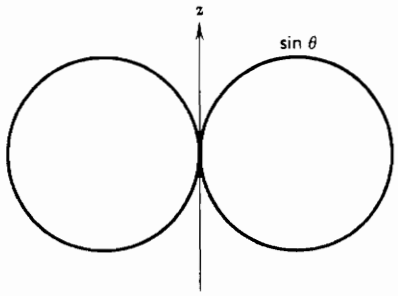

Figure 2.1.1-2. Radiation pattern for the normal-mode helix [4].

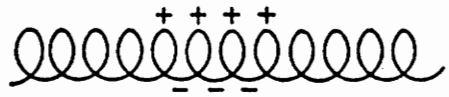

Figure 2.1.2-1. Instantaneous charge distribution for the second-order transmission mode on a helix of infinite length [1].

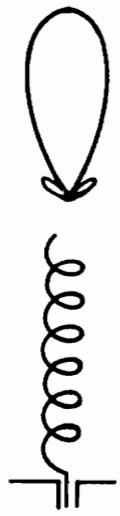

Figure 2.1.2-2. Radiation pattern for the axial-mode helix [1].

geometry of the helix, points opposite each other on a turn will be in phase. The far-fields produced by each point will then constructively interfere with each other along the axis of the helix. This remarkable occurrence gives rise to a fairly directive beam of radiation along the axis as shown in Figure 2.1.2-2. The helical geometry also naturally gives rise to circular polarization on the axis since the phase of the current changes by 90° over a quarter turn which causes the orthogonal far-field components to also differ by 90°.

Since the axial-mode helix behaves like a traveling-wave antenna, it is not surprising that it operates over a wide range of frequencies. Traveling-wave antennas often operate over such large bandwidths that the ratio of the upper frequency of operation to the lower can be as large as 2:1. After much experimentation, researchers seem to agree that the axial mode persists over a frequency range given roughly by:

$$\frac{3}{4}\lambda < C < \frac{4}{3}\lambda \qquad (2.1.2\text{-}1)$$

It has been shown that this frequency range corresponds to a bandwidth ratio of:

$$\frac{f_u}{f_l} = \frac{\frac{C}{\lambda_u}}{\frac{C}{\lambda_l}} = \frac{\frac{4}{3}}{\frac{3}{4}} = \frac{16}{9} = 1.78 \qquad (2.1.2\text{-}2)$$

where f_u and f_l are the upper and lower frequencies of operation, respectively [4]. At almost 2:1, this bandwidth gives the helix many broadband applications.

As stated above, the helical antenna operating in the axial mode is very nearly circularly polarized on its axis. The sense of the polarization depends on the winding of the helix. If the helix is wound in a right- (left-) handed sense, its polarization will also be right- (left-) hand sensed. Figure 2.1.2-3 shows left- and right-hand wound helices. Matched pairs of oppositely wound helical antennas are often used on antenna ranges to determine the polarization sense of test antennas by comparing their responses [5].

Like all traveling-wave antennas, the input impedance of the axial-mode helix is almost purely resistive. The impedance associated with a pure traveling

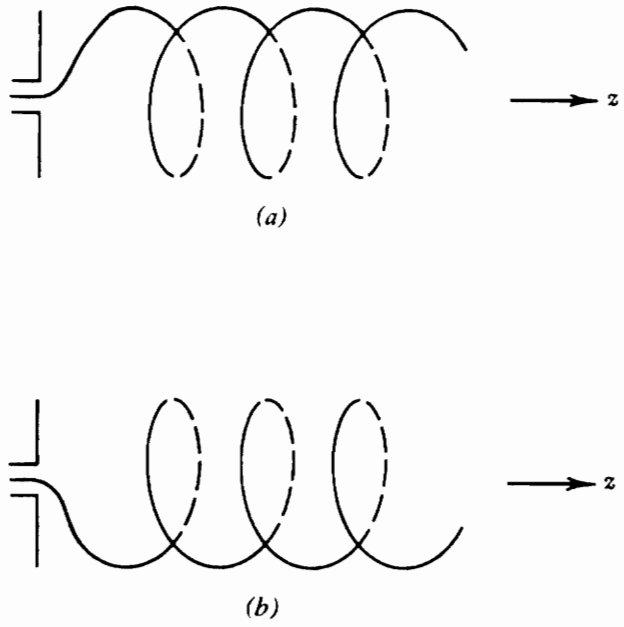

Figure 2.1.2-3. (a) Left-hand wound helix and (b) right-hand wound helix [4].

wave on a long helical coil acting as a transmission line is equal to the mostly real characteristic impedance of the coil. The helical antenna supports outward traveling waves and behaves in the same manner. Experiments have shown that the radiation resistance of the axial-mode helix lies between 100 and 150 ohms and is mostly real. This makes the axial-mode helical antenna a very efficient radiator since outward traveling waves are almost entirely radiated along the length of the wire and reflections at the end are small.

2.2 Theoretical Analysis of the Helical Antenna

Analytical expressions that characterize the radiation properties of an antenna are very useful and should be developed even if approximations are required to get them. They help in understanding the physics governing the antenna and also provide insight into how it might be optimized for better performance. As stated in the introduction, the helical antenna is difficult to analyze due to its complex geometry and, in fact, no exact solutions that describe its behavior have ever been developed. The following two sections briefly discuss how approximate expressions for the far-field patterns of the normal- and axial-mode helices are formulated.

2.2.1 Normal-Mode Helix

Several approximations are used to generate the far-field radiation patterns of the normal-mode helix. These approximations are valid provided the dimensions of the helix are small ($L \ll \lambda$). Figure 2.2.1-1 shows the helix and the coordinate system in which it will be analyzed. E_ϕ and E_θ are the two components of the far-zone electric field. These components and the coordinate system shown in Figure

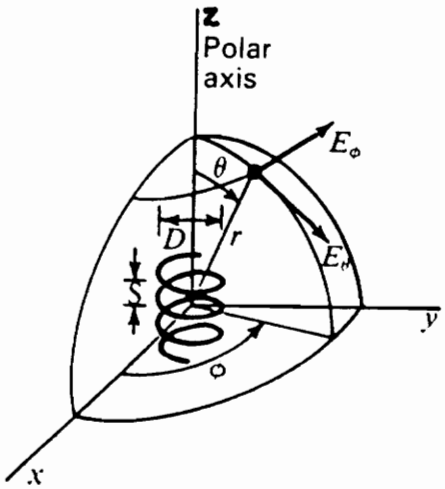

Figure 2.2.1-1. Coordinate system for the helix [1].

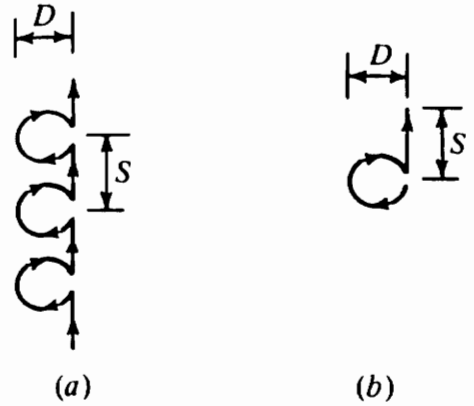

Figure 2.2.1-2. (a) Helix modeled by ideal loops and dipoles. (b) Model reduced to a single loop and dipole [1].

2.2.1-1 will be used throughout this work.

Since the dimensions of the helix are small with respect to wavelength, each turn can be modeled as a short dipole and a small loop connected in series as shown in Figure 2.2.1-2a. The loops have the diameter of the helix, D, and the dipoles have the length of the spacing between turns, s. This model can be further reduced to a single loop and dipole, as shown in Figure 2.2.1-2b, since each turn has the same far-field effect due to the "electrical compactness" of the helix.

With these approximations, the solution for the far-field of the normal-mode helix is reduced to a simple vector addition of the fields produced by two canonical antenna types. The far-zone electric field for an ideal dipole is a standard result in most antenna textbooks and is written as [4]:

$$\boldsymbol{E}_D = j\omega\mu I s \frac{e^{-j\beta \mathbf{r}}}{4\pi r} \sin\theta \, \widehat{\boldsymbol{\theta}} \tag{2.2.1-1}$$

where I = magnitude of the current
ω = angular frequency
μ = permeability of free space
β = phase constant $(2\pi/\lambda) = \omega\sqrt{\mu\varepsilon}$
ε = permitivity of free space

Similarly for an ideal loop:

$$\boldsymbol{E}_L = \eta\beta^2 \frac{\pi}{4} D^2 I \frac{e^{-j\beta \mathbf{r}}}{4\pi r} \sin\theta \, \widehat{\boldsymbol{\phi}} \tag{2.2.1-2}$$

where η = intrinsic impedance of free space $= \sqrt{\frac{\mu}{\varepsilon}}$
$\frac{\pi}{4}D^2$ = area of the loop

The total field produced by the normal-mode helix is the vector sum of the field components in (2.2.1-1) and (2.2.1-2):

$$\boldsymbol{E} = E_\theta \widehat{\boldsymbol{\theta}} + E_\phi \widehat{\boldsymbol{\phi}} = \boldsymbol{E}_D + \boldsymbol{E}_L \tag{2.2.1-3}$$

Field components are 90° out of phase (note that $j = e^{\frac{j\pi}{2}} = e^{j90^\circ}$ in (2.2.1-1)) and

vary as $\sin\theta$ which gives maximum radiation in directions normal to the helix axis. This was shown in Figure 2.1.1-2.

The normal-mode helix is elliptically polarized in general but can be made to be circularly polarized under certain conditions. Axial ratio, AR, is a quantity that describes the nature of the polarization and is defined as the ratio of the semi-major and semi-minor axes of the polarization ellipse. Since the two electric field components are 90° out of phase in the normal mode, the axial ratio becomes:

$$|AR| = \frac{|E_\theta|}{|E_\phi|} = \frac{|E_D|}{|E_L|} = \frac{4\omega\mu s}{\sqrt{\frac{\mu}{\varepsilon}}\,\omega\sqrt{\mu\varepsilon}\left(\frac{2\pi}{\lambda}\right)\pi D^2} = \frac{2s\lambda}{\pi^2 D^2} \qquad (2.2.1\text{-}4)$$

Circular polarization will occur in all directions (except along the axis where the field is zero) when this ratio is unity or when:

$$C = \pi D = \sqrt{2s\lambda} \qquad (2.2.1\text{-}5)$$

2.2.2 Axial-Mode Helix

Approximate expressions for the far-field pattern of the axial-mode helical antenna are generated by considering the helix to be an array of n (the number of turns) equally-spaced elements. Each element is a single turn of the helix and can be modeled as a traveling-wave loop antenna with a one-wavelength circumference. If each turn is assumed to be uniformly excited the array factor, AF, for the array-modeled helix is given by:

$$AF(\theta) = K\,\frac{\sin\left(\frac{n\psi}{2}\right)}{n\,\sin\left(\frac{\psi}{2}\right)} \qquad (2.2.2\text{-}1)$$

$$\begin{aligned} \text{where } \psi &= \beta s\cos\theta + \alpha \\ K &= \text{normalization constant} \\ \alpha &= \text{phase shift between elements} \end{aligned} \qquad (2.2.2\text{-}2)$$

which is a standard result for uniformly-excited equally-spaced arrays. (Note: the α used in (2.2.2-2) is different from the helix pitch angle.) The full far-field pattern is given by the array factor multiplied with the element pattern.

The phase shift between elements, α, has long been a matter of discussion due to the complex nature of wave propagation along the helix. Researchers have proposed many ways of describing its very unique and surprising behavior. A rather simple discussion is given here.

The axial-mode helix can be assumed to operate as an ordinary endfire array for which radiation is a maximum along the axis ($\theta = 0°$). The array factor, AF, is a maximum when $\psi = -2\pi m$ where m = 0, 1, 2, 3,.... The negative sign is necessary because the phase of each turn lags the previous turn and since the circumference of the axial-mode helix is about one wavelength the current wave has a difference of -2π (corresponding to m = 1) at each turn. Thus, for the ordinary endfire case on axis:

$$\psi = -2\pi = \beta s\cos(0) + \alpha \qquad (2.2.2\text{-}3)$$

and hence:

$$\alpha = -\beta s - 2\pi \qquad (2.2.2\text{-}4)$$

The total pattern of the axial-mode helix, $F(\theta)$, is found by multiplying the array factor, $AF(\theta)$, with the element factor. The element factor is approximately the pattern produced by a one-wavelength traveling-wave loop, $\cos\theta$. Thus for the ordinary endfire case:

$$F(\theta) = K\cos\theta\,\frac{\sin\left(\frac{n\psi}{2}\right)}{n\sin\left(\frac{\psi}{2}\right)} \qquad (2.2.2\text{-}5)$$

where ψ and α are given by (2.2.2-2) and (2.2.2-4), respectively.

The patterns measured from actual helices are considerably more directive than those predicted by the ordinary endfire condition. As it turns out, the axial-mode helix remarkably behaves more nearly like a Hansen-Woodyard increased-directivity endfire array. Under this condition, the interelement phase shift, α, is delayed by an extra $-\pi n$ over the ordinary endfire case and becomes:

$$\alpha = -\beta s - 2\pi - \frac{\pi}{n} \qquad (2.2.2\text{-}6)$$

The normalization factor, K, for the Hansen-Woodyard case can be found by solving for the pattern maximum at $\theta = 0$. The total far-field pattern for the helical antenna operating in the axial mode can finally be written as [4]:

$$F(\theta) = (-1)^{n+1} \sin\left(\frac{\pi}{2n}\right) \cos\theta \frac{\sin\left(\frac{n\psi}{2}\right)}{n \sin\left(\frac{\psi}{2}\right)} \qquad (2.2.2\text{-}7)$$

$$\text{where } \psi = \beta s(\cos\theta - 1) - 2\pi - \frac{\pi}{n} \qquad (2.2.2\text{-}8)$$

which is valid for both components of the far-field, E_θ and E_ϕ. Amazingly, the directivity of the axial-mode helix actually exceeds the directivity of a Hansen-Woodyard endfire array since the element pattern of one turn (approximated as $\cos\theta$ here) narrows the beam in the axial direction [5].

2.3 Optimization of the Axial-Mode Helix

A range of circumferences was given in Section 2.1.2 over which the helical antenna operates in the axial mode. In actuality, there are limits on the other

dimensions as well. These limits are based on numerous experiments and, though they are not sharply defined, some nominal values are given in Table 2.3-1.

Table 2.3-1.
Limits on Helix Parameter Values for Optimum Axial-Mode Performance.

Parameter	Value Range
• circumference	$\frac{3}{4}\lambda < C < \frac{4}{3}\lambda$
• pitch angle	$11^\circ < \alpha < 14^\circ$
• number of turns	$2 < n < 16$
• diameter of wire conductor	negligible effect
• diameter of ground plane	at least $\frac{1}{2}\lambda$

The limits for the other parameters defined at the beginning of Chapter 2 are not necessary since the cylindrical helix is uniquely defined by those in Table 2.3-1. (For example, fixing C and α fixes the spacing between turns, s).

What is remarkable about the axial-mode helix is that its radiation properties are not critically dependent on its geometry. Thus, there are no precise construction tolerances, making it one of the most popular antennas among amateur and professional circles alike. In fact, the helix can even operate in the axial mode outside the limits of Table 2.3-1, although there may be some deterioration in its electrical properties ($1\frac{1}{4}$ turn [6] and 18° pitch-angle helices [5] have been used successfully).

2.3.1 Helix Dimensions for Optimum Performance

Within the ranges specified above there are certain values for the parameters at which the helix performance is optimum (i.e., high gain, wide bandwidth, low axial ratio, etc.). The following sections present the experimental

results contained in the literature that seek to find these values.

Circumference

Most researchers seem to agree that the optimal circumference for the axial-mode helical antenna is around 1.1 λ. The solid line in Figure 2.3.1-1 is a plot of the peak gain (the highest gain achieved over the frequency range of the axial mode) as the pitch angle is varied. The dashed line shows the circumference of the helix at peak gain and is plotted against the right vertical axis. (Note: $\frac{\pi D}{\lambda_p}$ equals the circumference normalized to free-space wavelengths at the frequency of peak gain). The symbols in Figure 2.3.1-1 (circles and triangles) represent actual measurements and the lines are curve fitted to these points. Peak gain occurs at about the same circumference, 1.135 λ, regardless of the pitch angle. Other results show that for more turns the optimal circumference goes down (optimal $C_\lambda = 1.07\,\lambda$ for $n = 35$ turns [7], see Figure 2.3.1-3). Thus, there is a slight but complex interdependence between all the helical parameters making exact values for optimal performance elusive. Nonetheless, a circumference of 1.1 λ is a good estimate for the optimal circumference of the axial-mode helix.

Pitch Angle

It has long been accepted that the optimal pitch angle for the axial mode is 12.5°. The first textbook to address helical antennas [1] and the most recent one [8] confer on this. Figure 2.3.1-2 is a plot of gain versus frequency for helices with different pitch angles and fixed wire lengths. The 12.5° pitch-angle helix gives the highest gain out of the three. Experiments have shown that even lower pitch angles, such as 11°, produce even higher gain, but do so at the cost of decreased bandwidth [7].

Number of Turns

Having specified optimal values for the circumference and pitch angle, the only thing needed to uniquely specify the helix is its length. This can be quantized by one of three equivalent parameters: the number of turns (n), axial length (A), or conductor length (L). Figure 2.3.1-3 is a plot of the on-axis or peak gain versus number of turns for fixed-circumference and fixed pitch-angle helices. It shows

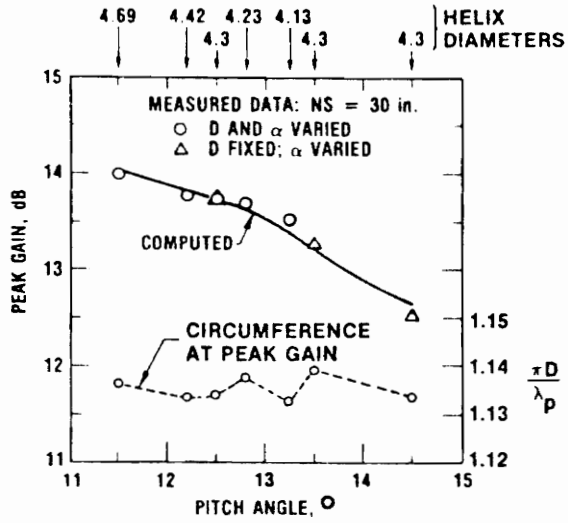

Figure 2.3.1-1. Peak gain (solid) and circumference at peak gain (dashed) of fixed length helices versus pitch angle [7]. Symbols (circles and triangles) are measured values and lines are curve fitted to these points.

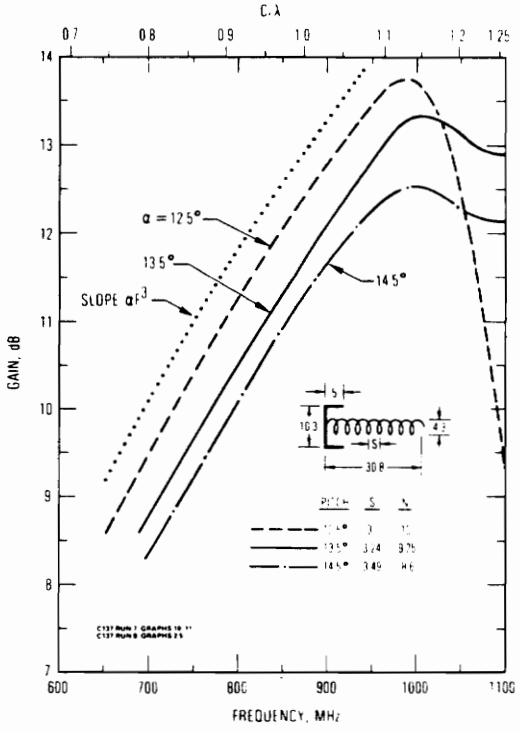

Figure 2.3.1-2. Measured gain of fixed-length, fixed-circumference helices for pitch angles of 12.5°, 13.5°, and 14.5° [7].

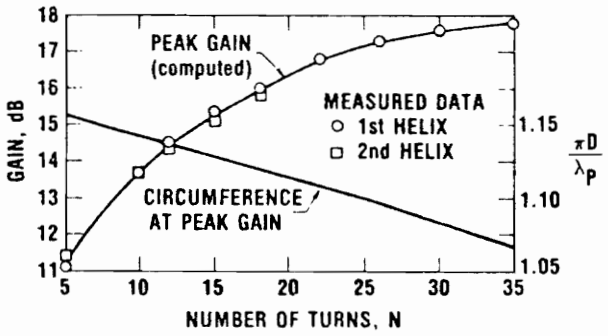

Figure 2.3.1-3. Peak gain and circumference at peak gain versus number of turns [7]. Symbols (circles and squares) are measured values and lines are curve fitted to these points.

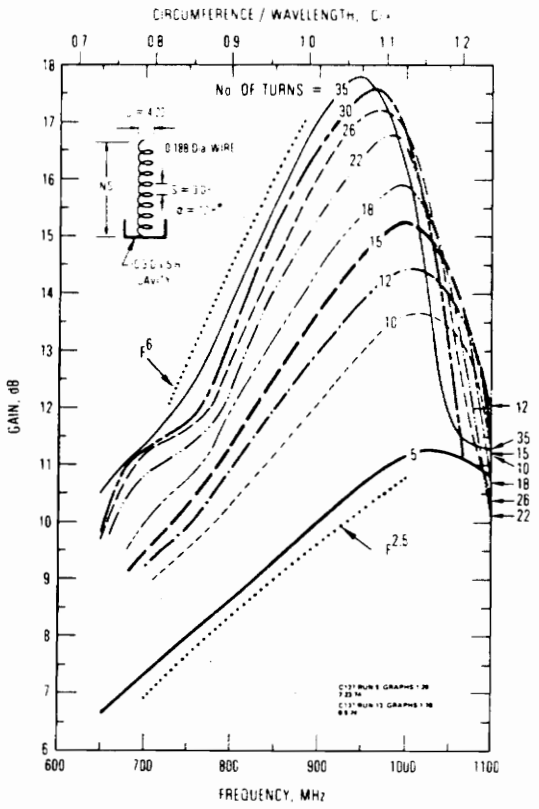

Figure 2.3.1-4. Measured gain versus frequency for fixed-circumference, fixed-pitch-angle helices of different lengths [7].

that the peak gain increases with the number of turns, which is not surprising since the directivity of an equally-spaced array increases as more elements are added to the array. This is another feature of the helix which makes it attractive to antenna designers; its gain (and/or beamwidth) can be tailored by adjusting the number of turns. Also shown in Figure 2.3.1-3 is a curve for the normalized circumference at peak gain versus the number of turns. The optimal circumference shows a slight decrease as more turns are added to the helix but for the most part it stays about 1.1 λ as discussed above .

Helices with many turns have a few disadvantages that should be mentioned here. Long helical antennas can be difficult to support; larger diameter tubing or wire is needed to obtain a self-supporting structure. Also, long helices are physically too large for many applications. Perhaps the biggest drawback, however, is that although gain goes up as the number of turns is increased, bandwidth drops significantly. This is shown in Figure 2.3.1-4 where curves of gain versus frequency are plotted for helices with 5 to 35 turns. (Data for Figure 2.3.1-3 were taken from these curves). It can be seen that the usable bandwidth decreases for helices with more turns. For example, the 3 dB bandwidth of the 15-turn helix in Figure 2.3.1-4 is approximately 260 MHz as compared to 190 MHz for the 35-turn helix. This can be seen more clearly if the bandwidth, as defined in (2.1.2-2), is plotted versus number of turns. The result is Figure 2.3.1-5 where the upper and lower frequencies of operation, f_u and f_l, are defined as the points where the gain falls 3 dB below its peak value.

Given these considerations, most helical antennas that have been developed for actual use have between 6 and 16 turns. In some applications where the desirable properties of helical antennas and high gain are required, helical arrays are used [9].

Conductor Diameter

Experiments have shown that the conductor diameter has little effect on the radiation properties of the axial-mode helical antenna [10]. Conducting tape wrapped on a cylindrical surface can be used if weight is a consideration or a thick conductor can be used if the helix must support itself.

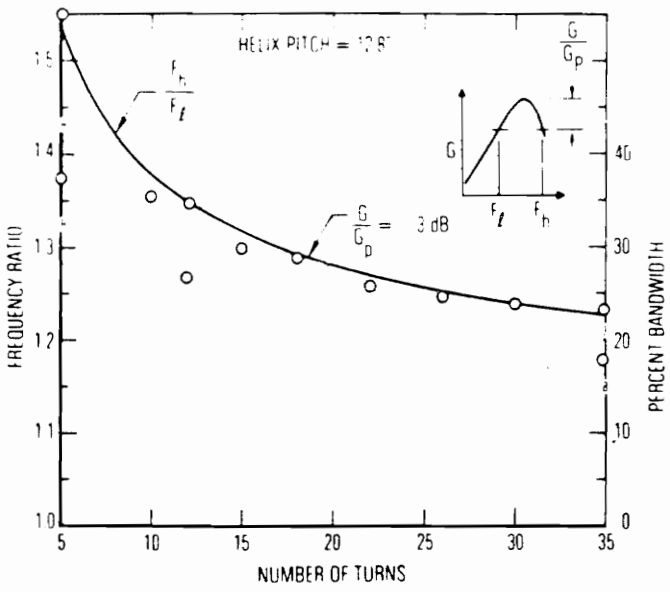

Figure 2.3.1-5. Bandwidth ratio, f_u/f_l, versus number of turns for the helices of Figure 2.3.1-4 [7]. Circles are measured values and line is curve fitted to these points.

Ground Plane

The effect of the ground plane is practically insignificant for the helix operating in the axial mode since reflected waves incident upon it are very weak [4]. Nonetheless, a ground plane that is at least $\frac{1}{2}\lambda$ in diameter at the lowest frequency is usually recommended.

Certain modifications to the standard circular ground plane have been explored. Meshed ground planes, as in Figure 2.3.1-6, have been used to eliminate eddy currents which can be detrimental to the radiation characteristics of the helix. Another modification which has become quite popular recently is a "cupped" ground plane, as shown in Figure 2.3.1-7. Researchers claim that this reduces backlobe radiation and increases directivity, particularly for long helices [5,11].

2.3.2 Expressions for Radiation Characteristics of the Axial-Mode Helix

Approximate expressions for the far-field radiation pattern of the axial-mode helix were discussed in Section 2.2.2 using array-modeling techniques. In this section, empirical relations that describe certain radiation characteristics of the helix are presented.

Gain

During his early work on the helical antenna, Kraus developed the following empirical relation for its directivity (or gain, G, since its efficiency is nearly unity) [1]:

$$G = 15C_{\lambda}^{2}ns_{\lambda} \qquad (2.3.2\text{-}1)$$

for $12^{\circ} < \alpha < 15^{\circ}$, $\frac{3}{4} < C_{\lambda} < \frac{4}{3}$, and $n > 3$. The subscripts, λ, indicate that the parameter is normalized to the free-space wavelength.

Many researchers have reported that Kraus's gain formula is overly optimistic and that actual helix measurements reveal considerably lower gain.

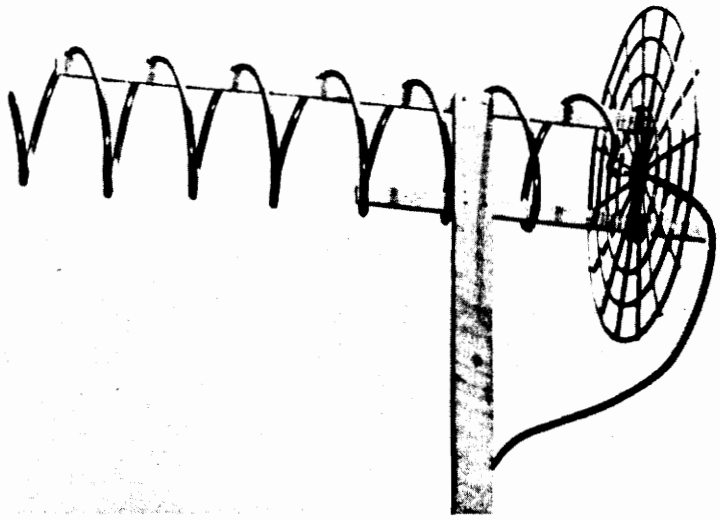

Figure 2.3.1-6. 7-turn, 12.5° pitch-angle helix mounted over a meshed ground plane [1].

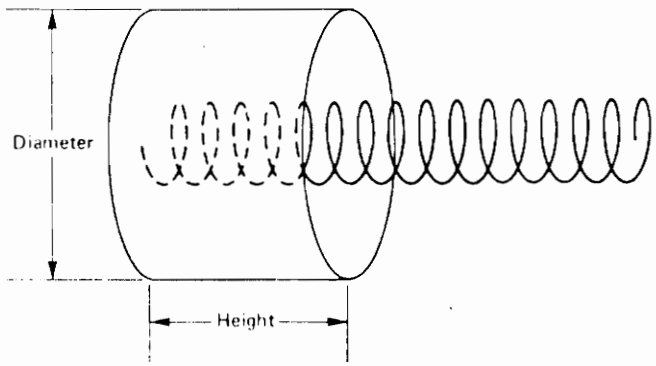

Figure 2.3.1-7. Helix mounted over a cupped ground plane [5].

King and Wong [7] developed a more accurate equation for peak gain, G_p, based on a much broader experimental data base:

$$G_p = 8.3\left(\frac{\pi D}{\lambda_p}\right)^{\sqrt{n+2}-1}\left(\frac{ns}{\lambda_p}\right)^{0.8}\left(\frac{\tan 12.5^\circ}{\tan\alpha}\right)^{\frac{\sqrt{n}}{2}} \qquad (2.3.2\text{-}2)$$

where λ_p is the free-space wavelength at peak gain. This equation has become the standard although some have reported that it may be off by as much as 1 or 2 dB from actual measurements [12]. The peak gain curves in Figures 2.3.1-1 and 2.3.1-3 were computed using this expression. The nearly exact agreement between computed and measured values is due to the fact that these measured values were part of the data base from which equation (2.3.2-2) was derived.

Half-Power Beamwidth

Kraus [1] developed the following equation for the half-power beamwidth, $HPBW$:

$$HPBW = \frac{52}{C_\lambda\sqrt{ns_\lambda}} \text{ degrees} \qquad (2.3.2\text{-}3)$$

for $12^\circ < \alpha < 15^\circ$, $\frac{3}{4} < C_\lambda < \frac{4}{3}$, and $n > 3$. Like his gain equation, this relation predicts helices to be more directive than they really are. King and Wong [13] have claimed that the actual half-power beamwidths are between 10 and 20 percent wider than those predicted by equation (2.3.2-3). They developed the following empirical relation:

$$HPBW = \frac{61.5\left(\frac{2n}{n+5}\right)^{0.6}}{\left(\frac{\pi D}{\lambda}\right)^{\frac{\sqrt{n}}{4}}\left(\frac{ns}{\lambda}\right)^{0.7}}\left(\frac{\tan\alpha}{\tan 12.5^\circ}\right)^{\frac{\sqrt{n}}{4}} \text{ degrees} \qquad (2.3.2\text{-}4)$$

Input Impedance

While operating in the axial mode the terminal impedance of the helical

antenna is mostly insensitive to changes in frequency. It is also almost purely resistive as mentioned in Section 2.1.2 which makes it a very efficient radiator. The following equation is an empirical relation for the radiation resistance which should be accurate to within $\pm 20\%$ [1]:

$$R = 140\, C_\lambda \text{ ohms} \tag{2.3.2-5}$$

for $12^\circ < \alpha < 15^\circ$, $\frac{3}{4} < C_\lambda < \frac{4}{3}$, and $n > 3$.

Axial Ratio

There is a certain degree of asymmetry in a helical antenna due to the way it is fed and truncated. This causes its polarization to be somewhat elliptical and not exactly circular as is often desired. Axial ratio was defined in Section 2.2.1 and is a measure of how well an antenna is circularly polarized. The following equation for the on-axis axial ratio is not an empirical relation but can be derived from the Hansen-Woodyard array model of the helical antenna [1]:

$$AR = \frac{2n+1}{2n} \tag{2.3.2-6}$$

The axial ratio approaches unity (pure circular polarization) as the number of turns is increased. This has been confirmed experimentally as shown in Figure 2.3.2-1, which is a plot of axial ratio versus number of turns. Certain modifications to the standard helix such as tapered ends and feeds can also be used to lower the axial ratio. These will be discussed in Section 2.5.

Equation (2.3.2-6) has been shown to be inaccurate in many cases [15] but it still can be useful as a quick and simple estimate of the axial ratio. Figure 2.3.2-2 is a plot of the axial ratio of radiation in the axial direction as frequency is changed. The dashed line is the axial ratio as predicted by (2.3.2-6) (in this case, $n = 7$ and $AR = \frac{15}{14} = 1.07$). The curve shows how well the helix remains circularly polarized over a wide frequency range. It is emphasized that equation (2.3.2-6) is only valid along the axis where the helix is closest to an axial ratio of unity. There has also been considerable amount of work done on characterizing and improving the axial ratio in off-axis directions [16].

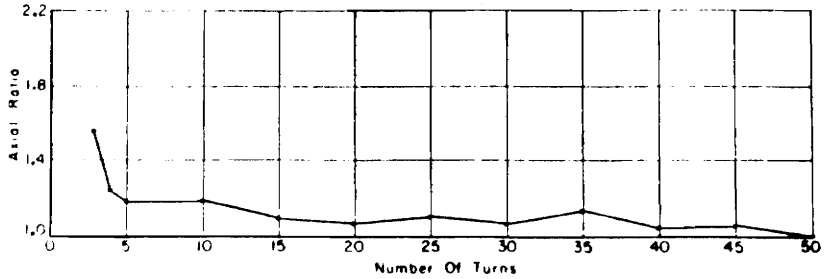

Figure 2.3.2-1. Measured on-axis axial ratio versus number of turns [14].

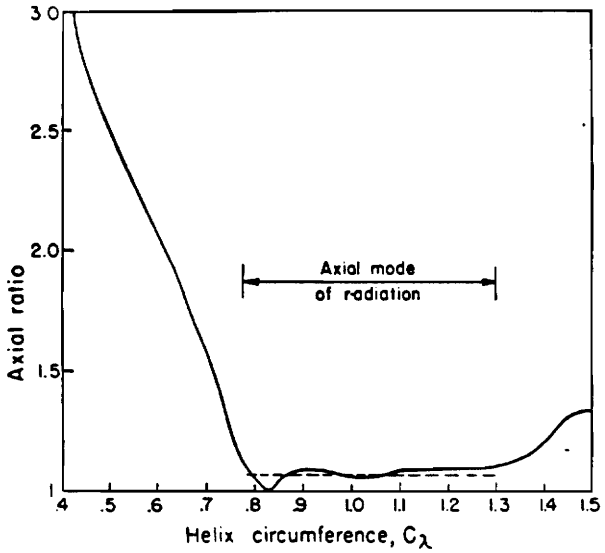

Figure 2.3.2-2. Measured on-axis axial ratio versus circumference normalized to wavelength (solid) and predicted value from (2.3.2-6) (dashed) [1].

Bandwidth

An empirical relation for the bandwidth (as a frequency ratio) of the helical antenna as defined in (2.1.2-2) has been developed [7]:

$$\frac{f_u}{f_l} \approx \left(\frac{0.91}{\frac{G}{G_p}} \right)^{\frac{4}{3\sqrt{n}}} \qquad (2.3.2\text{-}7)$$

where G_p is the peak gain and G is the gain at the limits of operating frequencies. If f_u and f_l are defined as the points where G is 3 dB down from G_p, i.e. $\frac{G}{G_p} = 0.5$, (2.3.2-7) then becomes:

$$\frac{f_u}{f_l} \approx (2.91)^{\frac{4}{3\sqrt{n}}} \qquad (2.3.2\text{-}8)$$

Figure 2.3.1-5 is a plot of this expression through a portion of the data from which it was derived. The bandwidth of the helical antenna deteriorates drastically from the frequency ratio of 1.78 (as given by equation (2.1.2-2)) as the number of turns is increased.

2.4 ESP Analysis of an Axial-Mode Helix

The ESP moment-method program is used in this section to analyze the radiation properties of a cylindrical helix operating in the axial mode. The test-case helix has 6 turns, a pitch angle of 14°, and a diameter of 0.2325 meter (C $\approx 1\ \lambda$ at 450 MHz). This antenna was chosen because actual measurements of a helix with these dimensions are available [1]. The two results are compared in this section.

2.4.1 Electromagnetic Surface Patch (ESP) Moment-Method Code

Antennas to be analyzed by ESP must first be modeled as a combination of straight wire segments and flat plates. ESP then uses the method of moments or, more specifically, the *piecewise sinusoidal Galerkin's method* to approximate the current distribution on each segment or plate [17]. Once these currents have been found it is a rather straightforward task to compute the antenna radiation characteristics (far-field pattern, input impedance, etc.).

Different versions of ESP have been around for about 20 years. The latest, Version III, has been available since 1987 and was used throughout this work. Previous investigations showed that ESP produces accurate far-field patterns for other types of wire antennas [18,19] and should demonstrate its accuracy for the problem at hand, i.e. comparison with a known helix result.

ESP is well-suited for studying wire antennas with complex geometries such as the helix. For this work, it was installed on a personal computer to make its results easily accessible. Even on a PC, ESP is capable of handling antennas broken into a large number of segments (up to several hundred, depending on the memory) although it may run considerably slower than if it was on a mainframe. Initial work on the spherical helix used a recently released moment-method code called *AWAS* (Analysis of Wire Antennas and Scatterers) developed by a group at Syracuse University [20]. This program is very user-friendly and provided a good starting point but, unfortunately, it can only handle up to 50 segments.

Another benefit of using ESP is that it provides an option of defining the wire geometry through a subroutine called *WGEOM* appended to the main program. This makes it easy to enter data points for many segments of a mathematically well-defined structure like the helix (the more segments, the better the approximation to the actual antenna). Clever use of input data to the subroutine also makes it possible to change the dimensions of an antenna without having to recompile.

One final reason ESP was chosen to analyze the spherical helix is that its flat plate feature permits modeling of a finite ground plane. Most moment method codes, including AWAS, approximate a ground plane as a perfectly conducting

sheet of infinite dimensions.

2.4.2 Measurements and Numerical Analysis of a 6 turn, 14° Helix

This section discusses how ESP was used to compute the radiation patterns of a 6-turn, 14° cylindrical helix and compares the results to measured patterns. The ESP subroutine WGEOM used to compute the data points for the helix is included in Appendix A. The mathematics for generating these points is rather simple. The equations of the helix are written in cylindrical coordinates (ρ, ϕ, z) as (referring to the coordinate system of Figure 2.2.1-1 and the helical dimensions of Figure 2-1):

$$z = \frac{s}{2\pi}\phi = \left(\frac{D}{2}\tan\alpha\right)\phi \qquad (2.4.2\text{-}1)$$

$$\rho = \frac{D}{2} \qquad (2.4.2\text{-}2)$$

where ϕ is in radians and s, D, and α are as previously defined. The equivalent cartesian coordinates (x, y, z) form of the helix equation for use with ESP is given by the following relations:

$$x = \rho\cos\phi = \frac{D}{2}\cos\phi \qquad (2.4.2\text{-}3)$$

$$y = \rho\sin\phi = \frac{D}{2}\sin\phi \qquad (2.4.2\text{-}4)$$

$$z = \left(\frac{D}{2}\tan\alpha\right)\phi \qquad (2.4.2\text{-}5)$$

After a number of experimental runs with ESP, it was determined that accurate patterns are produced for helical geometries modeled with 20 straight wire segments per turn. Thus, a 6 turn helix will be made up of 120 segments. The sub-program WGEOM approximates the geometry of the 6 turn, 14° helix as shown in Figure 2.4.2-1.

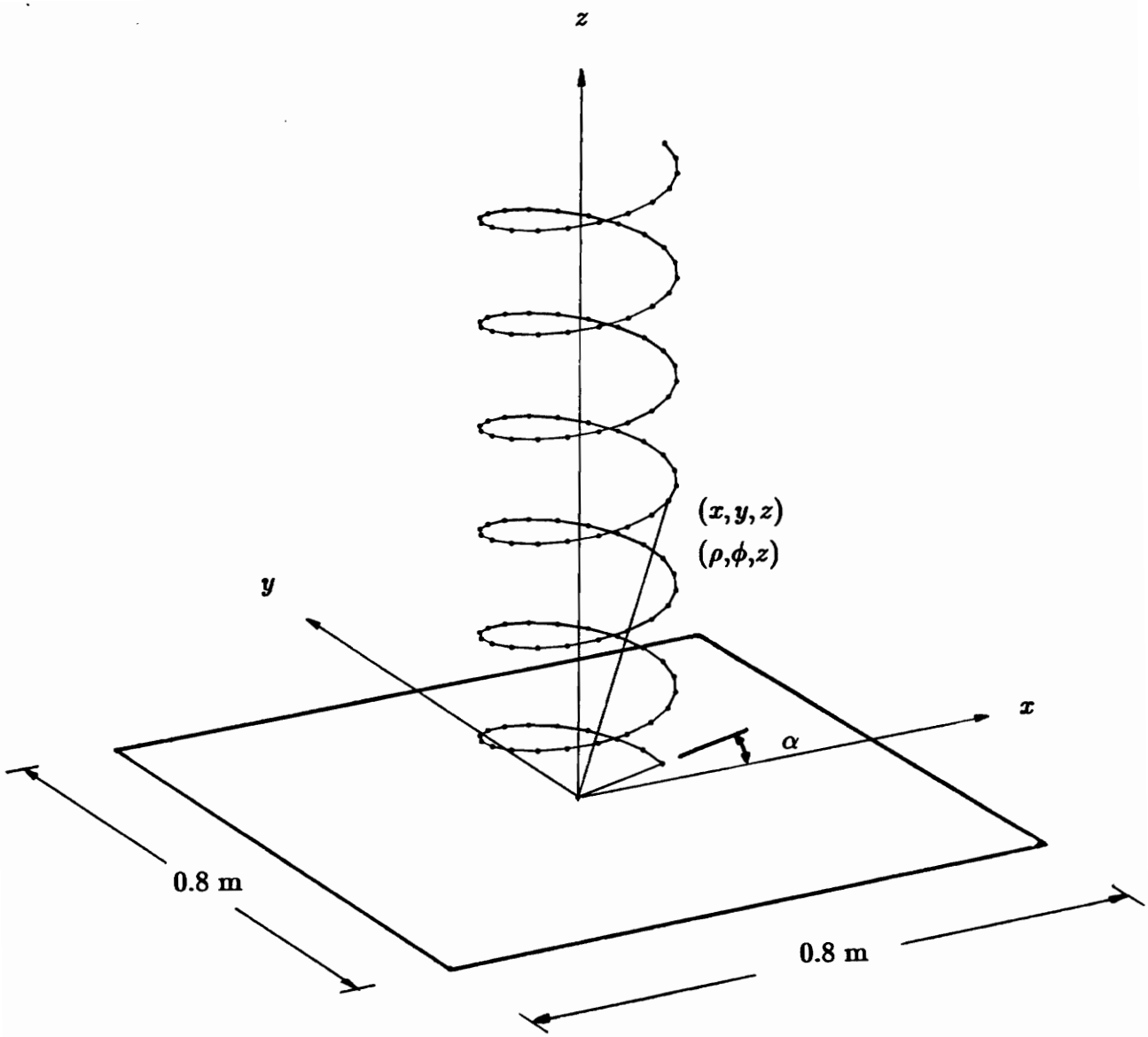

Figure 2.4.2-1. 6-turn, 14° helix modeled with straight wire segments for input into ESP (120 total segments, 20 per turn). Helix has a diameter of 0.23 m and is mounted over a square ground plane, 0.8 m on each side. Feeding wire makes angle α with ground plane.

The exact feeding arrangement or type of ground plane used for the original measurements was not specified in the published results [1]. These will not have a significant effect on the pattern calculations however. A square ground plane was used for simplicity and fast computational time. It is shown in Figure 2.4.2-1. The ground plane is 0.8 meter on each side, which is well over a half wavelength at the lowest frequency tested (275 MHz, where $\lambda = 1.09$ m). The ground plane used for the measurements was probably circular but since its dimensions are greater than a half wavelength, the square ground plane should not make much of a difference.

The helix is slightly offset from the ground plane so that it can be fed by a straight wire segment attached to the center conductor of the coaxial input. The feeding wire is arranged so that it forms an angle α (equal to the pitch angle of the helix) with its projection on the ground plane as shown in Figure 2.4.2-1. This type of feeding arrangement has been used on helical antennas in the past to lower the $VSWR$ [1].

Figure 2.4.2-2a shows the measured field patterns of the 6 turn, 14° helix as reported by Kraus [1]. Both components, E_θ and E_ϕ, are plotted on a linear scale at each frequency and have been normalized to the same maximum. (Refer to Figure 2.2.1-1 for how the field components and coordinate system are related.) The antenna operates in the axial mode over a frequency range from at least 300 MHz to 500 MHz, giving a bandwidth ratio of 1.67.

Figure 2.4.2-2b shows the results from an analysis of this antenna with ESP for the seven frequencies shown in Figure 2.4.2-2a. E_θ and E_ϕ are plotted as they were for the measured patterns in part (a). The pattern cuts are taken in the x-z plane, although it is not exactly clear which plane was used for the original measurements. It should not matter, however, since the axial-mode pattern of the helix is essentially symmetrical about the z-axis. The results from ESP compare remarkably well with the actual measurements. Both show that the helix begins to operate in the axial mode at 300 MHz or when its circumference is $0.73\,\lambda$ which also agrees well with the range specified in (2.1.2-1).

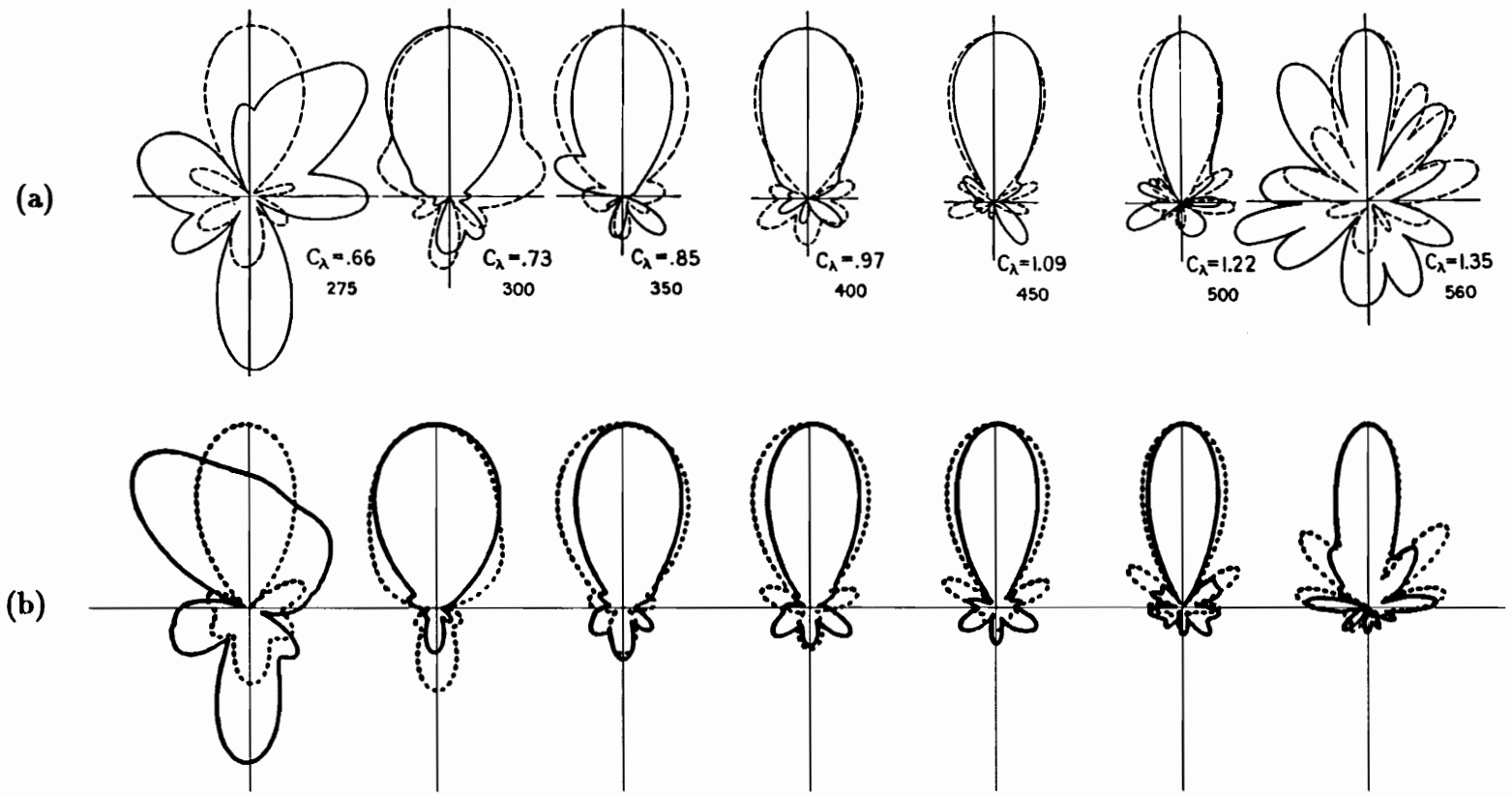

Figure 2.4.2-2. Field patterns of a 6-turn, 14° helix. Solid curves are for E_θ and dashed are for E_ϕ; both are plotted on a linear scale and normalized to the same maximum. (a) Measured patterns with frequency in MHz and normalized circumference given beneath each plot [1]. (b) Patterns computed by ESP at the same frequencies as those in (a).

Figure 2.4.2-3 contains plots of the phase difference between E_θ and E_ϕ computed using ESP for the upper half-plane ($-90^\circ \leq \theta \leq 90^\circ$)* at 350 and 400 MHz. These curves are useful in showing how well an antenna is circularly polarized. The requirement for circular polarization is that both components must have equal magnitude and be 90° out of phase. Figure 2.4.2-3 shows that E_θ and E_ϕ are 90 degrees out of phase for most of the main lobe in the axial mode (curves at the other frequencies between 300 and 500 MHz, not shown here, are similar to those in Figure 2.4.2-3). Circular polarization is only achieved on the axis. Off the axis, the magnitudes of the components are not quite equal and the phase difference between them departs from 90° which causes the polarization to become slightly elliptical. The phase difference curves for the patterns in Figure 2.4.2-2 (two of which were shown in Figure 2.4.2-3) show that circular polarization is maintained over a wide range of frequencies but not over a wide range of angles off boresight. Modifications to the standard helix can be used to lower the axial ratio and will be discussed in Section 2.5.

As expected, the far-field pattern reaches peak directivity when the circumference of the helix approaches 1.1 λ. In all of the patterns of Figure 2.4.2-2b, the sidelobe level is generally about -10 dB (although a linear scale was used in the figure) which also agrees well with published reports [7]. The half-power beamwidths are about 50 degrees in both the measured and ESP-generated plots verifying (2.3.2-5) for $HPBW$ which predicts a value of 48.6°. Incidentally, (2.3.2-4) which has been criticized for being inaccurate [13] predicts a half-power beamwidth for this antenna of 37.1°. At 560 MHz ($C_\lambda = 1.35$), the helix is no longer operating in the axial mode. Table 2.4.2-1 summarizes the comparison of the pattern characteristics computed by ESP, those measured on an antenna range, and those predicted by the empirical relations of Section 2.3.2.

*See the discussion in Appendix C for a more rigorous definition of the quantities and ranges used in these figures.

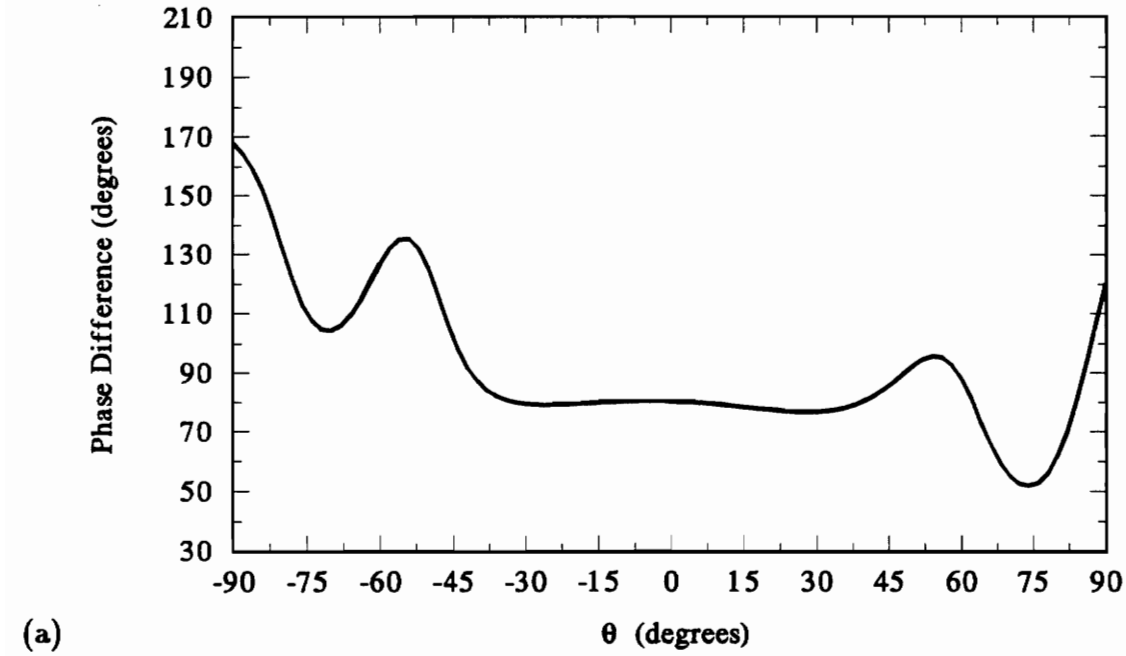

(a)

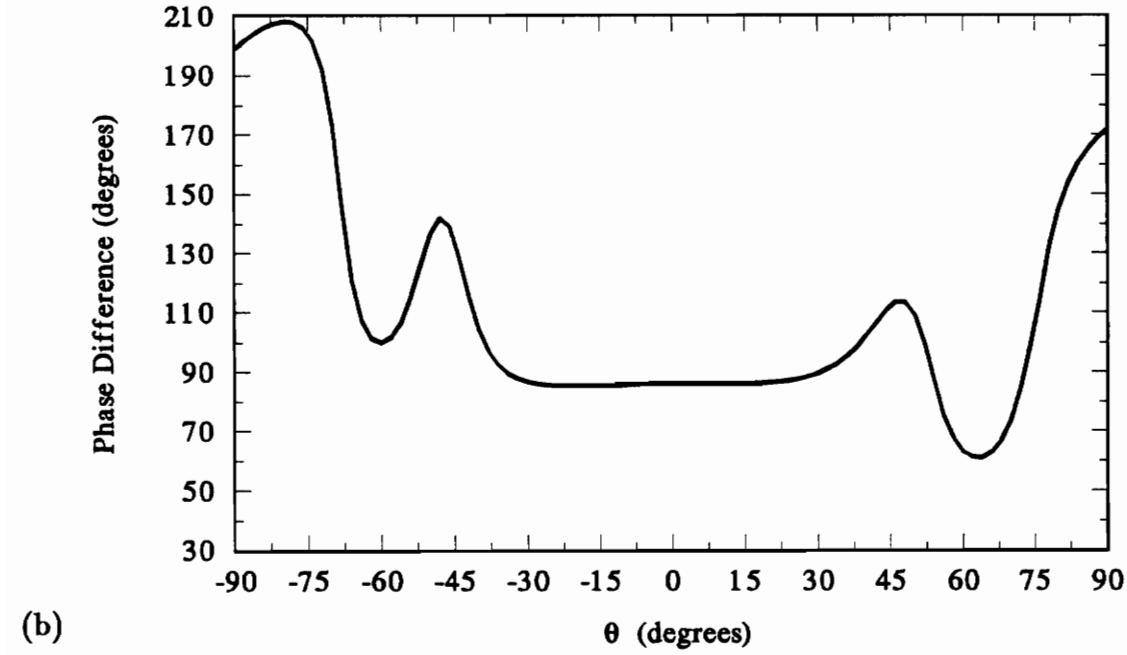

(b)

Figure 2.4.2-3. Phase difference between E_θ and E_ϕ computed using ESP at (a) 350 MHz and (b) 400 MHz for the upper half-plane.

Table 2.4.2-1.

Comparison of Numerical (ESP), Measured, and Empirically-Calculated Pattern Characteristics of a 6-turn, 14° helix with a Circumference of 1.1 λ.

Pattern Characteristic	Numerical (ESP)	Measured [1]	Empirical (eq. #)
• gain	12.3 dB	-	11.0 dB (2.3.2-2)
• bandwidth ratio	~ 1.70	~ 1.70	1.79 (2.3.2-8)
• halfpower beamwidth	$\sim 50^\circ$	$\sim 50^\circ$	48.6° (2.3.2-4)
• sidelobe level	-12.5 dB	~ -10 dB	-

This comparison of ESP results to a known helix verifies that ESP can be used to accurately analyze electrically-long wire antennas. The square ground plane has also proved to be an effective approximation to a circular one and this helps to greatly cut down on computational time. (Recall, the measured patterns of Figure 2.4.2-2a came from a helix which was most likely mounted over a circular ground plane and compared well with the ESP-generated patterns of Figure 2.4.2-2b for a helix over a square ground plane.) Experience gained on this test run was very useful in the analysis of the spherical helical antenna.

2.5 Modifications of the Helix

After Kraus's initial discovery of the remarkable properties of the axial-mode helix, a euphoria of experimentation with the antenna swept through research circles. Antenna engineers proposed countless variations on the simple cylindrical helix over a flat ground plane in order to achieve the following improvements:

- Higher gain
- More bandwidth

- Lower axial ratio
- Lower sidelobe level
- Lower VSWR at the feed

Exotic variations of the helix have inundated the antenna literature for the last forty years and are far too numerous to make even a partial list here. Many of these proposals have proved to be useless but some have stood up to close scrutiny and have found a variety of applications. Of particular importance are the following:

- Cupped ground planes [5] - higher gain
- Tapered feeds and ends [16] - lower axial ratio and VSWR
- Helices of different diameters in series [11] - more bandwidth
- Parasitic windings [21] - higher gain

With regard to the winding of the helix, Kraus [1] has defined three ways it can be modified:

1) α constant, s and D variable
2) D constant, α and s variable
3) s constant, α and D variable

Figure 2.5-1 shows some different ways helices in these three classes may be tapered. The spherical helix, the subject of this work, fits in the final category shown: a constant spacing, s, with an envelope taper. The envelope taper for the spherical helix is a sphere as shown in Figure 1-2.

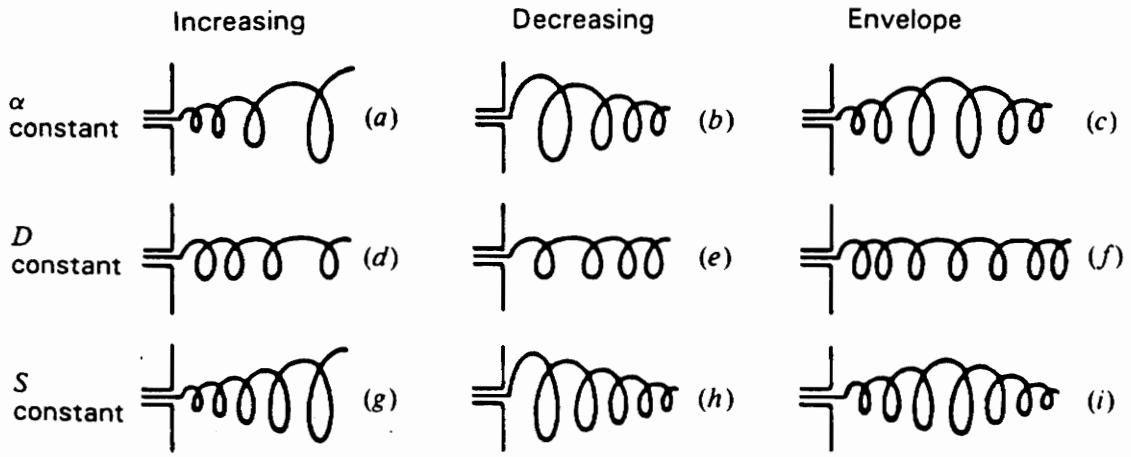

Figure 2.5-1. Variations of winding and tapering the axial-mode helical antenna [1]. (a) α held constant while s and D vary. (b) D held constant while α and s vary. (c) s held constant while α and D vary.

2.6 Applications of the Helix

The axial-mode helical antenna has found a wide variety of applications but has probably been most useful in the area of satellite communications. Fairly high gain and excellent circular polarization over a wide range of frequencies make it ideal for transmitting and receiving broadband satellite signals. In mobile satellite communications (land, sea, and air), low-to-medium gain helices are used because of their broad beamwidths and low axial ratio. In situations where high gain and reasonable circular polarization are required, parabolic reflectors with helical feeds are often used.

Figure 2.6-1 is a picture of the actual antenna used on the fleetsatcom satellites. Two helical antennas are used; one is the feed for the reflector and the other operates with its own cupped ground plane. It is interesting to note that, in both cases, the helices have tapered ends. In fact, most helical antennas built today, except perhaps in amateur circles, use some sort of modification as discussed in Section 2.5.

High gain helical arrays are also useful in satellite communications [9]. They provide the ability of tailoring the radiation pattern to a specific contour while still retaining the desirable properties of the helix. Figure 2.6-2 is a picture of an S-band phased array used on the Tracking and Data Relay Satellite System (TDRSS). The helical elements have tapered ends to reduce the axial ratio and cupped ground planes to minimize mutual coupling. The reference from which this was taken states that simplicity of construction was one of the reasons helical elements were chosen [23]. This is a serious concern even for high budget projects.

The spherical helical antenna is also simple to build. Several prototypes were constructed and tested throughout the course of this work (details are given in Chapter 5). The performance of this new antenna is discussed in the following chapters.

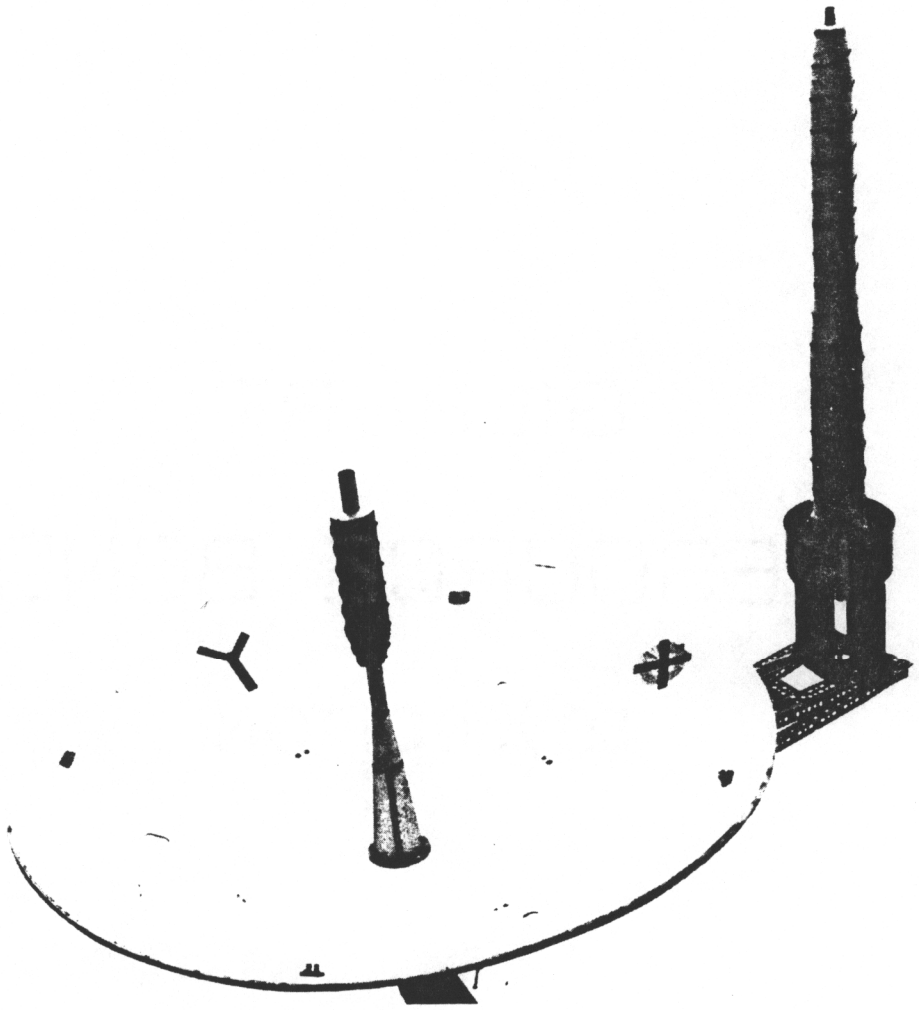

Figure 2.6-1. Antenna system for the Fleetsatcom satellites using helices operating between 240 and 400 MHz [22].

[8] 122 page

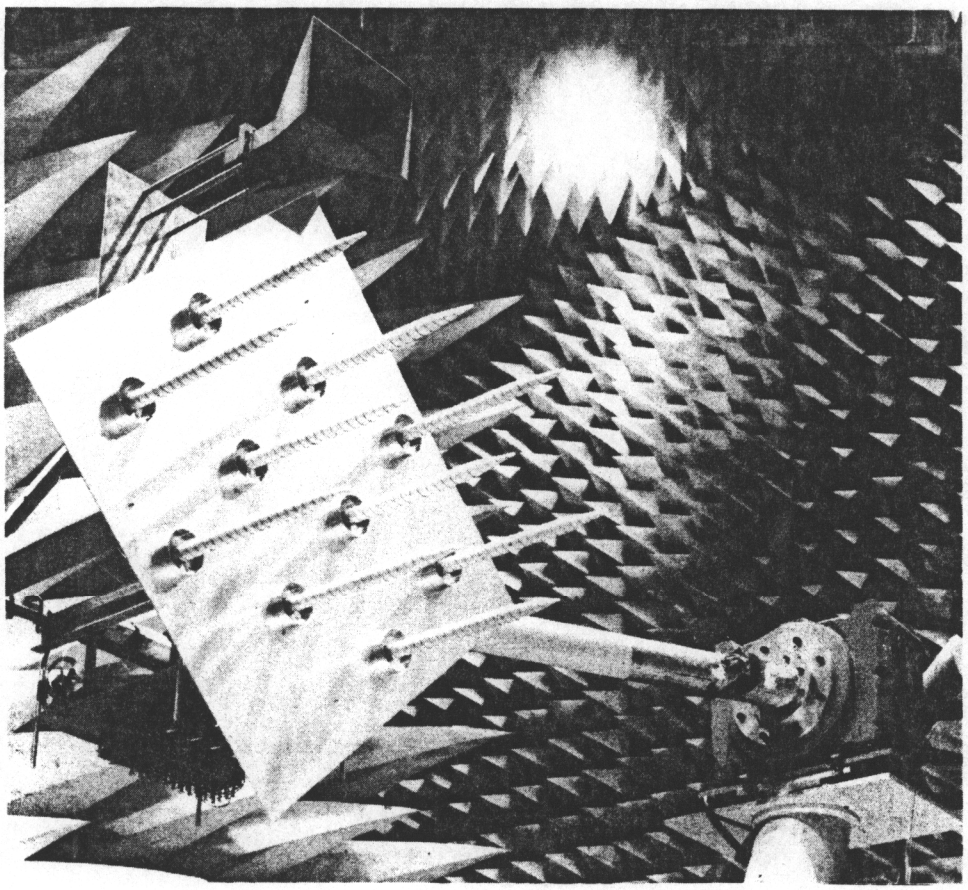

Figure 2.6-2. Phased array using helical antennas for the Tracking and Data Relay Satellite System (TDRSS) [23].

3. The Spherical Helical Antenna

The spherical helical antenna is very similar to the conventional helical antenna except that it is wound over a sphere instead of a cylinder. The sphere is centered over a coaxial input; the inner conductor becomes the helical winding and the outer conductor becomes the ground plane. This was shown in Figure 1-2.

The spherical helix is wound such that it maintains a constant spacing s between turns (see Figure 3.2-1). This was done so that mathematical expressions that describe the structure could be easily formulated. The spherical helix with a fixed spacing is also advantageous because it is easy to construct. As stated in Section 2.5, fixing the spacing and varying the diameter to produce a spherical envelope forces the pitch angle of the helix to be variable. Chapter 5 gives the details of the making and testing of these antennas.

With the spherical helix so-defined it is only necessary to specify the circumference (or diameter) of the spherical envelope and the number of turns (or spacing) to uniquely describe the structure. The spherical helices under consideration in this work have between 3 and 10 turns (the number of turns does not have to be an integer). With fewer turns, the structure departs from having a spherical shape and with more turns it becomes too much like a spherical resonant cavity. In order to accommodate between 3 and 10 turns on a sphere, the pitch angle (though varying) will be below the lower limit specified in Table 2.3-1 for optimum axial-mode performance. It is still expected, however, that the spherical

helix will operate in an axial mode since other researchers have produced axial radiation with helical dimensions outside those specified in Table 2.3-1 [1, 5, 6]. This investigation addresses whether the spherical helical geometry will provide any improvement over the radiation characteristics of the helix, specifically bandwidth and circular polarization. It is also possible that entirely new modes of operation will emerge.

The spherical helical antenna is even more difficult to analyze than the helical antenna. It cannot be easily modeled as an array, as was done for the helix, because the turns have different diameters and could not be assumed to have the same far-field response. The best available way to study its behavior is to use numerical techniques. ESP will be used to examine the spherical helix in Chapter 4.

If the spherical helix operates in an axial mode with a spherical circumference of 1 λ, as might be expected, it will be a very electrically compact antenna. Its diameter, D, will be:

$$D = \frac{C}{\pi} = \frac{1\lambda}{\pi} \approx 0.3\,\lambda \tag{3-1}$$

This is a beneficial feature of the spherical helical antenna since physical size is often an important consideration in antenna design. A helical antenna that has dimensions for optimal performance and takes up the same space as the spherical helical antenna would have very few turns. For example, a 12.5° helix with an axial length, A, of 0.3 λ would have:

$$n = \frac{A}{s} = \frac{A}{C\,\tan\alpha} = \frac{0.3\,\lambda}{1\lambda\,\tan 12.5^{\circ}} \approx 1.2 \text{ turns} \tag{3-2}$$

Thus, it can be realized that the average pitch angle of the spherical helix must be fairly low in order to accommodate several turns over an axial length of only 0.3 λ.

3.1 Previous Work Related to the Spherical Helix

An extensive literature survey did not uncover any previous work on the spherical helix as it is defined in this chapter. This could be due to the fact that it is very difficult to derive analytic solutions for the antenna even under special conditions. This section presents some of the research on spherically-shaped radiators that, to some degree, resemble the spherical helical antenna.

About 30 years ago, research was done on a class of radiators known as spherical spiral antennas which look very similar to the spherical helical antenna [24, 25, 26]. Exact mathematical solutions were developed for the far fields of a spherical boundary with an anisotropically-conducting surface [24]. The sphere is only conductive along lines that spiral from each pole and is non-conductive elsewhere. Considering an antenna as an anisotropic boundary-value problem is an elegant approach to antenna analysis [25].

The geometry and equations that describe the spiral lines are shown in Figure 3.1-1 for two of the cases examined. The spherical spiral antenna in Figure 3.1-1a looks very similar to the spherical helix. However, the solution to the anisotropically-conducting surface model requires that there be an infinite number of spiral turns along the sphere. The spherical helix presented in this work has only between 3 and 10 turns; most of the spherical surface is nonconducting. Additionally, the spherical spiral antenna is "excited by fields at a gap around the equator" [24] whereas the spherical helix is mounted above a ground plane and is excited by a coaxial input at the pole.

The work on spherical spiral antennas was motivated by the small spherical shape of satellites in the early 1960's. These satellites often required isotropic patterns since their attitudes were not stabilized with respect to the earth [26]. Other mechanical considerations prohibited protruding antennas which excluded dipole elements. This led to the development of broadband isotropic antennas that conformed to the surface of the satellite. A picture of such an antenna is shown in Figure 3.1-2. This satellite was used in the TRANSIT satellite program for taking measurements of ionospheric refraction.

(a)

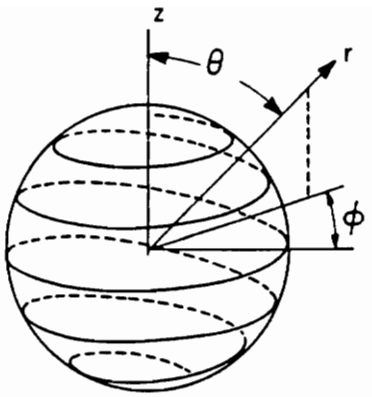

$$\phi = \frac{a}{2} \log \frac{1-\cos\theta}{1+\cos\theta}$$

$$\frac{d\phi}{d\theta} = \frac{a}{\sin\theta}$$

(b)

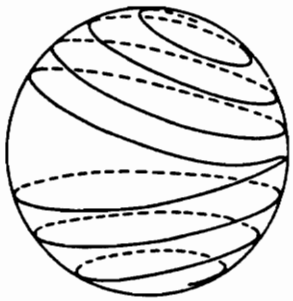

$$\phi = b \log \sin\theta$$

$$\frac{d\phi}{d\theta} = \frac{b\cos\theta}{\sin\theta}$$

Figure 3.1-1. Two previously investigated geometries [24] of spherical spiral antennas. (a) Geometry looks similar to spherical helix, (b) geometry is different than spherical helix.

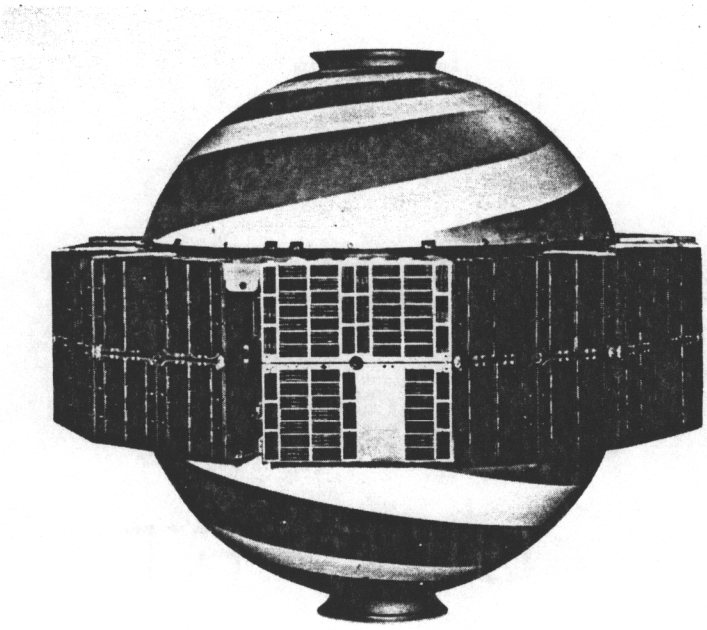

Figure 3.1-2. The spherical spiral antenna used on the TRANSIT 3B satellite [29].

The purpose of experimenting with the spherical helix is to see if any improvements can be made to the standard cylindrical helix or if any new noteworthy radiation characteristics can be found. Others have experimented with different envelopes and tapers for the same reason but, surprisingly, no one has examined the spherical helix which seems to be a very fundamental geometry. A notable departure from the cylindrical helix is the *conical helix* shown in Figure 3.1-3 which is reported to have increased bandwidth [8, 30]. The *half-ellipsoid helical antenna* shown in Figure 3.1-4 is another variation which is reported to have a wider bandwidth than the standard helical antenna [31]. It is interesting to note that, in both of these cases, the antennas operate in an axial mode just like the helix despite having geometries markedly different from the helix. It is expected that the spherical helix will behave similarly, although broadband operation is not expected since its varying pitch angle is very low.

3.2 Geometry of the Spherical Helix

The geometry of the spherical helix with equal spacing between turns is shown in Figure 3.2-1. The sphere, real or fictitious, over which the wire is wrapped is centered at the origin of cartesian (x,y,z), cylindrical (ρ,ϕ,z), and spherical (r,θ,ϕ) coordinate systems. The parameters that describe the geometry of the spherical helix are similar to those for the cylindrical helix:

$$
\begin{aligned}
a &= \text{radius of sphere} \\
N &= \text{number of turns} \\
s &= \text{spacing between turns} = \frac{2a}{N} \\
D &= \text{diameter of sphere} = 2a = Ns \\
C &= \text{circumference of sphere} = \pi D \\
d &= \text{diameter of conductor}
\end{aligned}
$$

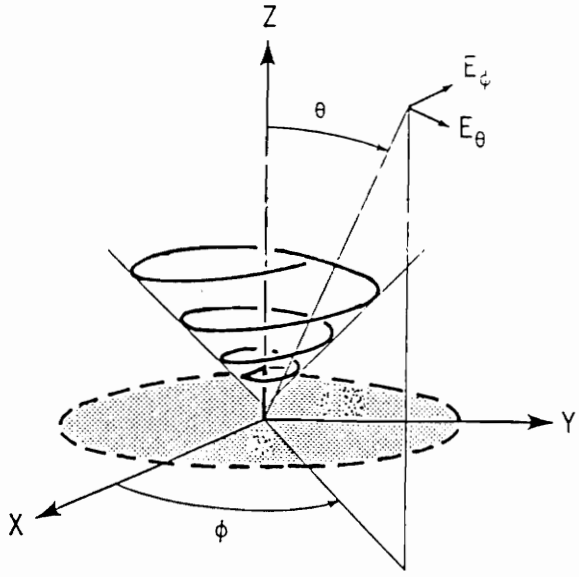

Figure 3.1-3. The conical helical antenna [8].

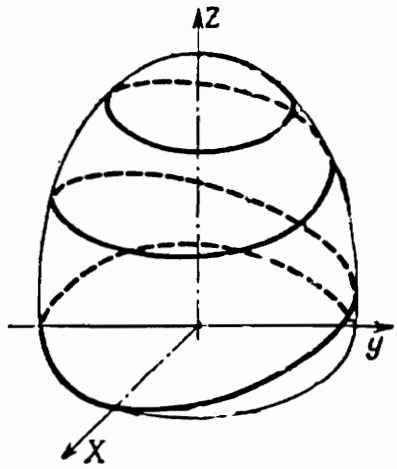

Figure 3.1-4. The half-ellipsoid helical antenna [31].

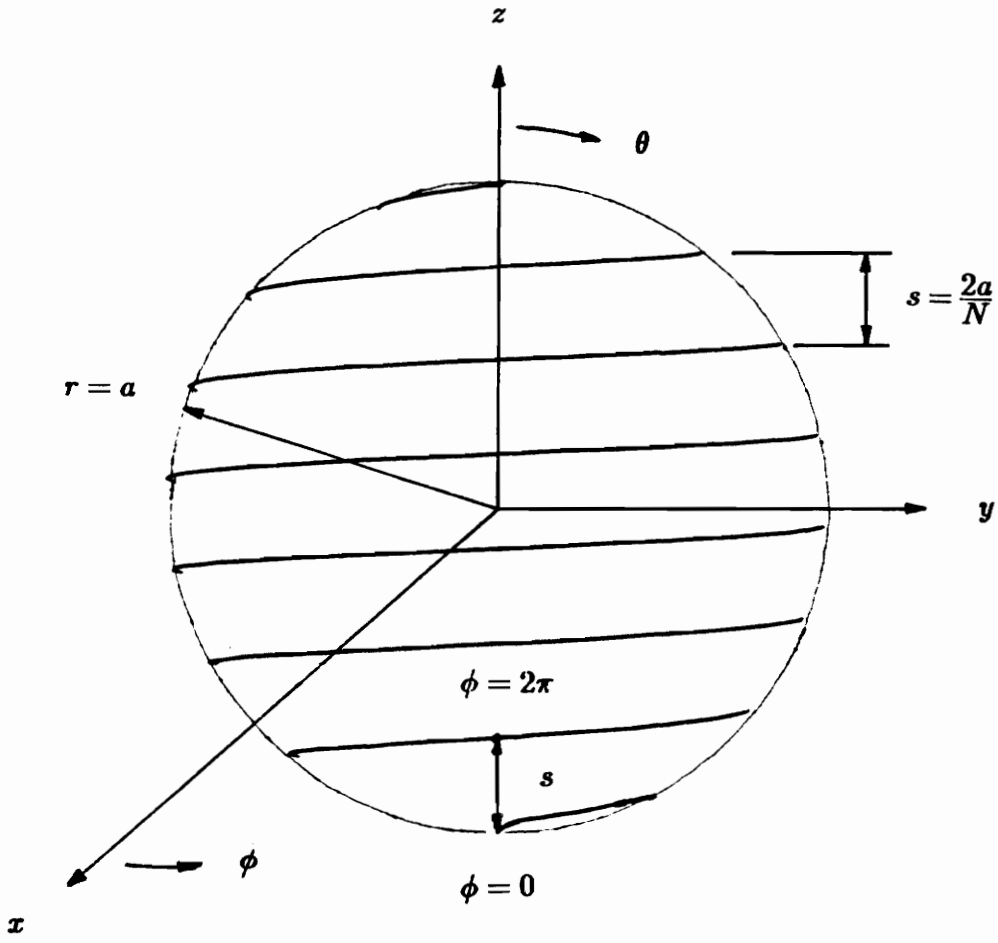

Figure 3.2-1. Geometry and dimensions of the spherical helix.

The only two parameters required to completely specify the spherical helix are the radius of the sphere, a, and the number of turns, N. This is due to the condition imposed on the winding that each turn, though different, must traverse the same axial distance, namely s or $\frac{2a}{N}$ (which is along the z-axis in Figure 3.2-1). This condition also makes the mathematical relations describing the helix easy to derive and, as will be seen later, makes the structure a rather simple one to build.

Expressions for the geometry of the spherical helix will now be derived. By definition, each spherical turn sweeps out 2π radians of the angle ϕ and displaces the same distance along the z-axis. Thus, there is a linear relationship between z and ϕ over the entire length of the spherical helix which sweeps out a total of $2\pi N$ radians of the angle ϕ. It can be expressed as:

$$z = m\phi + b \tag{3.2-1}$$

for $0 \leq \phi \leq 2\pi N$. The coordinates (ϕ, z) of two known points can be used to find m and b. Referring to Figure 3.2-1, the following points are chosen:

$$\phi = 0, \quad z = -a$$
$$\phi = 2\pi, \quad z = -a + s$$

Inserting these into (3.2-1) and solving a simple system of two equations in two unknowns yields:

$$z = \frac{s}{2\pi}\phi - a \tag{3.2-2}$$

for $0 \leq \phi \leq 2\pi N$. The parameter s can be removed by replacing it with $\frac{2a}{N}$. Equation (3.2-2) now becomes:

$$z = a\left(\frac{\phi}{N\pi} - 1\right) \tag{3.2-3}$$

for $0 \leq \phi \leq 2\pi N$. The linear relationship between z and ϕ is shown in Figure 3.2-2.

At this point, the derivation of equations for the spherical helix is simplified by converting to spherical coordinates (r, θ, ϕ). The coordinate transformation of z

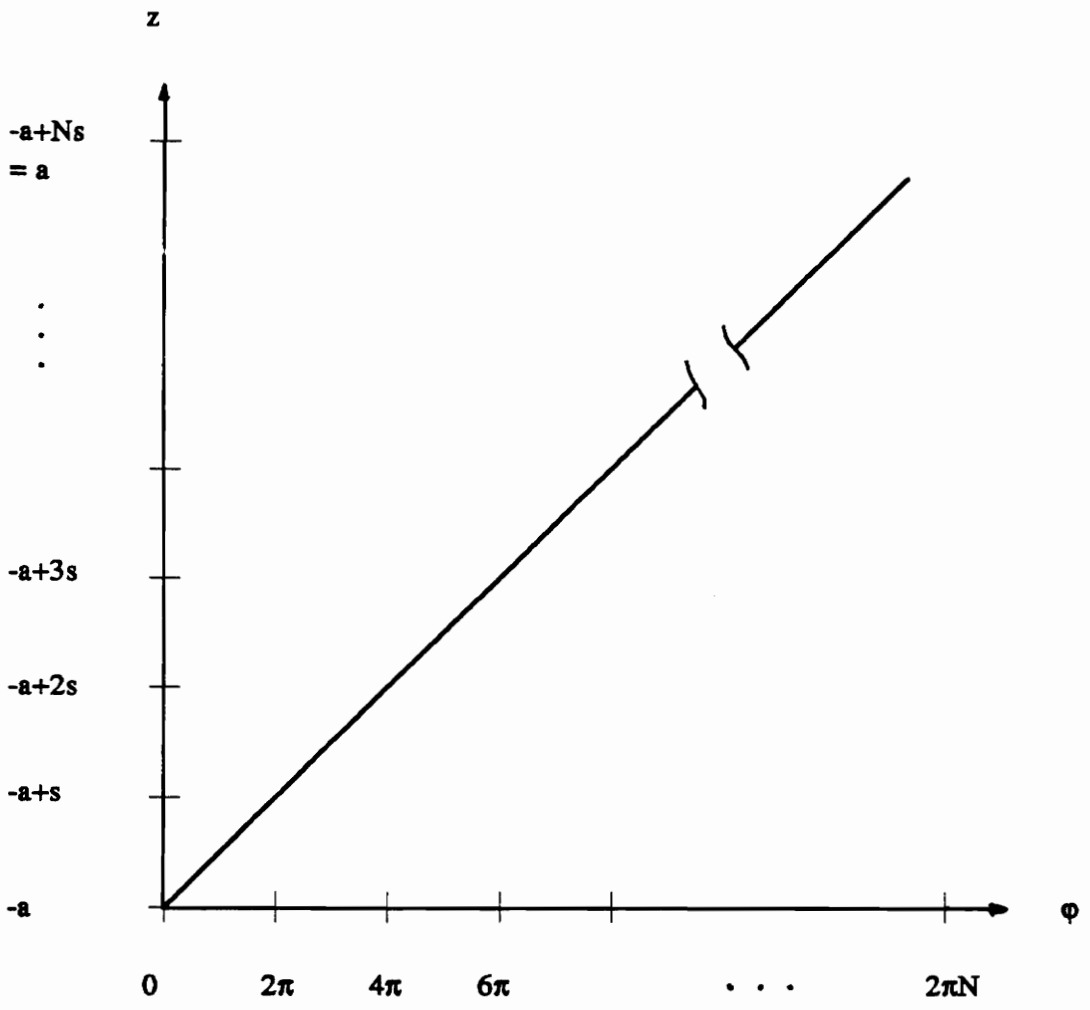

Figure 3.2-2. Linear relationship between z and ϕ coordinate of the spherical helix.

into spherical coordinates is given by:

$$z = r\cos\theta = a\cos\theta \tag{3.2-4}$$

Finally, the mathematical expressions for the spherical helix can be found by combining equations (3.2-3) and (3.2-4) and recognizing that the coordinate r is always equal to the radius of the sphere, a. They are:

$$r = a \tag{3.2-5}$$

$$\theta = \cos^{-1}\left(\frac{\phi}{N\pi} - 1\right) \tag{3.2-6}$$

for $0 \leq \phi \leq 2\pi N$.

The above relations can be extended to also describe spherical helices that do not completely wrap around the sphere from pole to pole. This type of structure, called a "*truncated spherical helix*," is specified by the actual number of turns it has, labeled n, and the total number of turns it would have if completely wound around the sphere, already labeled N. An example of a truncated spherical helix with $n = 5.5$ and $N = 8$ is shown in Figure 3.2-3. Future work may reveal that this variation improves the radiation characteristics compared to the full spherical helix since it looks less like a resonant cavity. This will again be proposed in Section 6.2. Equations (3.2-5) and (3.2-6) can be made to accommodate the option of truncated spherical helices simply by changing N to n in the range for ϕ. For a full spherical helix, $n = N$ and for a truncated spherical helix $n < N$.

The antenna geometry must be inputted to ESP in cartesian coordinates. In addition, it is also more convenient to have the base of the sphere at the origin; this puts the feed point also at the origin. The following three equations, coupled with (3.2-5) and (3.2-6), provide the necessary spherical-to-cartesian transformation and also shift the base of the sphere to the origin (simply by adding the radius of the sphere, a, to the z-component).

$$x = a\sin\theta\cos\phi \tag{3.2-7}$$

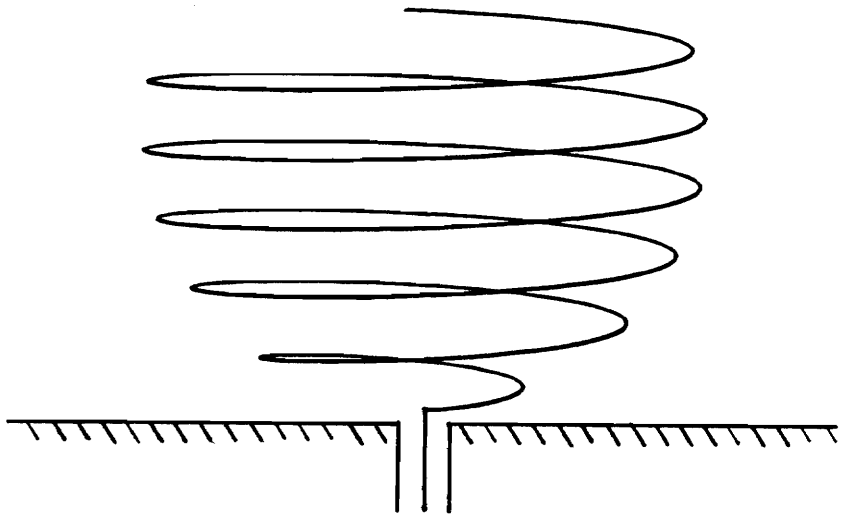

Figure 3.2-3. Truncated spherical helical antenna with 5.5 turns out of a possible 8 ($n = 5.5,\ N = 8$).

$$y = a \sin\theta \sin\phi \tag{3.2-8}$$

$$z = a \cos\theta + a \tag{3.2-9}$$

The ESP subroutine WGEOM was written to compute the data points for the spherical helix using (3.2-5) through (3.2-9) and is included and discussed in Appendix B.

4. Numerical Analysis of the Spherical Helical Antenna

The investigation of the spherical helix began with a numerical analysis of its radiation characteristics including pattern, polarization, and input impedance using the moment-method code ESP. The scope of this project was to examine how these characteristics are affected by the spherical circumference and the number of turns, the two parameters that completely define the spherical helix (see Chapter 3). Measurements were then made on the Virginia Tech antenna range in order to confirm the results of the numerical analysis. Details of construction and pattern measurements are given in Chapter 5. This chapter presents the results of the numerical analysis of the spherical helical antenna with ESP. The wire geometry of the spherical helix, as described in Section 3.2, is produced for ESP by the subroutine WGEOM which is listed in Appendix B.

Many different cases were investigated with ESP over a wide range of frequencies (by varying the frequency, the circumference of the sphere normalized to wavelengths was varied). The results for 3, 4, 5, 7, and 10-turn spherical helices were examined and compared. A few truncated geometries were investigated as well. In all of the cases, a spherical diameter of 3.7 centimeters was used and, according to the discussion in Section 3.2, the geometry of the full spherical helix is completely defined by the number of turns and diameter of the sphere.

As a starting point to the numerical analysis, it was assumed that the spherical helix would have some type of axial-mode behavior when its circumference was on the order of one wavelength as was the case for the cylindrical helix. The circumference of the sphere used here, 11.6 centimeters ($C = \pi D = 3.7\pi$), is equal to one wavelength at 2.6 GHz. A final frequency range of 1.8 GHz to 7.4 GHz (corresponding to normalized circumferences of: $0.67\,\lambda < C < 2.85\,\lambda$) with calculations every 0.4 GHz was chosen for the analysis because the spherical helix operates in two fairly stable modes over this range. Table 4-1 summarizes the range of variables for both the numerical and experimental investigations.

Table 4-1.

Range of Variables for the Investigation of the Spherical Helix.

Parameter	Value Range
• number of turns, N	$3 < N < 10$
• frequency, f	1.8 GHz $< f <$ 7.4 GHz
• circumference, C	$0.67\,\lambda < C < 2.85\,\lambda$

During the numerical analysis of the spherical helical antenna it was discovered that the number of turns has relatively little effect on its general performance; results from a 3-turn and a 10-turn spherical helix are remarkably similar. The number of turns on a conventional helical antenna has a significant impact on its behavior; Section 2.3.1 discussed how the helix becomes more directive as the number of turns is increased. The gain as well as some of the other characteristics of the spherical helix seem to be almost solely dependent upon the way the conductor is wrapped around a sphere. For this reason, it is only necessary to present a single set of standard results for the spherical helical antenna and, to this end, a 7-turn spherical helix was chosen to be discussed in Section 4.1 since it has roughly the median number of turns of all the spherical helices studied in this work. Section 4.2 highlights a few special cases where the spherical helix is

circularly polarized and Section 4.3 compares the spherical helix to a similarly-sized cylindrical helix.

4.1 A 7-Turn Spherical Helical Antenna

The numerical analysis of a 7-turn spherical helical antenna, like the one pictured in Figure 1-2, is presented in this section as a representative case for this new class of antennas. A square ground plane, .1 m on each side, was used and the straight-wire approximation used 20 segments per turn for a total of 140 segments. The structure, as "seen" by ESP, is shown in Figure 4.1-1.

The lowest frequency at which measurements are desired is 1.8 GHz where the circumference of the sphere is about 0.67 λ (approximately the lower limit of axial-mode operation for the cylindrical helix). At 1.8 GHz, a 0.1 meter square ground plane is 0.6 wavelengths in its smallest linear dimension which should be adequate for the spherical helix. (Recall, Section 2.3.1 stated that the ground plane for a helical antenna should be at least $\frac{1}{2}\lambda$ in diameter.) At higher frequencies it is electrically larger. Results were also generated for 7-turn spherical helices over ground planes larger than 0.1 m on each side and there was no significant difference between their radiation characteristics. For this reason and to cut down on the long computational time required for large ground planes, a 0.1 meter square ground plane is used for all the spherical helical antennas analyzed by ESP in this work.

The following four sections present the numerically computed radiation characteristics of a 7-turn spherical helix: far-field patterns, polarization, gain, and input impedance. As stated before, the results are nearly the same for all spherical helices between 3 and 10 turns, and it seems likely that with even more turns its behavior would not depart greatly from these results.

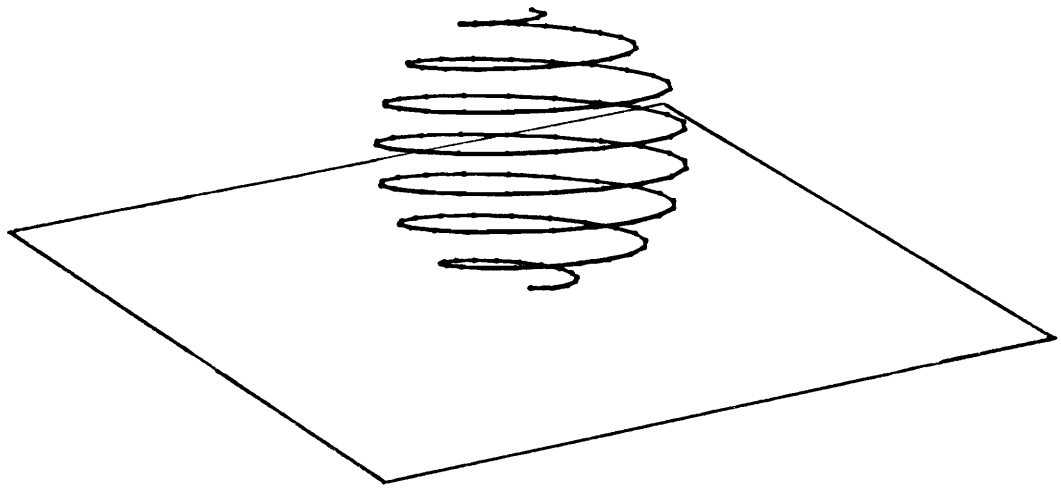

Figure 4.1-1. 7-turn spherical helix modeled with straight wire segments for input into ESP (140 total segments, 20 per turn). It is 3.7 centimeters in diameter and is mounted over a solid square ground plane, 0.1 m on each side.

4.1.1 Far-Field Patterns

Appendix C contains the computed far-field radiation plots for a 7-turn spherical helix over a frequency range from 1.8 GHz to 7.4 GHz, which corresponds to normalized circumferences of 0.67 λ and 2.85 λ. In part (a) of each figure, the gain of both far-field components in the x-z plane is plotted on a dB scale. The gain, given by G_θ and G_ϕ, is referenced to an isotropic linearly-polarized antenna. In part (b), the phase difference between the far-field components is plotted for the upper half-plane and will be discussed in Section 4.1.2.

The far-field patterns in Appendix C show that the spherical helix radiates in an axial mode over the approximate range of 0.75 λ to 2.0 λ (Figures C-2 through C-10). Other results, not shown in Appendix C, also indicate that it has a normal mode like the conventional helix similar to the pattern shown in Figure 2.1.1-2. The normal mode is not pursued further here because it is electrically small and therefore inefficient. The bandwidth ratio of the axial-mode pattern is:

$$\frac{f_u}{f_l} = \frac{\frac{C}{\lambda_u}}{\frac{C}{\lambda_l}} = \frac{2}{\frac{3}{4}} = \frac{8}{3} = 2.67 \qquad (4.1.1\text{-}1)$$

This value can be somewhat deceiving, however, because some of the other radiation characteristics of the spherical helix, like polarization and input impedance, vary significantly over this frequency range, as will be seen later.

The lower limit of the axial mode, 0.75 λ, is expected since this is also the lower limit of the axial-mode cylindrical helix as given by (2.1.2-1). The upper limit, 2.0 λ, is higher than that of the standard helix of 1.33 λ.

The patterns of both components in the axial mode are nearly equal in magnitude and have very large beamwidths. The 10 dB beamwidth, which is often used to characterize parabolic feeds, may be a more appropriate measure of this antenna's radiation pattern than the 3 dB beamwidth. The 10 dB beamwidth of the spherical helix is about 120° for both far-field components. The 3 dB beamwidths are about 60°. Unlike the conventional helix, the spherical helix does

not become more directive as the number of turns is increased. Figure 4.1.1-1 shows the far-field patterns for 3 and 10-turn spherical helices with circumferences of 1.5 λ. Comparing these two plots and Figure C-6, it is seen that the beamwidth does not decrease when more turns are added to the sphere.

Figure C-10 shows that as the circumference of the sphere increases to about 2 λ its broad beam pattern develops a null on the axis. This type of pattern is sometimes called a *bifurcated* pattern because it has two main lobes that branch off its axis. Figure C-15 shows that this type of radiation mode, referred to hereafter as the *axial-null mode*, is maintained up to a spherical circumference of about 2.8 λ. The behavior of this mode is somewhat similar to the behavior of the third radiation mode of the cylindrical helix which radiates a far-field pattern as shown in Figure 4.1.1-2. This helical mode also occurs when the circumference of the helix is 2 λ and like the bifurcated spherical helix pattern, there is a null on-axis [5].

The axial-null mode of the spherical helix arises due to phase cancellation of the fields along the axis. Figure 4.1.1-3 shows how this happens. The discussion is similar to that for the axial mode of the conventional helical antenna presented in Section 2.1.2. The current distribution is shown for turns that are near the equator of a spherical helix with a circumference of 2 λ. Halfway around each turn the phase goes through a complete cycle of 360° but since its direction is reversed 180° by the geometry of the wire, points opposite each other on a turn will be out of phase. The far-fields produced by each point will then destructively interfere with each other along the axis of the spherical helix.

It is worth noting that the on-axis null, as typified by Figure C-10, is much less sharper than that of the third order cylindrical-helical mode shown in Figure 4.1.1-2. This is due to the fact that the circumference of the individual turns on the spherical helix varies and gives each turn a slightly different frequency at which it produces a null on-axis. The varying circumference of each turn also contributes to the broad beam nature of the axial-mode spherical helix since each turn approaches a one-wavelength circumference at different frequencies. The spherical envelope taper also provides a larger bandwidth than the conventional helix. The bandwidth ratio of the axial-mode pattern of the spherical helix is 2.67 as compared to 1.78 for the standard helix (see equations (2.1.2-2) and (4.1.1-1)).

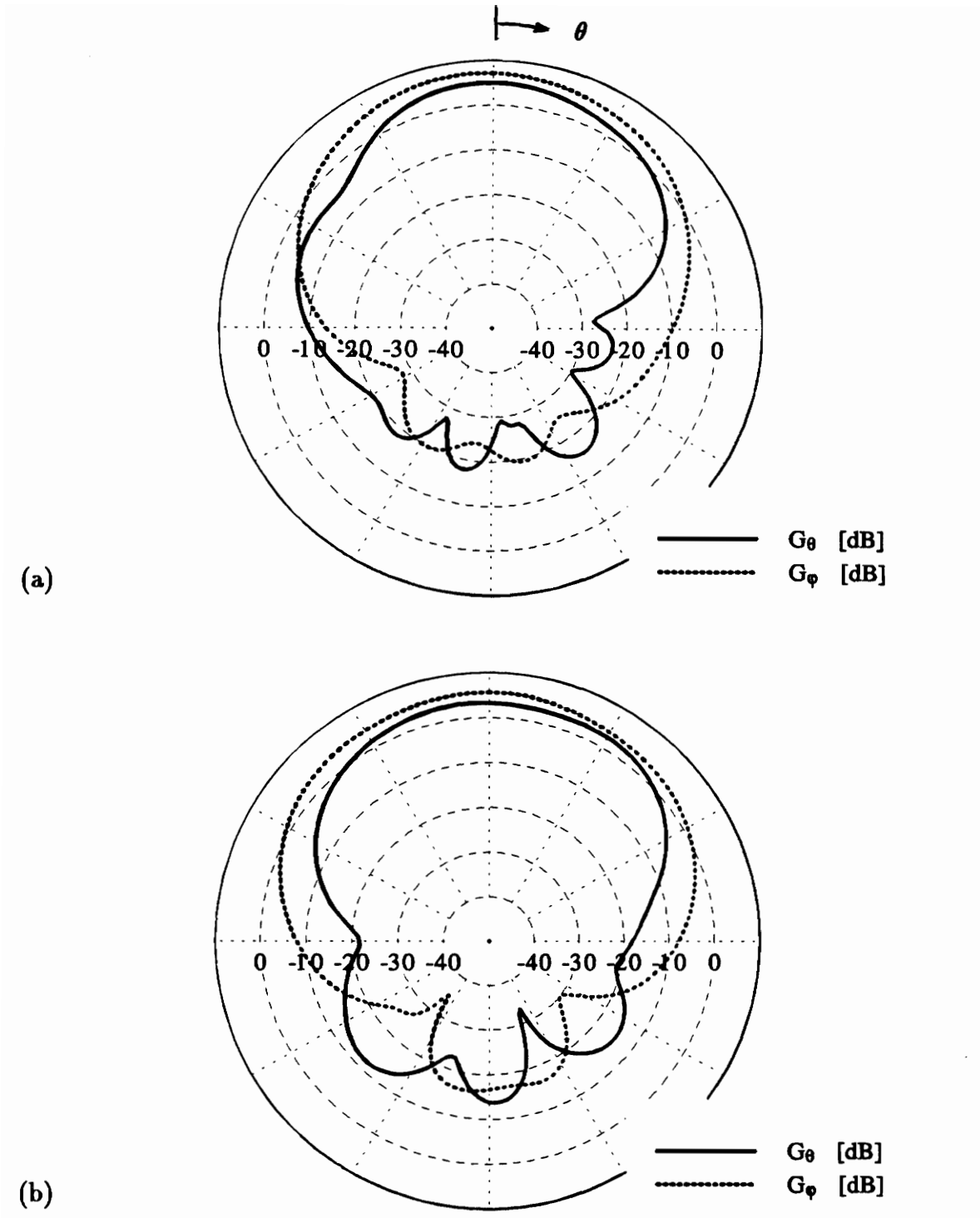

Figure 4.1.1-1. Computed far-field patterns in x-z plane for spherical helices 1.5 λ in diameter with (a) 3 turns and (b) 10 turns.

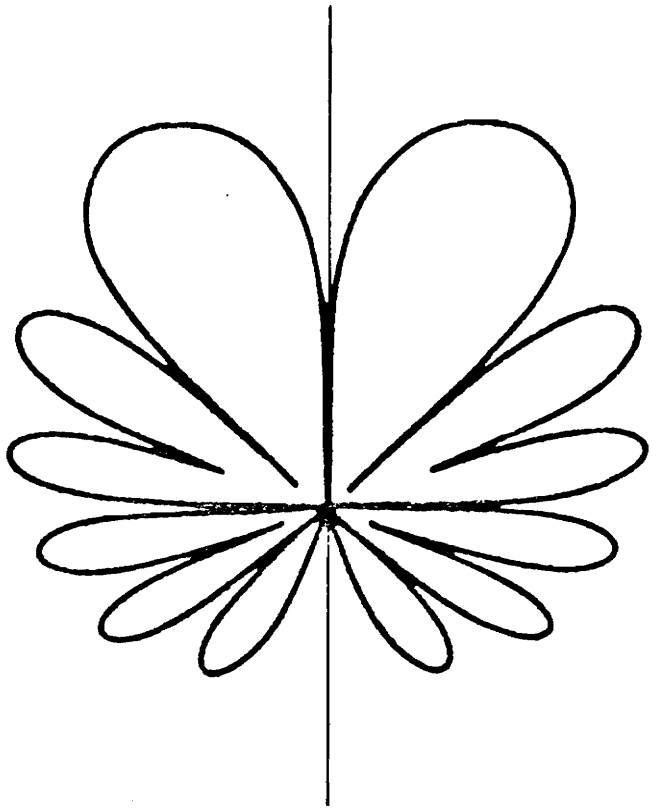

Figure 4.1.1-2. Far-field pattern of a cylindrical helix with a circumference of 2.0 λ [5].

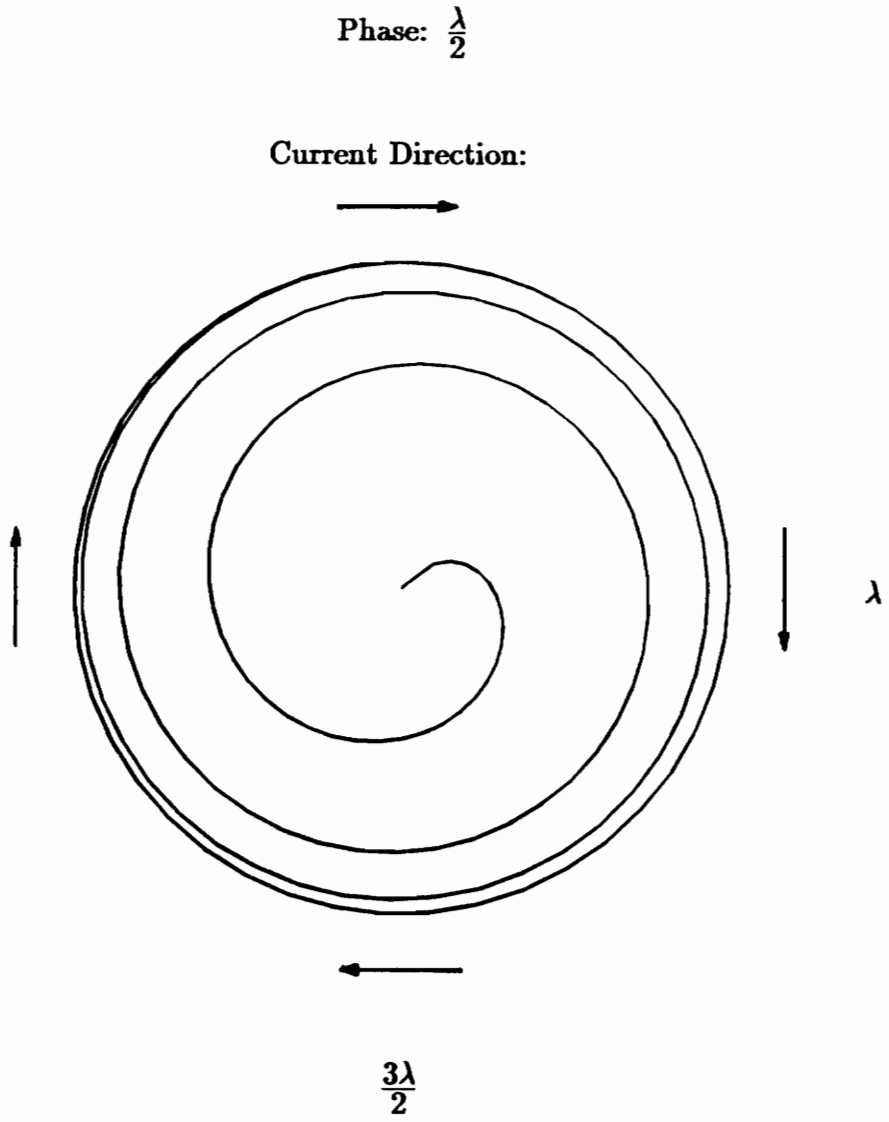

Figure 4.1.1-3. Top view of spherical helix with a circumference of $2\,\lambda$ showing how the current distribution on turns near the equator produces an on-axis null.

4.1.2 Polarization

The phase difference between the far-field components is plotted in part (b) of the figures in Appendix C, like they were in Figure 2.4.2-3 for the standard helix. It can be written explicitly as:

$$Phase\ Difference\ =\ \angle \boldsymbol{E}_{\theta}\ -\ \angle \boldsymbol{E}_{\phi} \qquad (4.1.2\text{-}1)$$

where $\angle \boldsymbol{E}_{\theta}$ and $\angle \boldsymbol{E}_{\phi}$ are the phases of the two electric-field components; they are computed by ESP. The phase difference between components coupled with their magnitudes (or gain as plotted in part (a) of the figures) describes the nature of the antenna's polarization.

The figures in Appendix C show that the phase difference fluctuates greatly with the frequency and angle θ. It also varies to some degree with the number of turns, though only a 7-turn case is shown here. In fact, of all the radiation characteristics of the spherical helix none seem to be more dependent on the number of turns than the phase difference between far-field components.

In general, the spherical helix is nonuniformly elliptically polarized. Although the magnitudes of the components are nearly equal over a wide frequency range, the phase difference between them does not stabilize at any given value. There are some special cases, however, where the phase difference approaches 90°, thereby giving rise to circular polarization. These will be discussed in Section 4.2.

The sense of the polarization of the spherical helix is determined the same way it was for the conventional helix. If it is wound in a right- (left-) handed sense then its polarization will also be right- (left-) hand sensed. The 7-turn spherical helix in Appendix C was wound in a right-hand sense by the subroutine WGEOM (see Appendix B). The phase difference, $\angle \boldsymbol{E}_{\theta} - \angle \boldsymbol{E}_{\phi}$, shows $\boldsymbol{E}_{\theta}$ to be leading $\boldsymbol{E}_{\phi}$ in most cases and by referring to the established coordinate system of Figure 2.2.1-1 it can be seen that the polarization is also right-hand sensed.

4.1.3 Gain

Appendix C shows the gain of both components, G_θ and G_ϕ, referenced to an isotropic linearly-polarized antenna as discussed in Section 4.1.1. It is also useful to find the total gain of the spherical helical antenna with respect to an isotropic circularly-polarized antenna. This can be achieved with the following expression [32]:

$$G = 10\ log(G_\theta + G_\phi) \quad [\mathrm{dB}_{ic}] \tag{4.1.3-1}$$

where G is gain in dB with respect to an isotropic circularly-polarized antenna and G_θ, G_ϕ is linear gain of G_θ,G_ϕ with respect to an isotropic linearly-polarized antenna as computed by ESP and shown in dB scale in Appendix C.

Figures 4.1.3-1a and 4.1.3-1b plot the gain as computed by (4.1.3-1) for the data in Figures C-6a and C-10a, respectively. These two cases are typical gain curves for all spherical helices operating in the axial and axial-null mode. In the axial mode, the gain is 9.5 dB along the axis (Figure 4.1.3-1a) and in the axial-null mode, the gain is about 7.3 dB on the main lobe peaks (Figure 4.1.3-1b). The 3 dB and 10 dB beamwidths for the axial mode are 64° and 111°, respectively. The 3 dB beamwidth for each main lobe of the axial-null mode is 33°.

As stated in Section 4.1.1, the number of turns of the spherical helix has little effect on the pattern and, hence, little effect on the gain as well. This is evident from Figure 4.1.1-1 which shows that both linear components of the gain are no greater with 10 turns than they are with 3 turns.

4.1.4 Input Impedance

The input impedance of the spherical helical antenna is complex, in general, and can be written as :

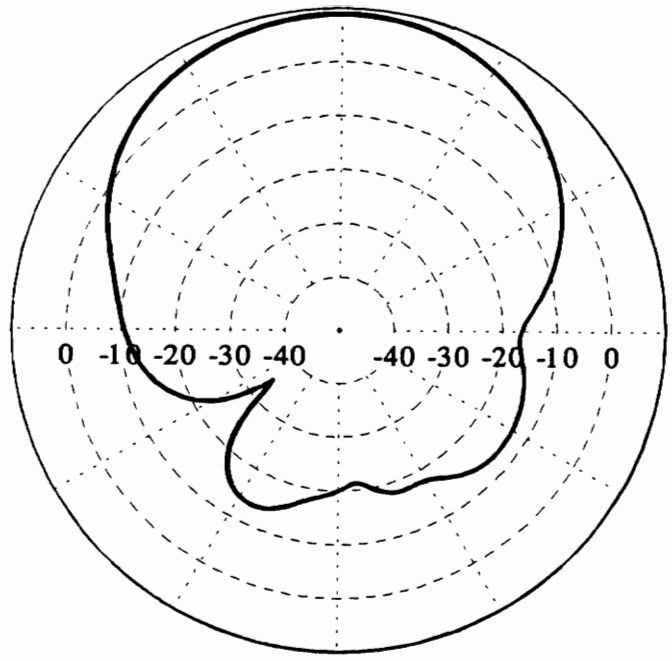

(a)

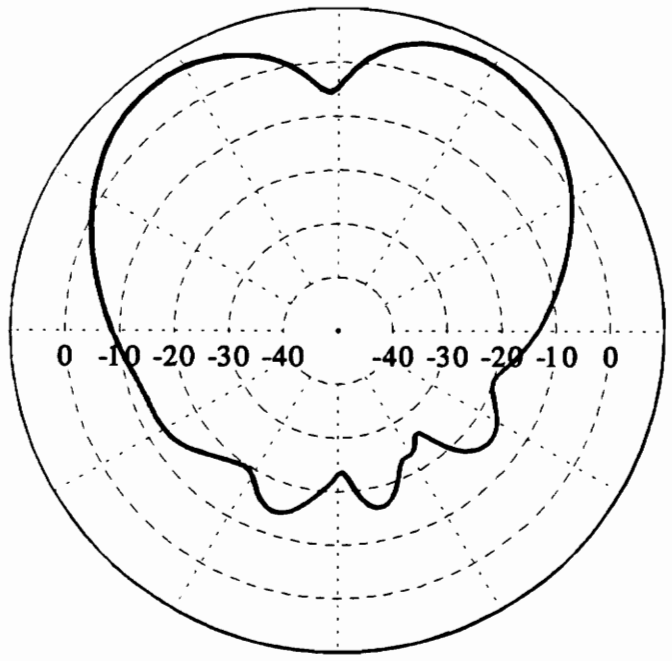

(b)

Figure 4.1.3-1. Gain with respect to a circularly-polarized isotropic antenna computed using ESP in the x-z plane for a 7-turn spherical helix with a circumference of (a) 1.46 λ and (b) 2.0 λ.

$$Z_{in} = R_{in} + jX_{in} \quad \text{[Ohms]} \tag{4.1.4-1}$$

One of the many advantages of the conventional helix is that its input impedance is almost purely real and does not change significantly in the axial mode of operation. This is due to the fact that the axial-mode helix is a traveling wave antenna as discussed in Section 2.1.2. Results for the spherical helix indicate that it is a resonant antenna and its input impedance is complex and varies significantly with frequency. Figure 4.1.4-1 plots the real and imaginary parts of the input impedance versus normalized circumference for the 7-turn spherical helix of Appendix C. The behavior of the input impedance in this figure is typical of all the spherical helices analyzed in this work. It is mostly reactive when it is electrically small ($\sim 0.7\,\lambda$), becomes oscillatory in the axial-mode region ($1.0\,\lambda$ - $2.0\,\lambda$), and levels off at approximately $70 - j50$ in the axial-null mode region ($2.0\,\lambda$ - $3.0\,\lambda$).

4.2 Special Cases of Circular Polarization

As discussed in Section 4.1.2, although the spherical helix is elliptically polarized, in general, there are some special cases where it is circularly polarized. Since circular polarization is often a very desirable property in antenna design an effort was made to find these cases.

4.2.1 Circular Polarization in the Axial-Null Mode

In the axial-null mode, particularly for a spherical circumference of about $2\,\lambda$, the phase difference between $\boldsymbol{E}_\theta$ and $\boldsymbol{E}_\phi$ is close to 90° on the main lobes for most spherical helices. This gives rise to a circularly-polarized bifurcated pattern

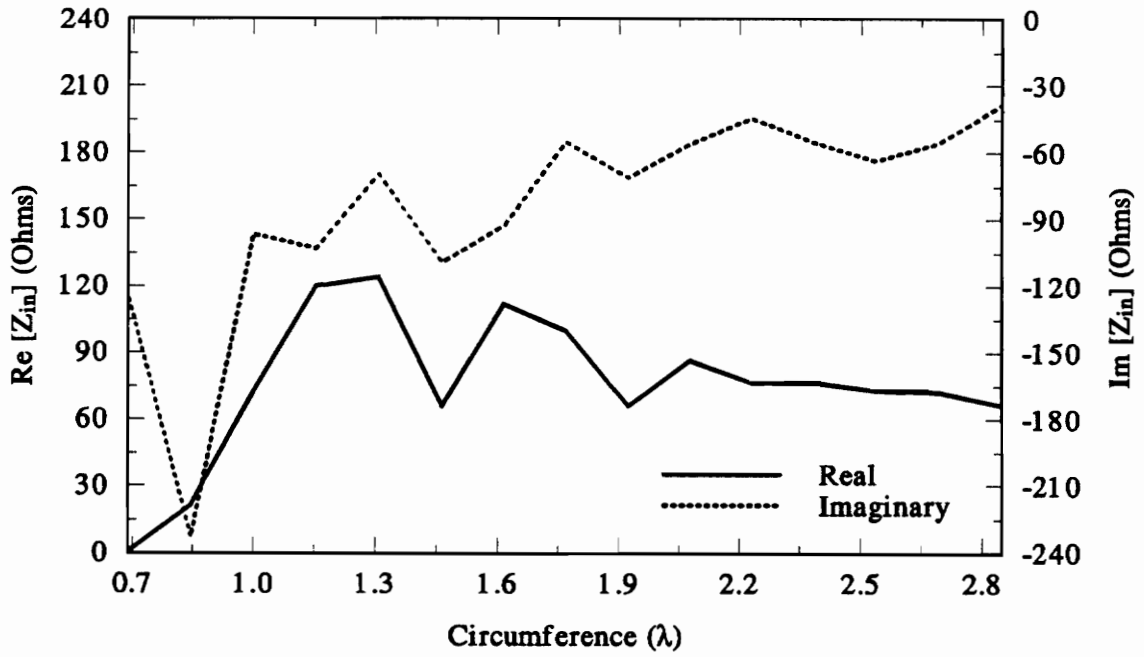

Figure 4.1.4-1. Input impedance versus normalized circumference computed using ESP for the 7-turn spherical helix in Appendix C.

since the magnitudes (or gain) of the components are nearly equal. An example of this occurrence is the 7-turn spherical helix with a circumference of 2.077 λ which is shown in Figure C-10. Both main lobes remain circularly polarized over a range of about 30° each, but not over a very wide bandwidth. Figures C-9 and C-11 show that the phase difference departs from 90° rather quickly as the frequency is changed. The bandwidth is about 400 MHz for a ping-pong ball sized spherical helix.

Due to the sensitivity of the phase difference to the number of turns not all of the spherical helices are close to circular polarization in the axial-null mode. Another example, however, is the 4-turn spherical helix with a circumference of 2.077 λ as shown in Figure 4.2.1-1. The circular polarization does not persist over a wide bandwidth in this case either.

4.2.2 Circular Polarization in the Axial-Mode

It was much more difficult to find any evidence of circular polarization in the axial-mode than it was in the axial-null mode because the phase difference between $\boldsymbol{E}_\theta$ and $\boldsymbol{E}_\phi$ fluctuates more unpredictably in the axial mode. Nevertheless, it was found that a 10-turn spherical helix with a circumference of 1.25 λ operates in the axial mode and is circularly polarized. Figure 4.2.2-1 shows the gain and phase difference of $\boldsymbol{E}_\theta$ and $\boldsymbol{E}_\phi$ for this special case. What is remarkable and potentially useful about this pattern is that it remains circularly polarized over a beamwidth of almost 120°. The conventional helical antenna does not maintain circular polarization off-axis, a drawback which has motivated researchers to look for ways of improving it. Tapered ends and feeds have proven somewhat successful in this regard [16] but no modification to the helix has yet produced circular polarization over an angle as large as that for this spherical helix. The limitation with this antenna, however, is the narrow bandwidth in which it operates this way. Results have shown that it stays circularly polarized only over a bandwidth of about 50 MHz for a spherical helix the size of a ping pong ball.

Another investigation revealed that a 4-turn spherical helix with a

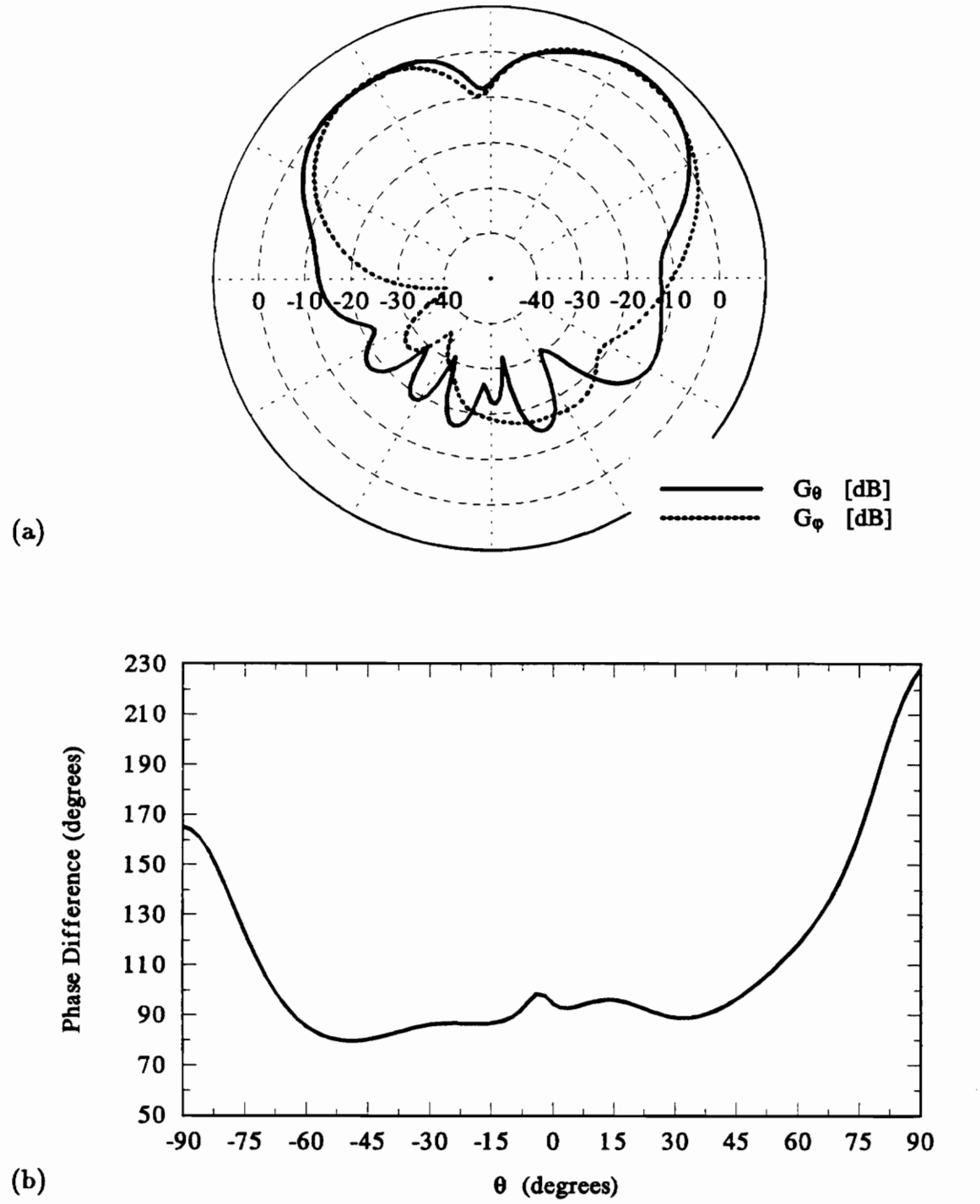

Figure 4.2.1-1. Computed far-field pattern in the x-z plane of a 4-turn spherical helical antenna with a circumference of 2.077 λ. (a) Gain of E_θ and E_ϕ with respect to an isotropic linearly-polarized antenna. (b) Phase difference between E_θ and E_ϕ.

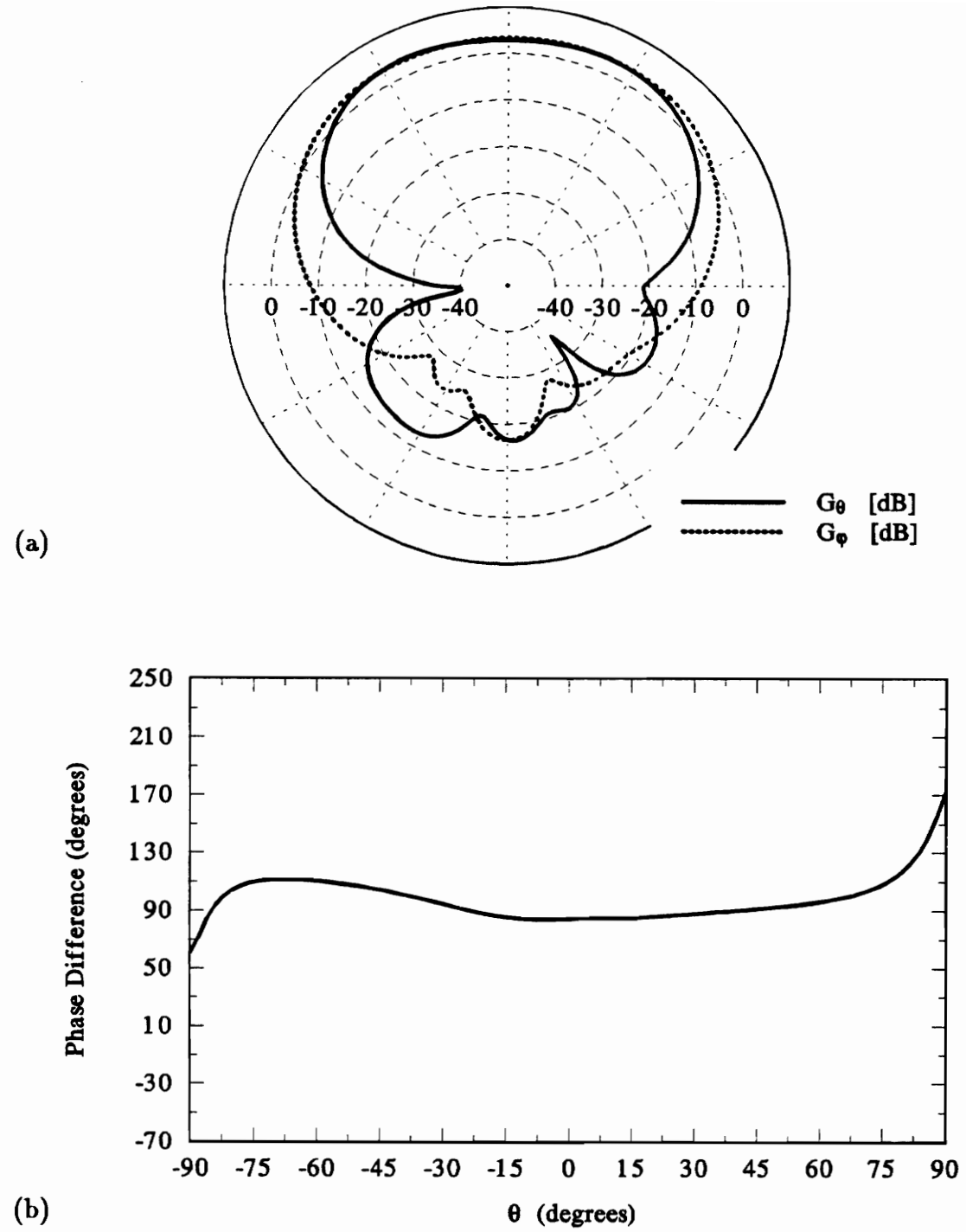

Figure 4.2.2-1. Computed far-field pattern in the x-z plane of a 10-turn spherical helical antenna with a circumference of 1.25 λ. (a) Gain of E_θ and E_ϕ with respect to an isotropic linearly-polarized antenna. (b) Phase difference between E_θ and E_ϕ.

circumference between $0.9\,\lambda$ and $1.6\,\lambda$ is nearly circularly polarized over a beamwidth slightly larger than 120°. A typical pattern for this case is shown in Figure 4.2.2-2 where the circumference of the spherical helix is $1.15\,\lambda$. Although the polarization is not as purely circular as it is for the 10-turn case due to slightly different field-component magnitudes, the bandwidth is much larger, about 800 MHz.

4.3 Comparison with a Standard Helix of Similar Physical Size

After observing the numerical results for the spherical helix it is obvious that this new antenna has radiation characteristics markedly different than the standard helix. This is due largely to the fact that a very low and variable pitch angle must be used in order to wind the helix on a sphere. This requirement has the advantage of making the spherical helical antenna an electrically-compact radiator as discussed in Chapter 3. It is much smaller than the conventional helix that has been so widely used and researched in the past and does not offer any improvement in the radiation characteristics of the axial mode.

In order to make a fair assessment of the spherical taper, a 5-turn spherical helix was compared to a 5-turn cylindrical helix of about the same physical size. The cylindrical helix was forced to occupy about the same physical volume as a ping pong ball (see introduction to Chapter 4 for the size of the spherical helix): the diameter was set to 3.7 centimeters and the pitch angle to 3.6° so that its axial length would also be 3.7 centimeters. The antenna would look something like the helix in Figure 1-1 except that it would be flattened such that its axial length was equal to its diameter. The results of this comparison are given in Figures 4.3-1 and 4.3-2 which show axial and axial-null mode patterns for the two antennas. Table 4.3-1 compares the radiation characteristics for the two antennas with normalized circumferences of $1\,\lambda$.

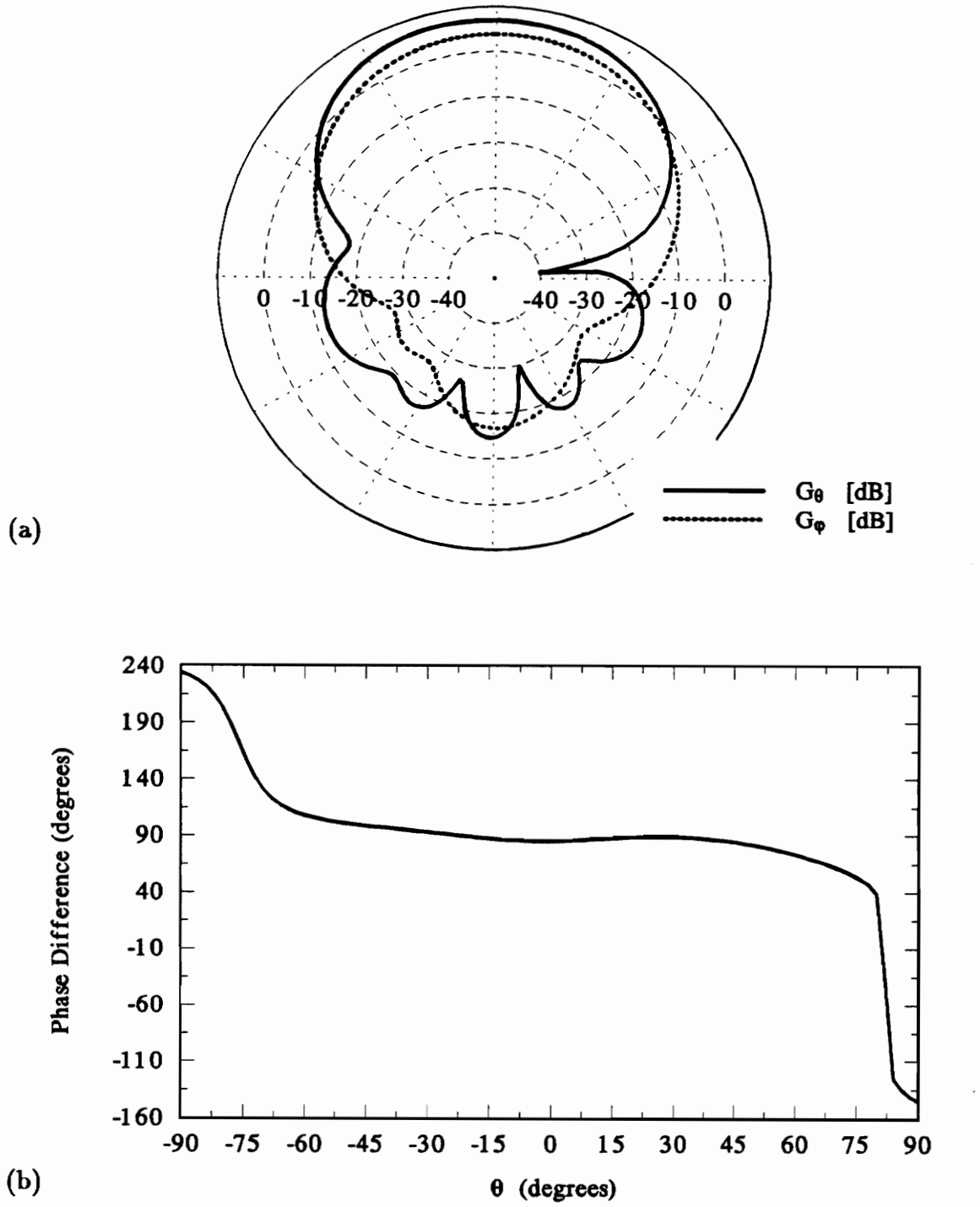

Figure 4.2.2-2. Computed far-field pattern in the x-z plane of a 4-turn spherical helical antenna with a circumference of 1.15 λ. (a) Gain of E_θ and E_ϕ with respect to an isotropic linearly-polarized antenna. (b) Phase difference between E_θ and E_ϕ.

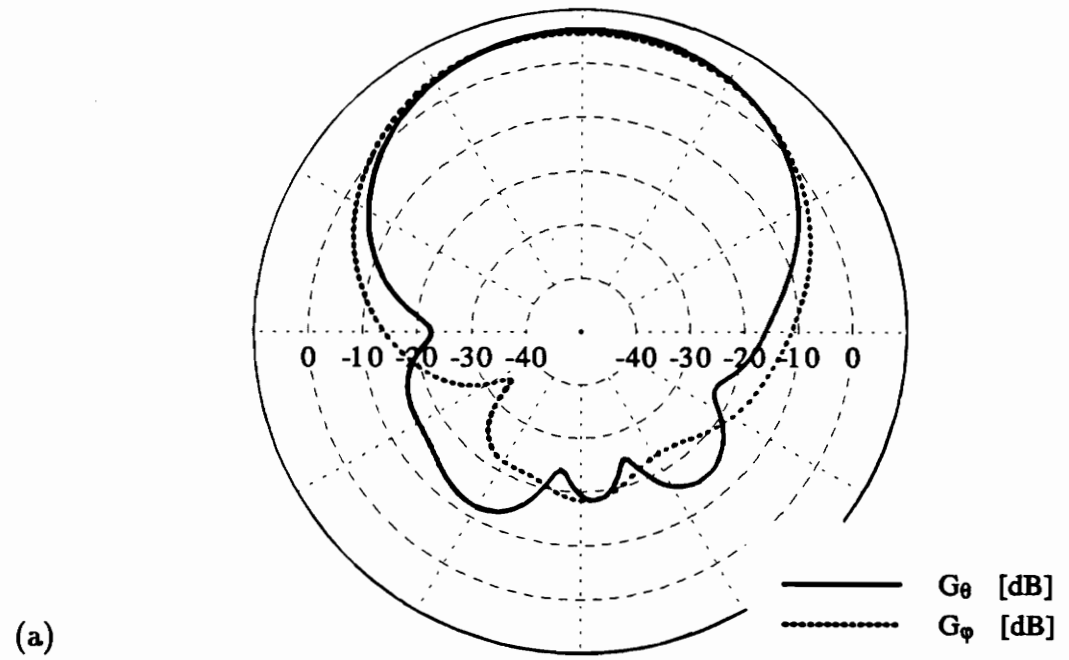

(a)

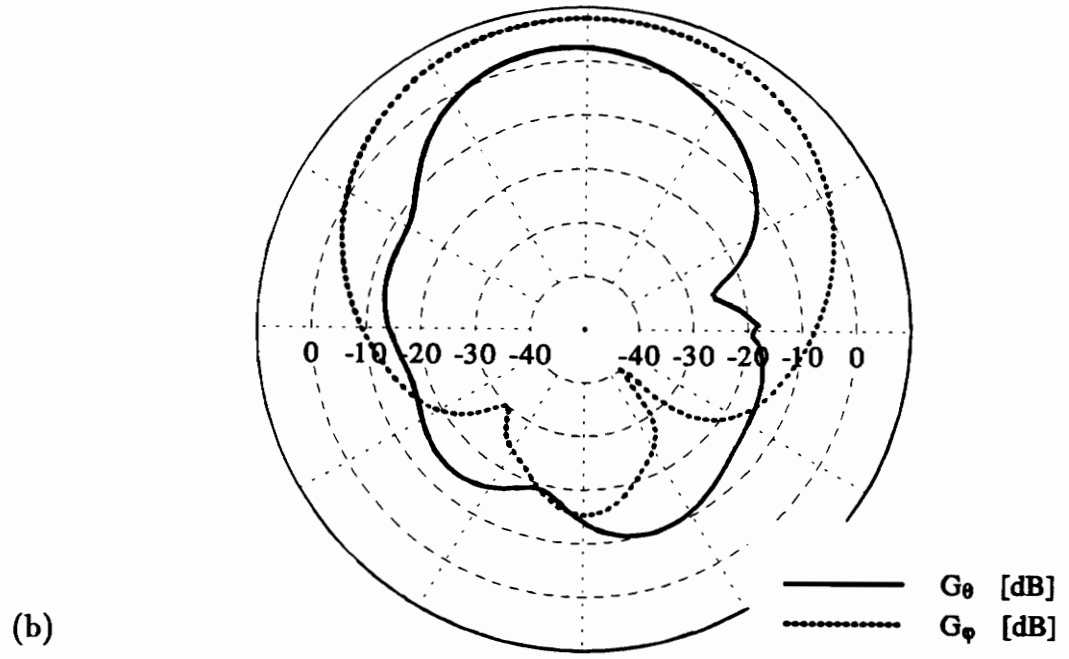

(b)

Figure 4.3-1. Computed far-field patterns in the x-z plane for a (a) 5-turn spherical helix and a (b) compact 5-turn cylindrical helix with circumferences of 1 λ. Both antennas occupy nearly the same volume.

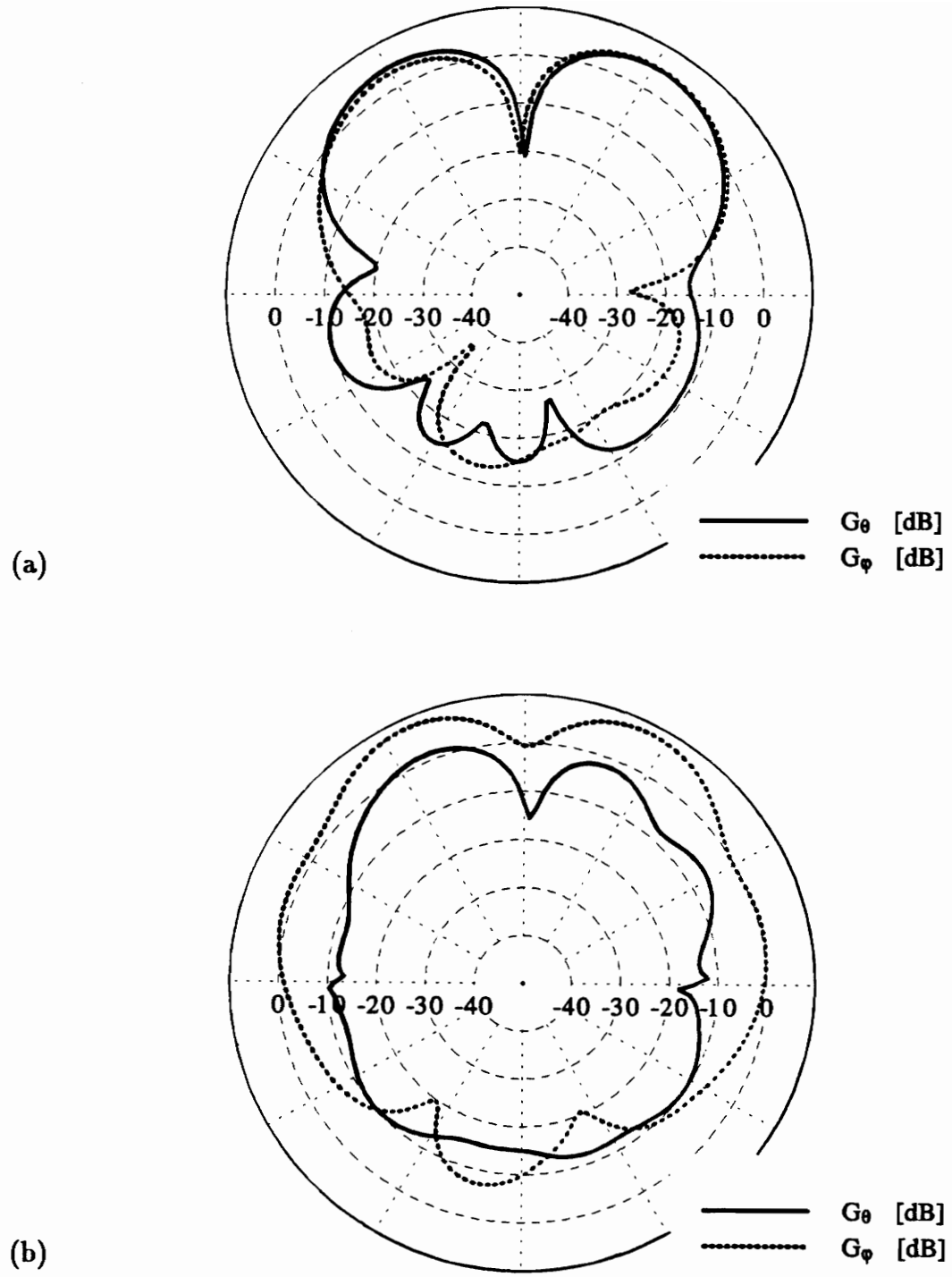

Figure 4.3-2. Computed far-field patterns in the x-z plane for a (a) 5-turn spherical helix and a (b) compact 5-turn cylindrical helix with circumferences of $2\,\lambda$. Both antennas occupy nearly the same volume.

Table 4.3-1.

Comparison of a 5-Turn Spherical Helix and a Compact 5-Turn Cylindrical Helix with Circumferences of 1 λ

Radiation Characteristic	Spherical Helix	Cylindrical Helix
• E_θ beamwidth (3 dB, 10 dB)	66.1°, 113.1°	44.3°, 88.8°
• E_ϕ beamwidth (3 dB, 10 dB)	75.2°, 128.5°	109.6°, 142.7°
• gain	9.3 dB_{ic}	9.4 dB_{ic}
• input impedance	$90.8 - j116.0$	$156.5 - j94.5$
• sidelobe level	~ -21.8 dB	~ -19.6 dB

For the cylindrical helix G_θ and G_ϕ differ by about 10 dB over the whole pattern in both modes whereas for the spherical helix they are nearly equal. This is an important difference making the spherical helix worthy of continued investigation since circular polarization is only achievable when the field components have equal magnitudes. Its compact size also makes it attractive for applications in which size is a factor.

5. Far-Field Measurements of the Spherical Helical Antenna

Several spherical helical antennas were constructed and tested on the Virginia Tech antenna range. Far-field measurements were taken over a wide range of frequencies and for both orthogonal components, E_θ and E_ϕ, for spherical helices with 4, 5, 7, and 10 turns. The results are presented in this chapter and compared to those generated numerically by ESP in Chapter 4. Section 5.1 will briefly describe how the antenna was constructed. Section 5.2 will present the measurements for the 7-turn spherical helix studied in Section 4.1 and Section 5.3 will focus on the results for the circularly-polarized cases studied in Section 4.2. Section 5.4 will conclude the chapter with measurements of an experimental spherical helix mounted in a spherical cavity.

5.1 Antenna Construction

The spherical helices tested in this work were built to conform as closely as possible to the way they were defined for the numerical analysis in Section 3.2.

The prototype was a 5-turn spherical helix wrapped around a ping-pong ball, which has a diameter of 3.7 centimeters. This is an appropriately-sized sphere because its desired operating range, 1.8 to 7.4 GHz ($0.69\,\lambda \leq C \leq 2.8\,\lambda$), falls well within the frequency range of the Virginia Tech Antenna Laboratory, 200 MHz to 28 GHz. This is why a 3.7 cm diameter spherical helix was used for the numerical analysis presented in Chapter 4.

Larger or smaller sized spheres could also be used so long as the normalized circumferences at which measurements are desired correspond to frequencies within the limits of the antenna range. To operate at higher frequencies, smaller spherical helices must be built. These were not constructed because it is difficult to wind wire around anything smaller than a ping-pong ball. Larger spherical helices were built, however, because they are easier to wind. Styrofoam balls, 10, 7.5 and 6 centimeters in diameter, proved useful for this purpose.

The first step in building a spherical helical antenna is finding two poles on the sphere, i.e., two directly opposite points on the surface. It is then useful to draw the equator and several equally-spaced longitudinal lines which make it easy to find the locations where the wire will pass through. Along the axis of the sphere, the spacing between turns ($s = \frac{D}{N}$) is equal, as discussed in Section 3.2. A contour gauge, which is basically a ruler that conforms to any curved surface, can be used to find the corresponding spacing on the surface of the sphere. The axial displacement of each turn is marked off on all of the longitudinal lines. Wire is then wound around the sphere from pole to pole so that each turn is just completed between adjacent demarcations on one of the longitudinal lines. The winding of all the spherical helical antennas in this work is right-hand sensed.

Superglue was originally used to adhere the wire to the spheres but some concern arose over its dielectric properties so masking tape, which is even easier to work with, was used instead. The dielectric constant of the spheres was also an important consideration. Ping-pong and styrofoam balls are good choices because they are composed mostly of air.

Finally, each spherical helix is mounted above a ground plane as was shown in Figure 1-2. It is fed with a coaxial cable, the center conductor being attached to the wire and the outer being attached to the ground plane. A practical

construction requirement is to slightly offset the spherical helix from the ground plane with a small (less than half a centimeter) straight wire segment in order to make a solid connection between the center conductor and the helix. This should not, however, have a significant effect on the far-field pattern.

Square and circular ground planes were tested. Both were made large enough so that they were at least $\frac{1}{2}\lambda$ wide at the lowest measured frequency. No significant difference was observed between patterns for the two in the upper half plane. Thus, the shape and size of the ground plane has relatively little effect on the behavior of the spherical helix as was the case for the conventional helix.

5.2 Measurements of a 7-turn Spherical Helix

The Virginia Tech antenna range was used to make far-field measurements of a 7-turn spherical helix at the same normalized circumferences as those used in the numerical analysis of Chapter 4. It is necessary to refer to normalized circumferences because a 10 cm diameter sphere was used for the actual measured spherical helix as opposed to the 3.7 cm diameter sphere used for the numerical calculations. Appendix D contains the measured patterns for the magnitude of both far-field components, E_θ and E_ϕ, corresponding to the ESP results in Appendix C. An attempt was made to take pattern cuts in the x-z plane as for the numerical results but there was some difficulty in aligning the antenna precisely. Nonetheless, numerical results show that the far-fields of the spherical helix are essentially symmetric about the z-axis so this did not pose too great a problem. The patterns of both components in Appendix D have been normalized to 0 dB.

There is some difficulty in measuring broad beam antennas such as the spherical helix on the antenna range due to reflections from a variety of metal surfaces. However, there is general agreement between the experimental results of Appendix D and the numerical results of Appendix C. At a circumference of 0.846 λ, Figure D-2 confirms with Figure C-2 that the spherical helix has begun to

operate in the axial mode and continues to do so up to a circumference of 2.077 λ, as shown in Figures D-10 and C-10. The experimental results also confirm that the spherical helical antenna is a broad beam radiator in this region with a 10 dB beamwidth of almost 120°. Sidelobe and back lobe radiation is generally 20 dB below the on-axis peak. This is an improvement over the standard helix which has a sidelobe level of about 10 dB (see Figure 2.4.2-2) and contributes to the relatively high gain of the spherical helix considering that it is a broad beam antenna. (A gain of 9.5 dB was computed in Section 4.1.3.)

Beyond 2 λ, there is less agreement between the measured and calculated patterns (Figures C,D-11 through C,D-15). Between 2 λ and 3λ, there is no observable on-axis null in the measured patterns although they do retain their general broad beam nature.

As an endnote to this general investigation, the spherical helical antenna does not appear to be affected by any similarity it may have to a spherical cavity. Initially, there was some concern that a spherical helix might store energy in the resonant modes of a spherical cavity but this does not seem to be happening. The lowest resonant frequency of a spherical cavity is from a Transverse Magnetic (TM) mode and is given by [33]:

$$f_r = \frac{2.744\ c}{C} \quad \text{Hz} \tag{5.2-1}$$

where c = speed of light
C = circumference of the sphere

Setting $f_r = \frac{c}{\lambda_r}$, this equation can be rearranged to:

$$C = 2.744\ \lambda_r \quad \text{m} \tag{5.2-2}$$

This is the normalized circumference of a spherical cavity at which the first resonant mode has appeared. A circumference of 2.744 λ occurs somewhere between those for the pattern measurements of Figures C,D-14 and C,D-15. Neither the numerically generated nor measured patterns seem to show any effect of a resonant cavity mode. Such an effect, if present, might be exhibited in the

input impedance of the spherical helix which was plotted in Figure 4.1.3-1. The imaginary or reactive part which represents stored power in the near field actually decreases after 2.7 λ. It is likely, however, that a cavity behavior will develop if the number of turns is increased such that the spacing between them becomes a small fraction of the wavelength.

5.3 Measurements of Circularly-Polarized Spherical Helical Antennas

Section 4.2 presented some special cases where spherical helices are circularly-polarized over a broad beamwidth. While it is not possible to measure the phases of the far-field components on the antenna range, it is possible to measure the relative difference between their magnitudes. The magnitudes of E_θ and E_ϕ must be equal for circular polarization. This section presents measurements for the two circularly-polarized (or nearly so) axial-mode spherical helices in Section 4.2.2.

Figure 5.3-1 shows the measured far-field of a 10-turn spherical helix with a circumference of 1.25 λ. The maximum of the E_ϕ pattern is normalized to 0 dB and E_θ is normalized relative to E_ϕ. An effort was made to avoid altering the gain of the test setup to allow comparison of component magnitudes. The measured patterns of the two components differ from each other only by about 2 dB and mimic each other almost exactly in the upper half-plane. Experimental error (interference, reflections, gain fluctuations, etc.) may have contributed to the difference between the components which are shown to be equal in the numerical predictions of Figure 4.2.2-1. Still, this antenna shows some promise as a narrowband broad beam circularly-polarized antenna.

Figure 5.3-2 shows the measured far-field pattern of a 4-turn spherical helix with a circumference of 1.154 λ. The numerically-computed patterns for this antenna were given in Figure 4.2.2-2 which showed it to be nearly circularly

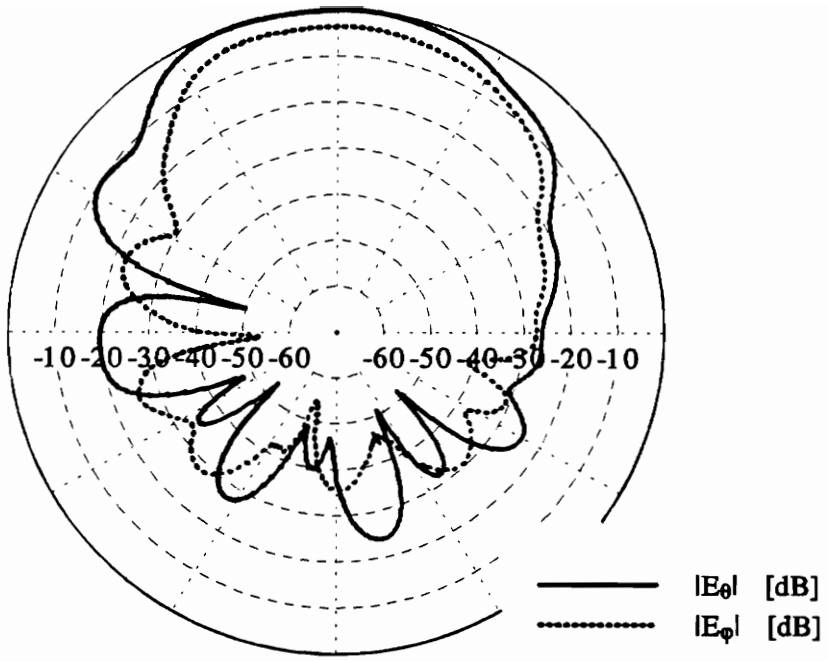

Figure 5.3-1. Measured far-field pattern of a 10-turn spherical helical antenna with a circumference of 1.25 λ.

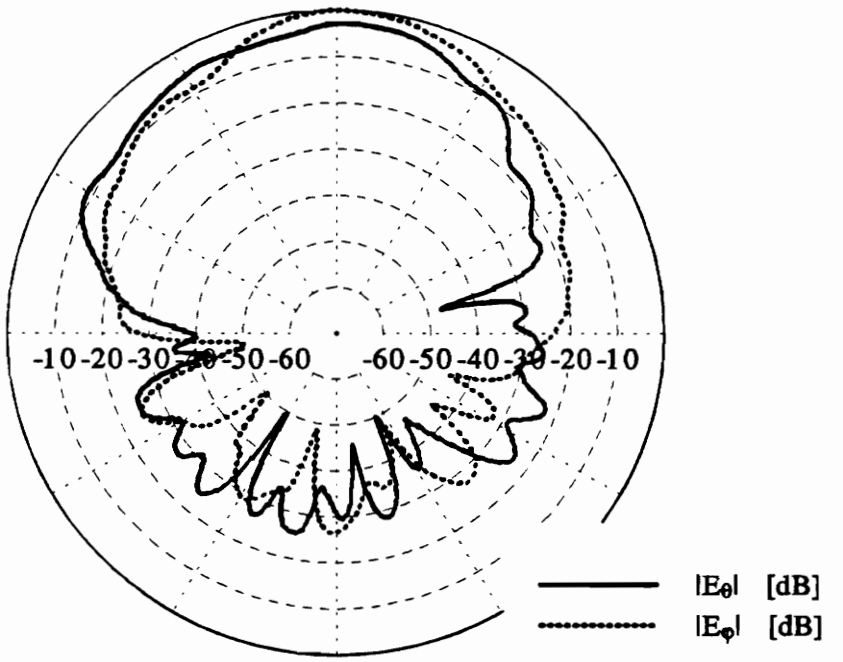

Figure 5.3-2. Measured far-field pattern of a 4-turn spherical helical antenna with a circumference of 1.154 λ.

polarized over a larger bandwidth than the previous 10-turn case. The measured results are in good agreement with the numerical calculations and allow some optimism for achieving circular polarization with the spherical helical antenna.

5.4 Measurements of a Spherical Helix Mounted in a Spherical Cavity

Cupped ground planes, as shown in Figures 2.3.1-7 and 2.6-1, have been used to cut down on unwanted modes and improve the gain of the standard helical antenna. Small elliptically-polarized helices have been used as antennas on high-speed aircraft mounted in cylindrical cavities flush with the surface of the plane [6]. Spherical helices mounted in spherical cavities may also be useful for this application since they are also physically compact.

It is very difficult to numerically model a spherical ground plane, even an approximate one, so the best way to evaluate this structure is through experimentation. Measurements were taken for a 4-turn spherical helix mounted in a spherical cavity as shown in Figure 5.4-1. The dimensions of the spherical cup and the placement of the spherical helix within it was rather arbitrarily chosen. Figure 5.4-2 compares the far-field patterns of this antenna with one over a flat ground plane. The results are promising and show that the axial mode of radiation is preserved with the spherical cavity.

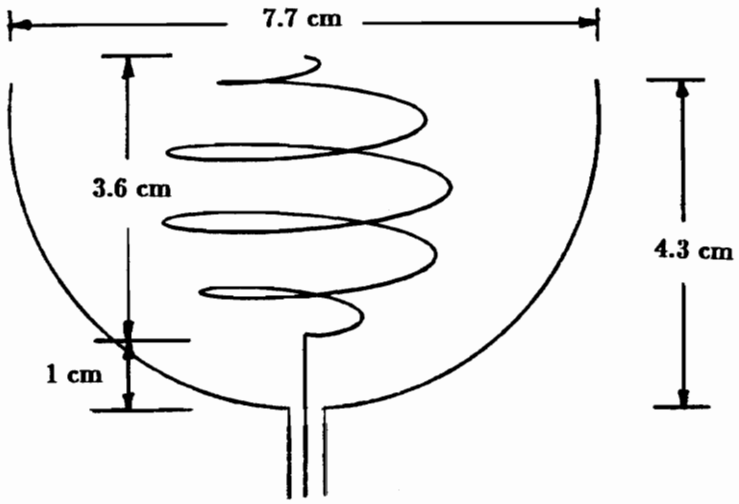

Figure 5.4-1. 4-turn spherical helix mounted in a spherical cavity.

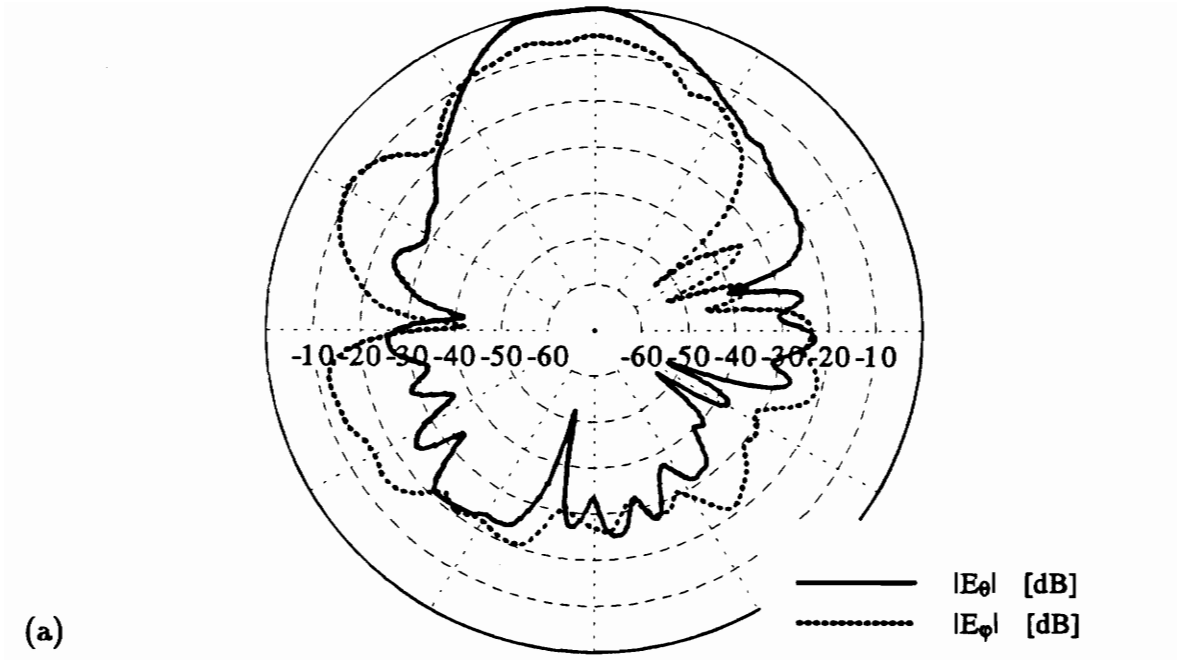

(a)

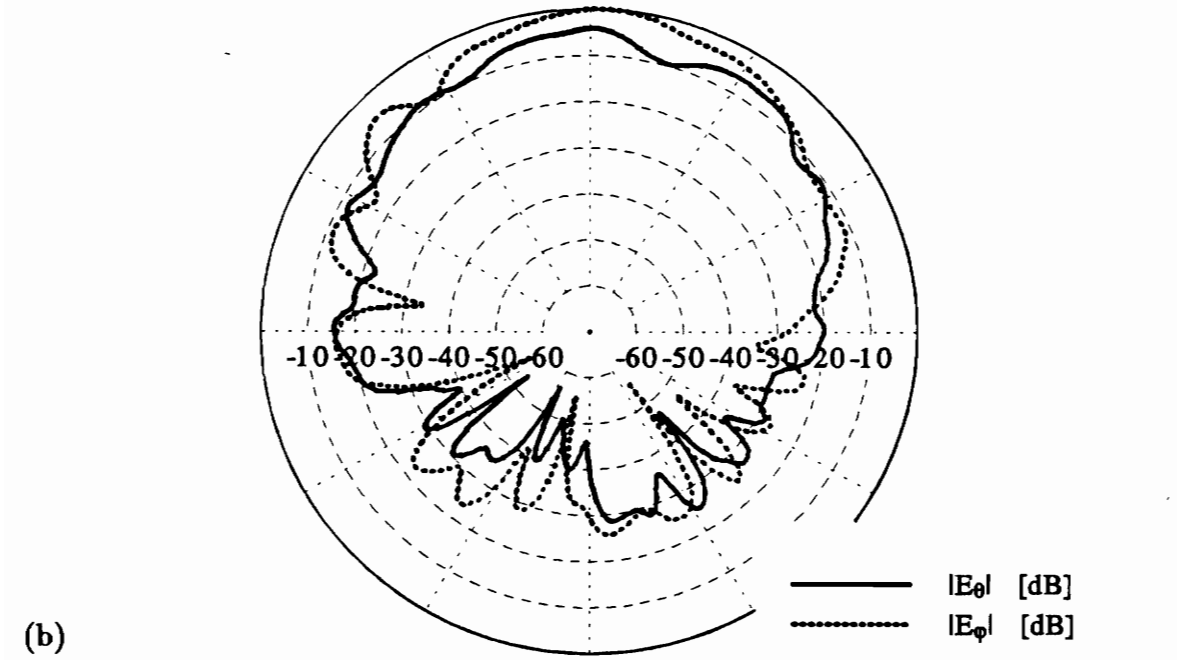

(b)

Figure 5.4-2. Measured far-field patterns for a 4-turn spherical helical antenna with a (a) square ground plane and a (b) spherical ground plane for a circumference of 1.308 λ.

6. Conclusions and Recommendations for Future Work

The spherical helical antenna was presented as a new variation of the well-established and widely-used cylindrical helical antenna. The wire antenna code ESP was used to analyze the structure because its complex geometry makes it difficult to develop even approximate analytic solutions for its behavior. Also, several spherical helices were built and tested in the Virginia Tech Antenna Laboratory. The experimental measurements and numerical predictions have yielded a general understanding of the spherical helical antenna and have also revealed certain conditions under which it is circularly polarized over a broad beamwidth. These results will be summarized in Section 6.1. Section 6.2 will offer suggestions for future work on the spherical helix.

As a final note, this investigation has been one in hundreds, perhaps thousands, of proposed modifications to the simple cylindrical helix first experimented with in 1946. Results from the spherical helix show that it has some unique properties which could be of interest in some applications. Chapter 2 presented an overview of the intensely-studied helical antenna and highlighted the remarkable properties that have given it a wide variety of applications: wide bandwidth, circular polarization, purely-resistive input impedance, etc.. Perhaps the truest testament to the value of the helical antenna is that it has stood up to 40 years of painstaking scrutiny, optimization, and modification and has remained

relatively unchanged from its original form. The spherical helix is markedly different from the cylindrical helix in many ways and is proposed not as an improvement to the helix but rather as a new wire antenna with its own distinct properties.

6.1 Summary of the Results

An extensive literature survey has revealed that the spherical helical antenna is, for the most part, a new antenna that has not been previously examined. There are some similarities to spherical radiators that have been studied in the past (Section 3.1) but the spherical helix as carefully defined in Section 3.2 is a unique structure. The following is a summary of its characteristics.

- The spherical helix is electrically small due to the fact that its axial length is equal to its diameter. A spherical helix operating at a frequency such that its circumference is 1 λ will have an axial length of 0.3 λ ($A = D = \frac{C}{\pi}$). A 10-turn cylindrical helix with a circumference of 1 λ and a pitch angle of 12.5° will have an axial length of 2.2 λ ($A = ns = nC\tan\alpha$). Thus, the spherical helix has the advantage over the cylindrical helix of being much smaller. Another result of its shape is that in order to wind several turns around a sphere the pitch angle must be low. (Section 3.2)

- All spherical helices seem to have the same general behavior (radiation patterns, polarization, input impedance, etc.) regardless of the number of turns. Their radiation characteristics are dependent upon the spherical envelope taper. (Chapter 4)

- The spherical helix has two radiation modes of interest, the so-called "axial" and "axial-null" modes. (Section 4.1.1)

- The axial mode operates over the approximate range: $0.75\lambda \leq C \leq 2.0\lambda$. The magnitudes of the components, E_θ and E_ϕ, are nearly equal, in general, and have large beamwidths; the 3 dB and 10 dB beamwidths are typically about 60° and 110° respectively. The on-axis gain is about 9 dB and the sidelobe and back lobe levels are about 20 dB below the peak. Polarization varies considerably over angle and frequency and is elliptical in general. (Section 4.1)

- The axial-null mode operates over the approximate range: $2.0\,\lambda \leq C \leq 2.8\,\lambda$. E_θ and E_ϕ are equal, in general, and have about a 10 dB null on-axis. The two main lobes have a maximum gain of about 7 dB and halfpower beamwidths of about 33°. The polarization is close to circular for $C = 2.0\,\lambda$ and is non-uniformly elliptical in general. (Section 4.1)

- The input impedance is complex since the spherical helix behaves more like a resonant antenna than a travelling-wave antenna and is not affected to any large degree by the number of turns. It oscillates in the axial mode but stabilizes at approximately $70 - j50$ in the axial-null mode. (Section 4.1.4)

- Under certain circumstances, the spherical helix is circularly polarized over a broad beamwidth but only over a narrow bandwidth. Experimental results seem to confirm this. (Section 4.2)

- Comparison with a comparably-sized cylindrical helix shows that equal magnitudes for E_θ and E_ϕ are possibly unique to the spherical helical geometry. This gives promise for finding and optimizing cases of circular polarization. (Section 4.3)

6.2 Recommendations for Future Work

During the course of this investigation, many choices had to be made as to which direction the work was going to proceed. Many avenues are yet to be explored. The following is a list of suggestions and modifications for future study of the spherical helix that could help to optimize its radiation characteristics.

- **Circular Polarization.** Circular polarization over a wide beamwidth has been achieved with the spherical helix but only over a narrow bandwidth. There may be some configurations in which it is circularly polarized over a wider bandwidth. It would be helpful to know what mechanism makes the 10-turn spherical helix circularly polarized for a circumference of almost exactly $1\frac{1}{4}\lambda$ (Section 4.2.2).

- **Truncated spherical helix.** A few of these cases were tried with ESP but no improvements were made over the full spherical helix. The subroutine WGEOM in Appendix B is capable of generating these geometries (Section 3.2). Perhaps using many more turns, say 10 to 30, would yield better results.

- **Different Winding.** The spherical helix as defined in Section 3.2 has a constant axial spacing between turns. This causes the turns to be somewhat "bunched up" near the equator and spread apart near the poles. It may be beneficial to redefine the spherical helix so that it has a constant pitch angle (low) which would make more use of the spherical surface.

- **Spherical Cavity Mount.** The spherical helix mounted in a spherical cavity was presented in Section 5.4 as a small elliptically-polarized antenna with promising applications. Further experimental results are needed to fully evaluate the usefulness of this structure and determine optimal dimensions for the spherical cavity.

REFERENCES

1. J. D. Kraus, *Antennas*, 2nd ed., McGraw Hill: New York, 1988.

2. A. Safaai-Jazi, Professor of Electrical Engineering, Virginia Tech, Personal discussion, May 1990 through August 1992.

3. R. E. Collin, *Field Theory of Guided Waves*, McGraw-Hill: New York, 1960.

4. W. L. Stutzman and G. A. Thiele, *Antenna Theory and Design*, John Wiley and Sons: New York, 1981.

5. T. A. Milligan, *Modern Antenna Design*, McGraw Hill: New York, 1985.

6. A. Bystrom, Jr. and D. G. Berntsen, "An experimental investigation of cavity-mounted helical antennas," *IRE Trans. Antennas Propagat.*, vol. AP-4, pp. 53-58, January 1956.

7. H. E. King and J. L. Wong, "Characteristics of 1 to 8 wavelength uniform helical antennas," *IEEE Trans. Antennas Propagat.*, vol. AP-28, pp. 291-296, 1980.

8. H. Nakano, *Helical and Spiral Antennas - A Numerical Approach*, Research Studies Press: New York, 1987.

9. N. D. Fox, "A detailed analysis of the helical array as a high performance portable ground station antenna," Master's Thesis, Virginia Tech, 1988.

10. T. E. Tice and J. D. Kraus, "The influence of conductor size on the properties of helical beam antennas," *Proc. Inst. Elec. Eng.*, p. 1296, November 1949.

11. J. L. Wong and H. E. King, "Broadband quasi-taper helical antennas," *IEEE Trans. Antennas Propagat.*, vol. AP-27, pp. 72-78, January 1979.

12. K. F. Lee and P. F. Wong, "Directivities of helical antennas radiating in the axial mode," *Proc. Inst. Elec. Eng.*, pp. 121-122, April 1984.

13. J. L. Wong and H. E. King, "Empirical helix antenna design," *Proc. IEEE Antennas Propagat. Int. Symp.*, pp. 366-368, 1982.

14. T. S. M. Maclean and R. G. Kouyoumjian, "The bandwidth of helical antennas," *IRE Trans. Antennas Propagat.*, pp. 379-386, December 1959.

15. R. G. Vaughan and J. B. Andersen, "Polarization properties of the axial mode helix antenna," *IEEE Trans. Antennas Propagat.*, vol. AP-33, pp. 10-20, January 1985.

16. U. R. Kraft and G. Mönich, "Main-beam polarization properties of modified helical antennas," *IEEE Trans. Antennas Propagat.*, vol. AP-38, pp. 589-592, May 1990.

17. E. H. Newman and R. L. Dilsavor, *A User's Manual for the Electromagnetic Surface Patch Code: ESP Version III*, The Ohio State University, ElectroScience Laboratory, NASA Technical Report No. 716148-19, May 1987.

18. Poggio, Bevensee, and Miller, "Evaluation of some thin wire computer programs," *IEEE Antennas Propagat. Int. Symp. Dig.*, Atlanta, Ga., pp. 181-184, 1974.

19. D. F. Kelley, "Analysis of phased array antenna radiation patterns including mutual coupling," Master's Thesis, Virginia Tech, November 1990.

20. A. R. Djordjević, et al, *Analysis of Wire Antennas and Scatterers: Software and User's Manual*, Artech House: Norwood, Ma., 1990.

21. H. Nakano, J. Yamauchi, and Y. Samada, "Power gain of helical antenna," *Fourth Int. Conf. Antennas Propagat.*," pp. 127-130, April 1985.

22. H. E. King and J. L. Wong, "240-400 MHz antenna system for the fleetsatcom satellites," *Proc. IEEE Antennas Propagat. Int. Symp.*, pp. 349-352, 1977.

23. Y. T. Lo and S. W. Lee, *Antenna Handbook*, van Nostrand Reinhold: New York, 1988.

24. K. K. Mei and M. Meyer, "Solutions to spherical anisotropic antennas," *IEEE Trans. Antennas Propagat.*, vol. AP-12, pp. 459-463, July 1964.

25. Atia and Mei, "Characteristics of a spherical spiral satellite antenna," *Program and Abstracts of the URSI 1969 Spring Meeting*, Washington, D. C., pp. 67-68, April 21-24, 1969.

26. C. H. Chen, "A combination of synthesis and analysis approaches to the spherical antenna with anisotropic surfaces," *Int. Symp. Antennas Propagat. - Summaries of Papers*, Sendai, Japan, pp. 179-180, September 1-3, 1971.

27. B. R. -S. Cheo, V. H. Rumsey, and W. J. Welch, "A solution to the frequency-independent antenna problem," *IRE Trans. Antennas Propagat.*, vol. AP-9, pp. 527-534, November 1961.

28. H. B. Riblet, "A broad-band spherical satellite antenna," *Proc. Inst. Radio Eng.*, pp. 631-635, April 1960.

29. H. P. Williams, *Antenna Theory and Design, Vol. 2 - The Electrical Design of Antennae*, Sir Isaac Pitman and Sons: London, 1968.

30. J. S. Chatterjee, "Radiation field of a conical helix," *J. Appl. Phys.*, vol. 24, pp. 550-559, May 1953.

31. N. P. Timirev, "Radiation from half-ellipsoid helical antennas," *Telecommun. and Radio Eng.*, vol. 30, pt. 1, March 1976.

32. IEEE Antenna Standards Committee, *IEEE Standard Test Procedures for Antennas*, IEEE, 1979.

33. C. A. Balanis, *Advanced Engineering Electromagnetics*, John Wiley: New York, 1989.

Appendix A. Subroutine WGEOM for Helices

The Fortran source code is presented for the ESP subroutine WGEOM that was used to produce the geometry of the cylindrical helix as outlined in Section 2.4.2. The ESP User's Manual [18] contains a full explanation of how to define the geometry of a wire antenna with a subroutine and integrate it with the main program. WGEOM is very useful because it allows the user to change the parameters of the wire structure without having to recompile the program.

The five READ statements in the subprogram accept the input parameters for the cylindrical helix. They are:

- **NSEGHEL** - Number of segments on the helix. This parameter determines how many straight-wire segments will approximate the helix.

- **ZOFFSET** - Distance helix is offset from ground plane in meters. This parameter was used to make the first segment between the coaxial input and the helix form an angle α (equal to the pitch angle of the helix) with the ground plane for the helix studied in Section 2.4.2.

- **NTURNS** - Number of turns of the helix.

- **PITCHANG** - Pitch angle, α, of the helix in degrees.

- **HELRAD** - Radius of the helix in meters.

As an example, the input file for the computation of the 6-turn, 14° helical geometry of Section 2.4.2 and shown in Figure 2.4.2-1 is given below. This data can be included at the end of the input for the READ statements in ESP (carefully outlined in [18]).

```
120
0.029
6.
14.
0.11625
```

The subroutine, WGEOM, for the cylindrical helix is listed below.

```
C*********************************************************************
C*
C*                SUBROUTINE WGEOM - Cylindrical Helix
C*
C*         Computes the wire geometry for a cylindrical helix
C*      approximated by straight wire segments for input to ESP
C*                    see Chapter 3 of Reference [18]
C*
C*********************************************************************
C
C234567
      SUBROUTINE WGEOM(IA,IB,X,Y,Z,NM,NP,NAT,NSA,NPLA,VGA,BDSK,ZLDA,
     +NWG,VG,ZLD,WV,NFS1,NFS2,NRUN,A)
      DIMENSION IA(1),IB(1),X(1),Y(1),Z(1),
     +NSA(1),NPLA(1),BDSK(1)
      COMPLEX VGA(1),ZLDA(1),VG(1),ZLD(1)
      REAL PIE, HELRAD, NTURNS, PITCHANG
C
C
C  Total number of wire segments desired on helix, NSEGHEL
      READ(5,*)NSEGHEL
C
C  Distance helix will be offset from ground plane, ZOFFSET [meters]
      READ(5,*)ZOFFSET
C
C  Total number of wire segments, NM (definition required by ESP)
      NM = NSEGHEL + 1
```

```
C
C  Total number of wire points, NP (definition required by ESP)
      NP = NM + 1
C
C  Total number of wire attachment points, NAT (one wire is
C  attached to the square plate making the ground plane - definition
C  required by ESP)
      NAT = 1
C
C  Number of turns of helix, NTURNS
      READ(5,*)NTURNS
C
C  Pitch angle of helix, PITCHANG [degrees]
      READ(5,*)PITCHANG
C
C  Radius of helix (half the diameter), HELRAD [meters]
      READ(5,*)HELRAD
C
      PIE = 3.1415927
C
C  Convert pitch angle from degrees to radians
      PITCHANG = PITCHANG*PIE/180.
C
C  SEGPHI is the change in the angle phi (radians) over each segment
      SEGPHI = 2.0*PIE*NTURNS/REAL(NSEGHEL)
C
C  Coordinates of first wire point, the origin (required by ESP)
      X(1) = 0.0
      Y(1) = 0.0
      Z(1) = 0.0
C
C  Nodes of the first segment
      IA(1) = 1
      IB(1) = 2
C
C
C  Coordinates of the rest of the wire points and nodes.
C
      DO 100 J = 2,NP
        PHI = SEGPHI*REAL(J-2)
        X(J) = HELRAD*COS(PHI)
        Y(J) = HELRAD*SIN(PHI)
        Z(J) = HELRAD*TAN(PITCHANG)*PHI + ZOFFSET
          IF (J .EQ. NP) GOTO 100
        IA(J) = J
        IB(J) = J+1
  100 CONTINUE
C
C
C  Check that smallest segment is greater than twice the wire radius
C  (otherwise ESP results may be invalid - see ESP manual)
```

```
C
      SLENGTH = SQRT( (X(NP)-X(NP-1))**2 + (Y(NP)-Y(NP-1))**2 +
     +          (Z(NP)-Z(NP-1))**2 )
C
      IF (SLENGTH .LE. A*2.) WRITE(*,*)'   WARNING - At least one
     +segment is smaller than twice the wire radius'
C
C
C  Following inputs are required by ESP:
C
C  Wire "location" of attachment point, NSA
      NSA(1) = 1
C
C  Plate number geometry is attached to, NPLA
      NPLA(1) = 1
C
C  Complex voltage generator, VGA
      VGA(1) = (1.0,0.0)
C
C  Outer disk radius of disk monopole (should be about .2
C  wavelengths lambda), BDSK
      BDSK(1) = 0.2*WV
C
C
      RETURN
      END
```

Appendix B. Subroutine WGEOM for Spherical Helices

The Fortran source code is presented for the ESP subroutine WGEOM that was used to produce the geometry of the spherical helix as outlined in Section 3.2. The ESP User's Manual [18] contains a full explanation of how to define the geometry of a wire antenna with a subroutine and integrate it with the main program. WGEOM is very useful because it allows the user to change the parameters of the wire structure without having to recompile the program.

The five READ statements in the subprogram below accept the input parameters for the spherical helix. They are:

- **NSEGSP** - Number of segments on the spherical helix. This parameter determines how many straight-wire segments will approximate the spherical helix.

- **ZOFFSET** - Distance spherical helix is offset from ground plane in meters. This parameter was set to zero for all of the spherical helices analyzed in this work but is included as an option for future work.

- **NTOTAL** - Total number of turns spherical helix would have if completely wound around sphere (labeled N in Section 3.2).

- **NACT** - Actual number of turns of spherical helix. This parameter provides a way to define truncated spherical helices as discussed in Section 3.2. For all of the cases presented in this work, NACT = NTOTAL.

- **AS** - Radius of sphere in meters.

As an example, the input file for the computation of the 7-turn spherical helical geometry of Section 4.1 and shown in Figure 4.1-1 is given below. This data can be included at the end of the input for the READ statements in ESP (carefully outlined in [18]).

```
140
0.0
7
7
0.018364
```

The subroutine, WGEOM, for the spherical helix is listed below.

```
C***********************************************************************
C*
C*                SUBROUTINE WGEOM - Spherical Helix
C*
C*         Computes the wire geometry for a spherical helix
C*      approximated by straight wire segments for input to ESP
C*                   see Chapter 3 of Reference [18]
C*
C***********************************************************************
C
C234567
      SUBROUTINE WGEOM(IA,IB,X,Y,Z,NM,NP,NAT,NSA,NPLA,VGA,BDSK,ZLDA,
     +NWG,VG,ZLD,WV,NFS1,NFS2,NRUN,A)
      DIMENSION IA(1),IB(1),X(1),Y(1),Z(1),
     +NSA(1),NPLA(1),BDSK(1)
      COMPLEX VGA(1),ZLDA(1),VG(1),ZLD(1)
      REAL PIE, AS, NTOTAL, NACT
C
C
C  Total number of wire segments approximating spherical helix,
C  NSEGSP
      READ(5,*)NSEGSP
C
C  Length of segment offsetting sphere from ground plane, ZOFFSET
```

```
C  If ZOFFSET is not zero there will be one additional segment
      READ(5,*)ZOFFSET
      IF (ZOFFSET .GT. 0.0) INDX = 1
C
C  Total number of wire segments, NM (definition required by ESP)
      NM = NSEGSP + INDX
C
C  Total number of wire points, NP (definition required by ESP)
      NP = NM + 1
C
C  Total number of wire attachment points, NAT (one wire is
C  attached to the square plate making the ground plane - definition
C  required by ESP)
      NAT = 1
C
C  Total number of turns sphere would have if completely wound,
C  NTOTAL
      READ(5,*)NTOTAL
C
C  Actual number of turns sphere has, NACT
      READ(5,*)NACT
C
C  Radius of sphere, AS (meters)
      READ(5,*)AS
C
      PIE = 3.1415927
C
C  SEGPHI is the change in the angle phi (radians) over each segment
      SEGPHI = 2.0*PIE*NACT/REAL(NSEGSP)
C
C  Coordinates of first wire point, the origin (required by ESP)
      X(1) = 0.0
      Y(1) = 0.0
      Z(1) = 0.0
C
C  Nodes of the first segment
      IA(1) = 1
      IB(1) = 2
C
C  Coordinates of second wire point and nodes of the second segment
C  if there is the spherical helix is vertically offset from the
C  ground plane
        IF (INDX .EQ. 0) GOTO 101
      X(2) = 0.0
      Y(2) = 0.0
      Z(2) = ZOFFSET
      IA(2) = 2
      IB(2) = 3
C
C
C  Coordinates of the rest of the wire points and nodes.
```

```
C
  101 DO 100 J = 2+INDX,NP
        PHI = SEGPHI*REAL(J-1-INDX)
        TH = ACOS((PHI/(PIE*NTOTAL))-1.0)
        X(J) = AS*SIN(TH)*COS(PHI)
        Y(J) = AS*SIN(TH)*SIN(PHI)
        Z(J) = AS*COS(TH) + AS + ZOFFSET
          IF (J .EQ. NP) GOTO 100
        IA(J) = J
        IB(J) = J+1
  100 CONTINUE
C
C
C  Check that smallest segment is greater than twice the wire radius
C  (otherwise ESP results may be invalid - see ESP manual)
C
      SLENGTH = SQRT( (X(NP)-X(NP-1))**2 + (Y(NP)-Y(NP-1))**2 +
     +          (Z(NP)-Z(NP-1))**2 )
C
      IF (SLENGTH .LE. A*2.) WRITE(*,*)'   WARNING - At least one
     +segment is smaller than twice the wire radius'
C
C
C  Following inputs are required by ESP:
C
C  Wire "location" of attachment point, NSA
      NSA(1) = 1
C
C  Plate number geometry is attached to, NPLA
      NPLA(1) = 1
C
C  Complex voltage generator, VGA
      VGA(1) = (1.0,0.0)
C
C  Outer disk radius of disk monopole (should be about .2
C  wavelengths lambda), BDSK
      BDSK(1) = 0.2*WV
C
C
      RETURN
      END
```

Appendix C. Numerically-Calculated Far-Field Patterns of a Spherical Helix

The far-field radiation plots are compiled for the 7-turn spherical helix discussed in Section 4.1 over a frequency range from 1.8 GHz to 7.4 GHz, which corresponds to normalized circumferences of 0.67 λ and 2.85 λ, respectively. In part (a) of each figure, the gain of both far-field components is plotted in the x-z plane which can be written in terms of θ and ϕ as:

$$0^\circ \leq \theta \leq 180^\circ \quad \text{for } \phi = 0^\circ \text{ (right half-plane)} \quad \text{and } \phi = 180^\circ \text{ (left half-plane)}$$

Pattern cuts are shown only for the x-z plane since the pattern of the spherical helix is essentially, but not perfectly, symmetrical about the z-axis. The gain of each component is referenced to an isotropic linearly-polarized antenna and can be shown to be related to the magnitude of the electric field components by:

$$G_\theta = 10\, log\left(C\left|E_\theta\right|^2\right) = 10\, log(C) + 20\, log\left(\left|E_\theta\right|\right) \text{ dB} \qquad \text{(D-1)}$$

$$G_\phi = 10\, log\left(C\left|E_\phi\right|^2\right) = 10\, log(C) + 20\, log\left(\left|E_\phi\right|\right) \text{ dB} \qquad \text{(D-2)}$$

where C is a constant that is related to the radiation intensity of an isotropic source (see reference [4]). Thus, relative comparisons can be drawn between the patterns in this appendix (G_θ and G_ϕ) and the measured patterns in Appendix D (E_θ and E_ϕ in dB normalized to 0 dB).

In part (b) of each figure, the phase difference between the far-field components as discussed in Section 4.1.2 is plotted for the upper-half x-z plane given by:

$$-90^\circ \leq \theta \leq 90^\circ$$

Strickly speaking, θ varies between 0° and 180° in spherical coordinates. Here, $-90^\circ \leq \theta \leq 0^\circ$ and $0^\circ \leq \theta \leq 90^\circ$ ranges are used for $\phi = 180^\circ$ and $\phi = 0^\circ$, respectively.

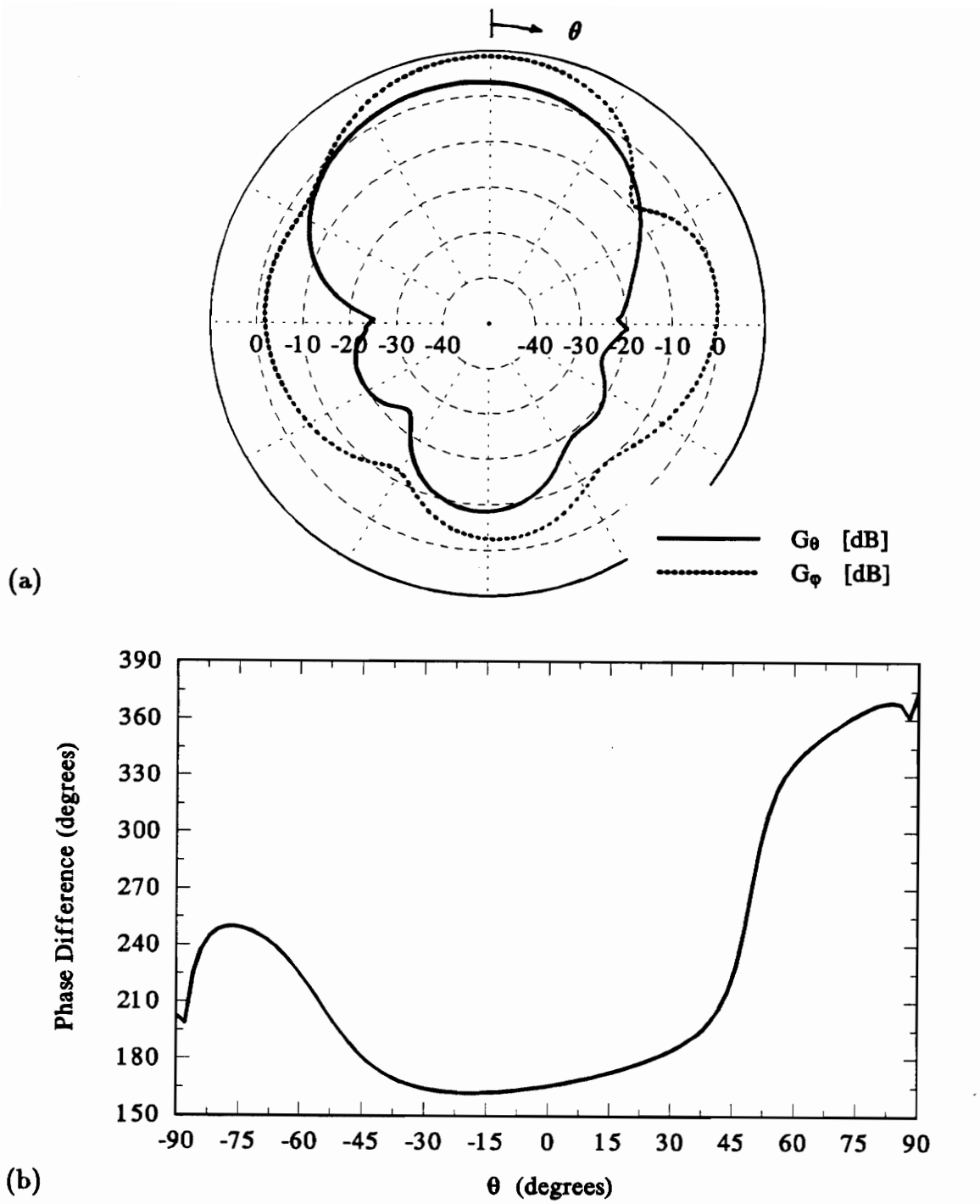

Figure C-1. Computed far-field pattern in the x-z plane of a 7-turn spherical helical antenna with a circumference of 0.692 λ. (a) Gain of E_θ and E_ϕ with respect to an isotropic linearly-polarized antenna. (b) Phase difference between E_θ and E_ϕ.

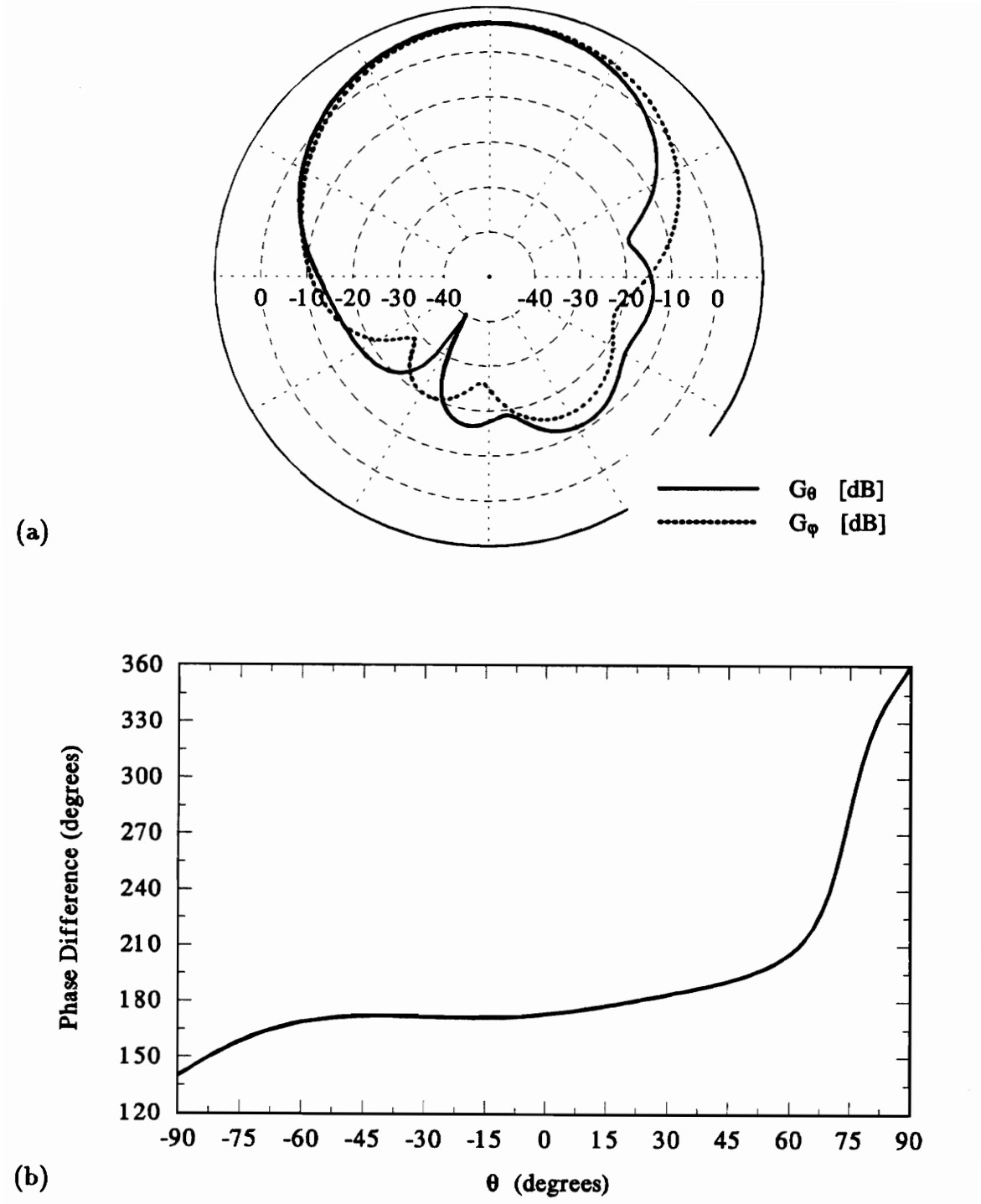

Figure C-2. Computed far-field pattern in the x-z plane of a 7-turn spherical helical antenna with a circumference of 0.846 λ. (a) Gain of E_θ and E_ϕ with respect to an isotropic linearly-polarized antenna. (b) Phase difference between E_θ and E_ϕ.

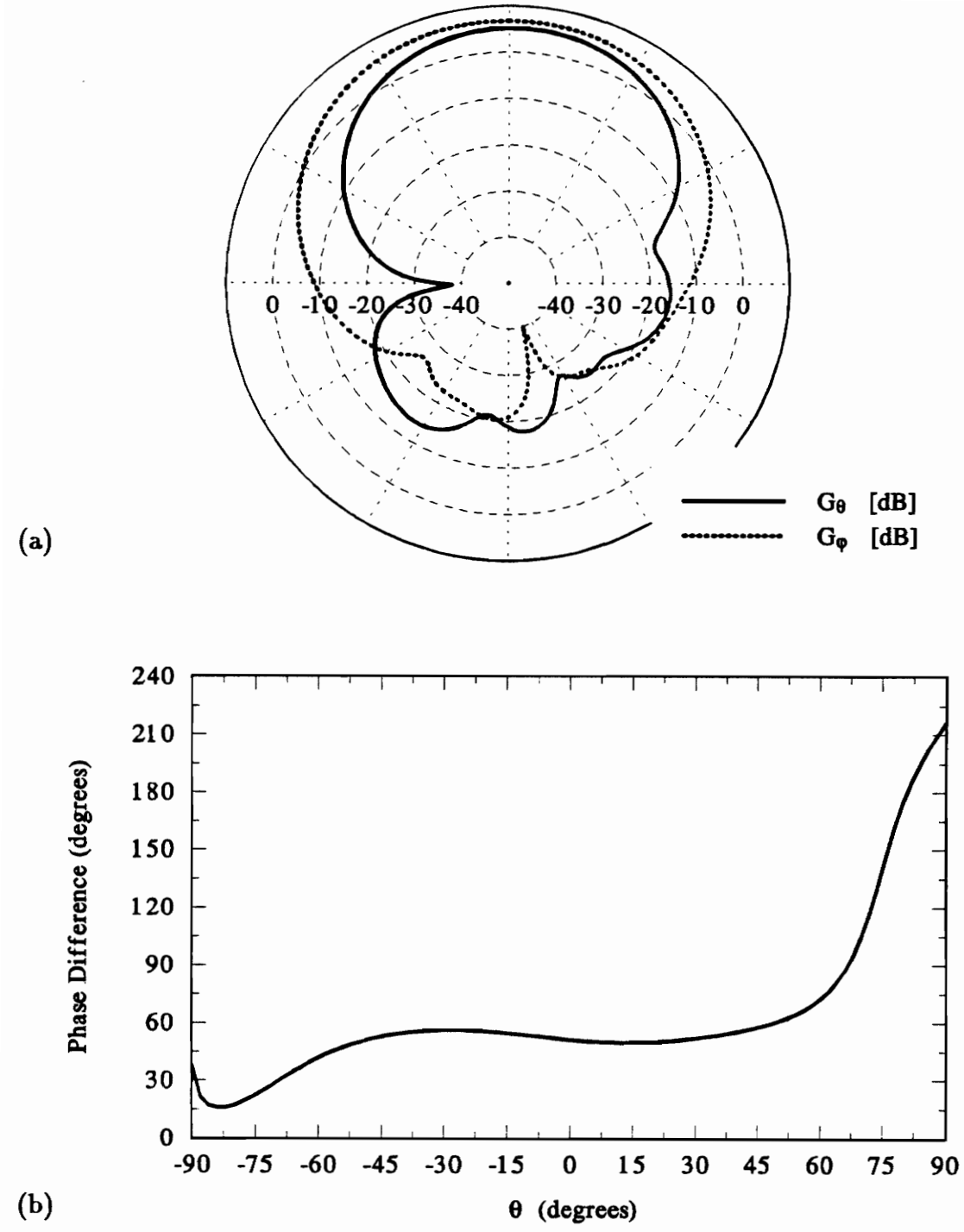

Figure C-3. Computed far-field pattern in the x-z plane of a 7-turn spherical helical antenna with a circumference of 1.0 λ. (a) Gain of E_θ and E_ϕ with respect to an isotropic linearly-polarized antenna. (b) Phase difference between E_θ and E_ϕ.

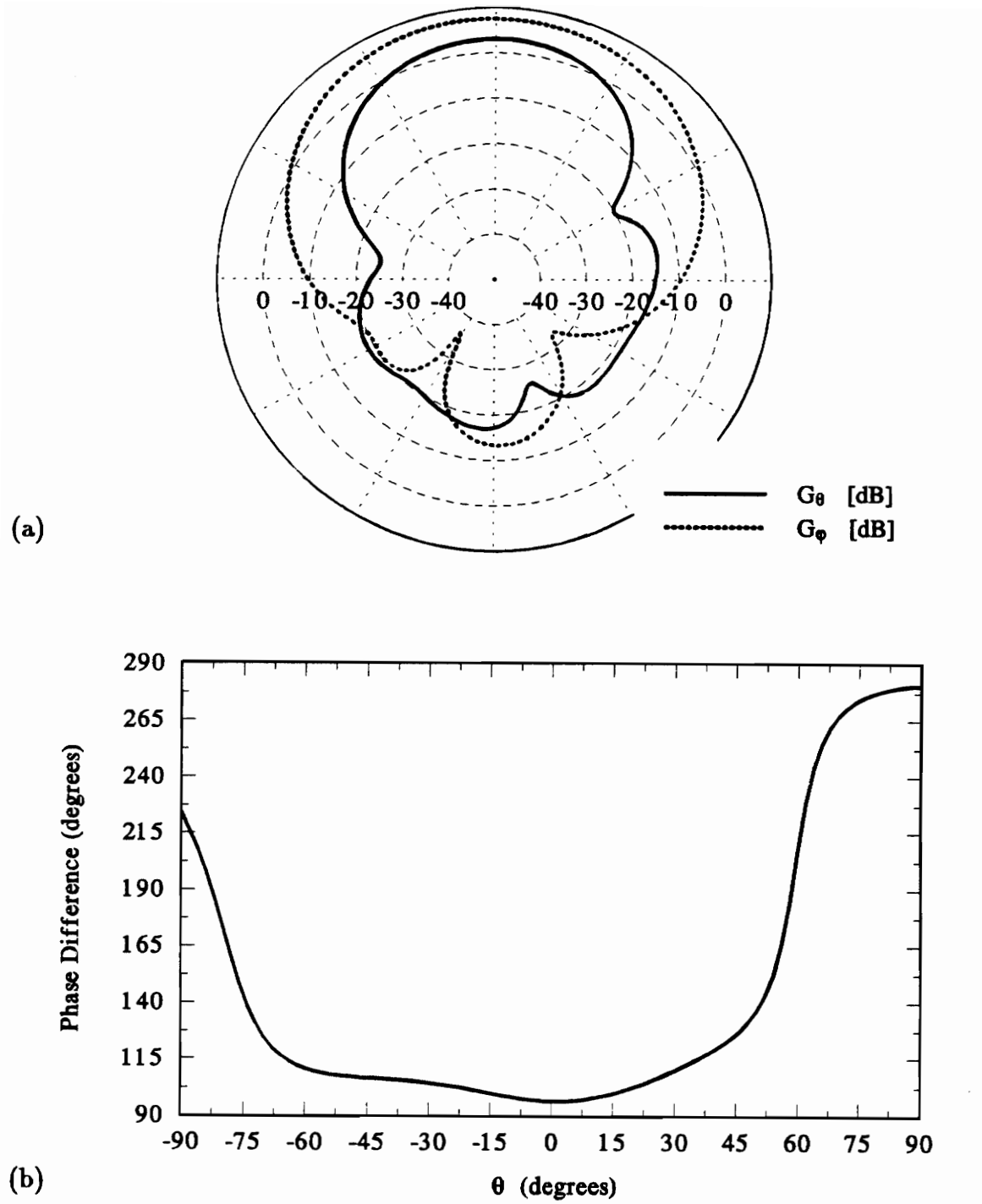

Figure C-4. Computed far-field pattern in the x-z plane of a 7-turn spherical helical antenna with a circumference of 1.154 λ. (a) Gain of E_θ and E_ϕ with respect to an isotropic linearly-polarized antenna. (b) Phase difference between E_θ and E_ϕ.

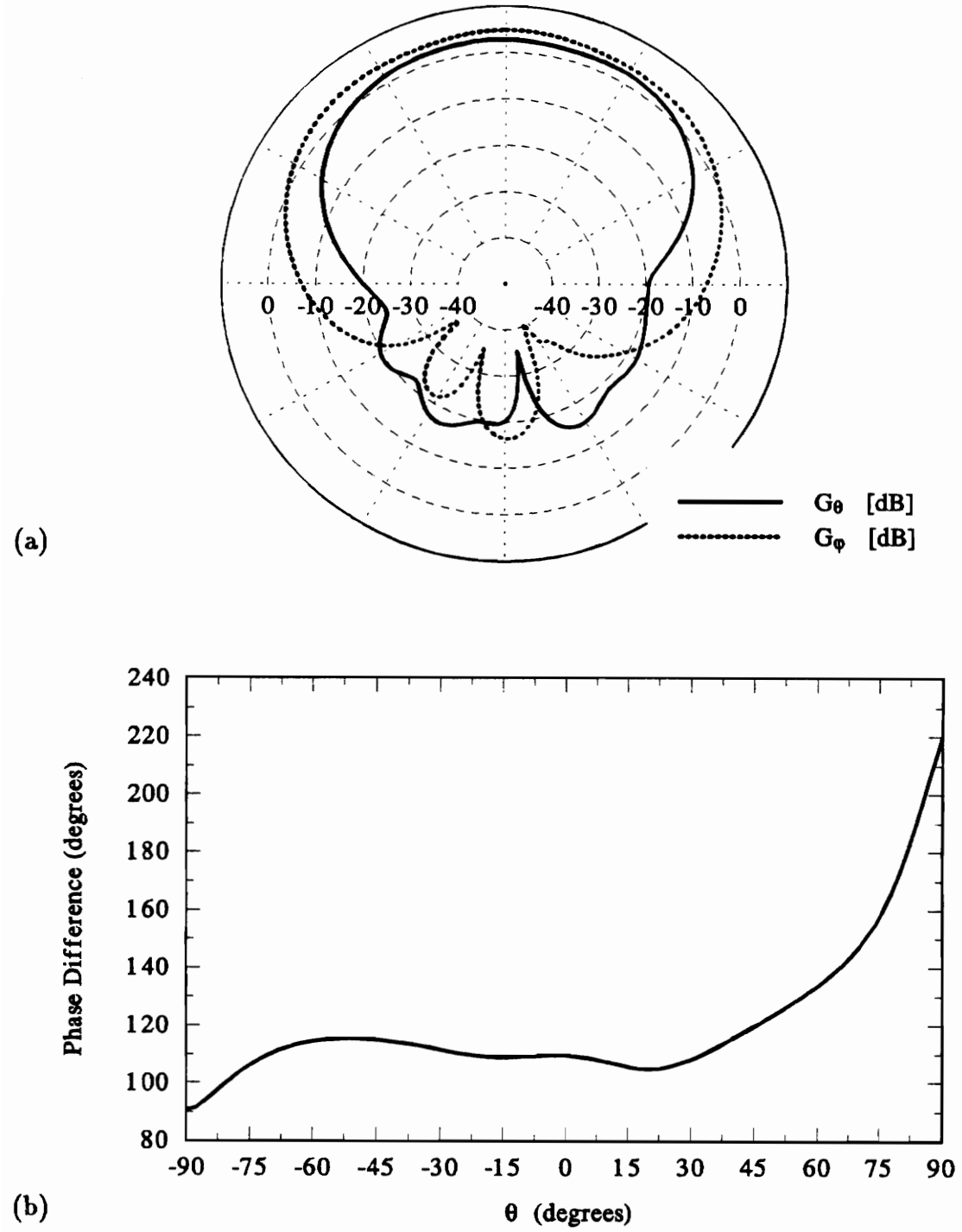

Figure C-5. Computed far-field pattern in the x-z plane of a 7-turn spherical helical antenna with a circumference of 1.308 λ. (a) Gain of E_θ and E_ϕ with respect to an isotropic linearly-polarized antenna. (b) Phase difference between E_θ and E_ϕ.

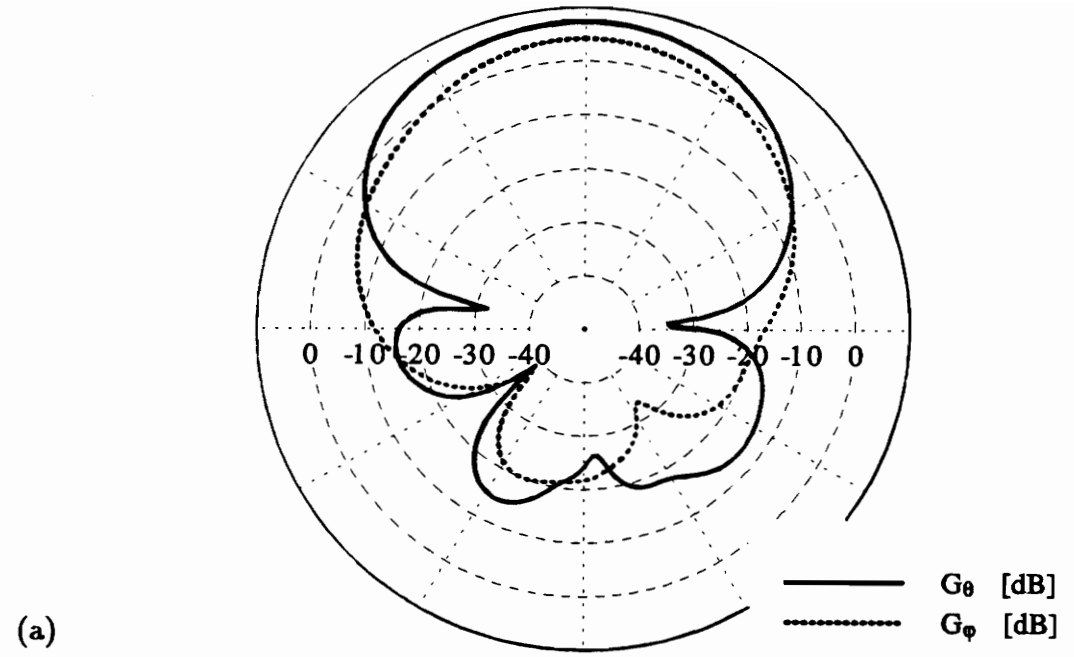

(a)

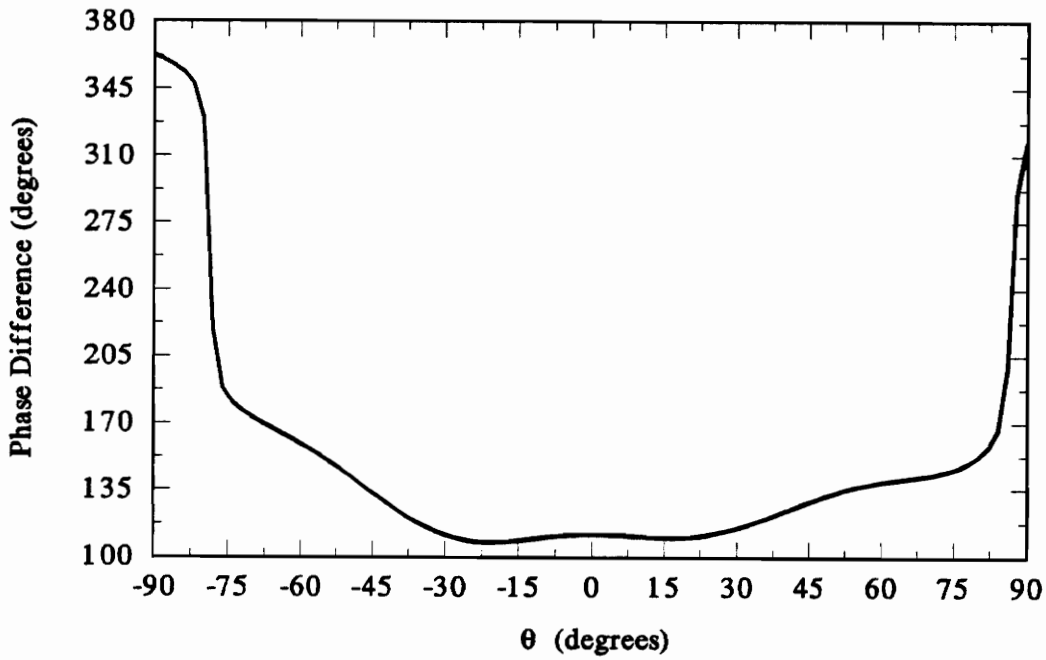

(b)

Figure C-6. Computed far-field pattern in the x-z plane of a 7-turn spherical helical antenna with a circumference of 1.462 λ. (a) Gain of E_θ and E_ϕ with respect to an isotropic linearly-polarized antenna. (b) Phase difference between E_θ and E_ϕ.

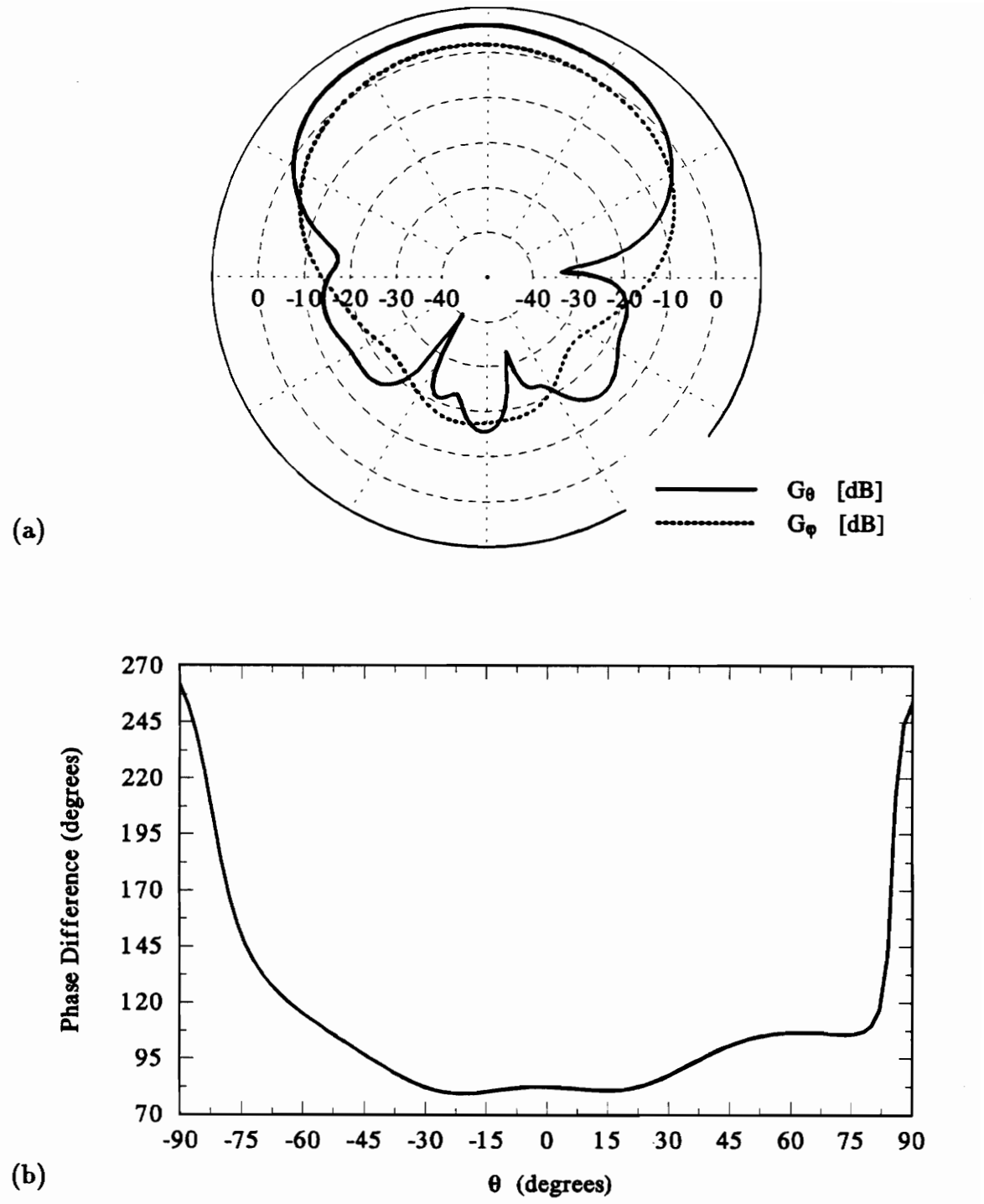

Figure C-7. Computed far-field pattern in the x-z plane of a 7-turn spherical helical antenna with a circumference of 1.615 λ. (a) Gain of E_θ and E_ϕ with respect to an isotropic linearly-polarized antenna. (b) Phase difference between E_θ and E_ϕ.

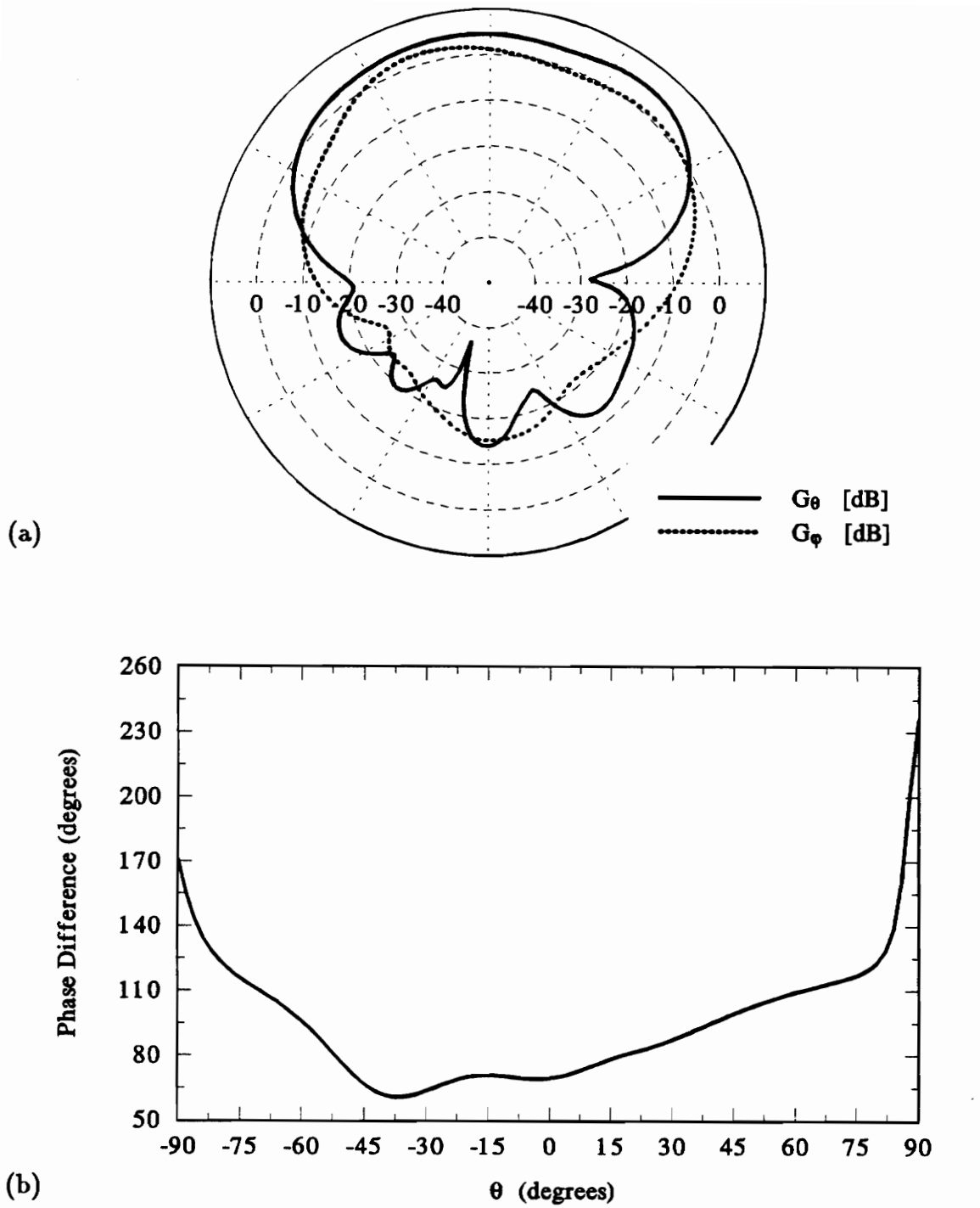

Figure C-8. Computed far-field pattern in the x-z plane of a 7-turn spherical helical antenna with a circumference of 1.769 λ. (a) Gain of E_θ and E_ϕ with respect to an isotropic linearly-polarized antenna. (b) Phase difference between E_θ and E_ϕ.

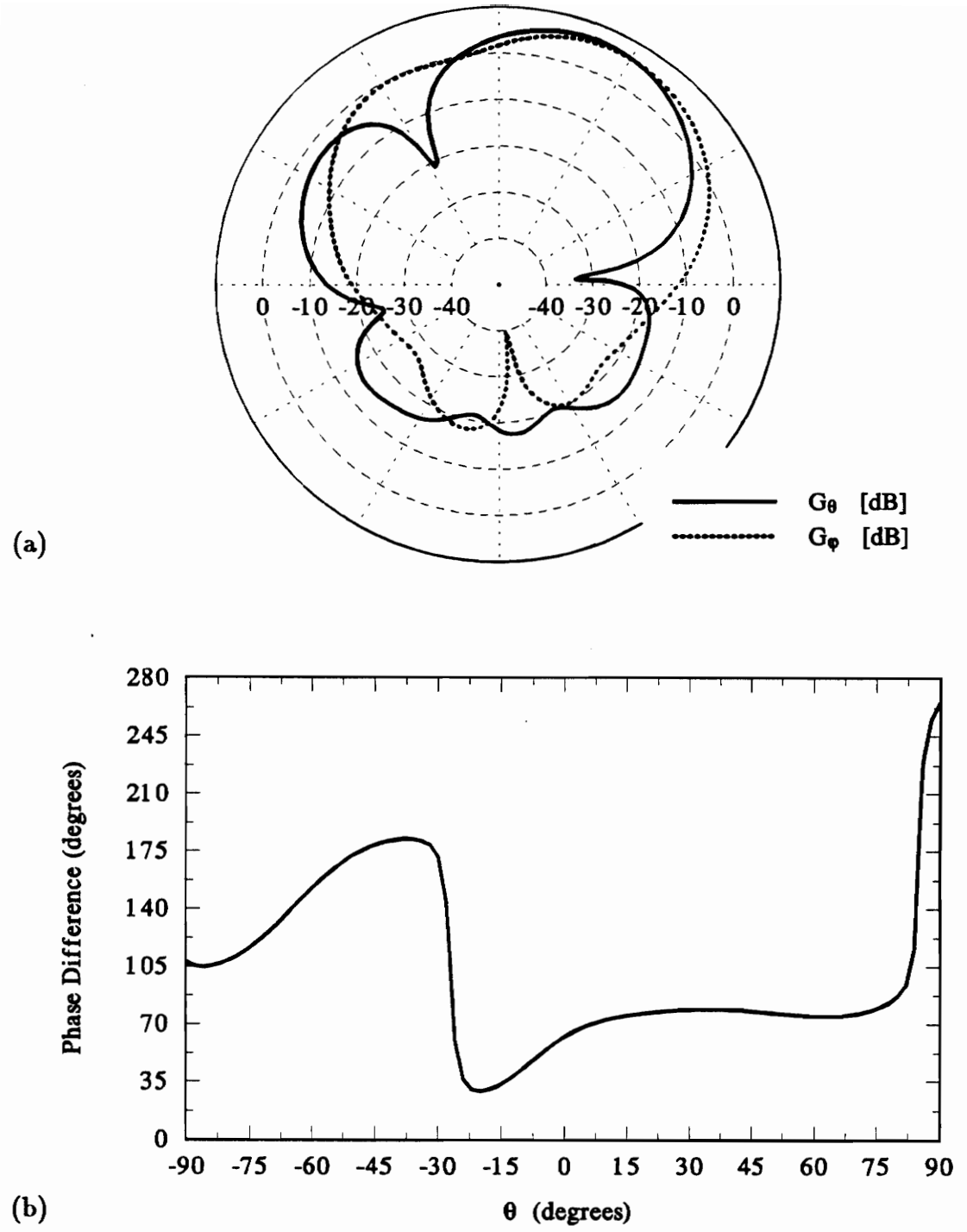

Figure C-9. Computed far-field pattern in the x-z plane of a 7-turn spherical helical antenna with a circumference of 1.923 λ. (a) Gain of E_θ and E_ϕ with respect to an isotropic linearly-polarized antenna. (b) Phase difference between E_θ and E_ϕ.

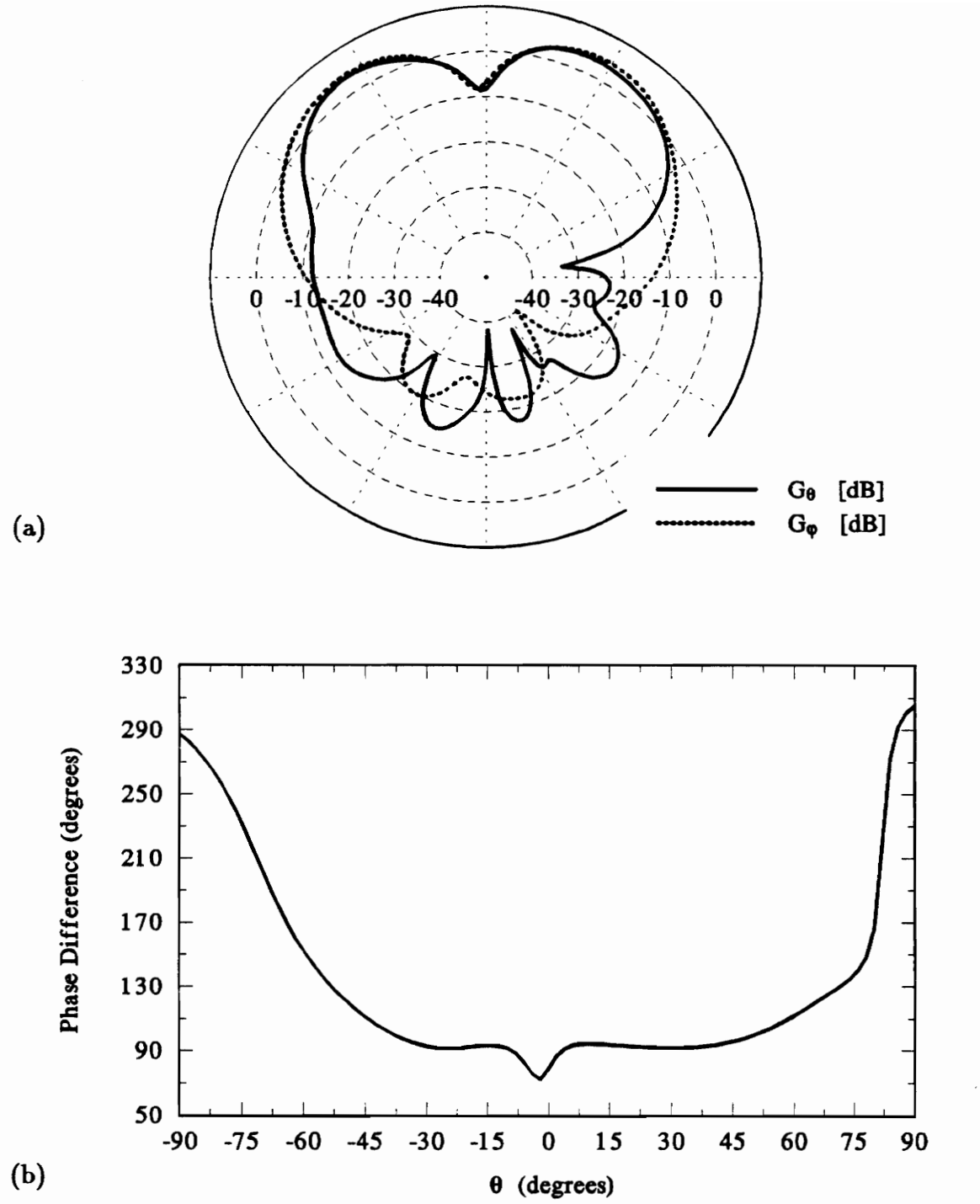

Figure C-10. Computed far-field pattern in the x-z plane of a 7-turn spherical helical antenna with a circumference of 2.077 λ. (a) Gain of E_θ and E_ϕ with respect to an isotropic linearly-polarized antenna. (b) Phase difference between E_θ and E_ϕ.

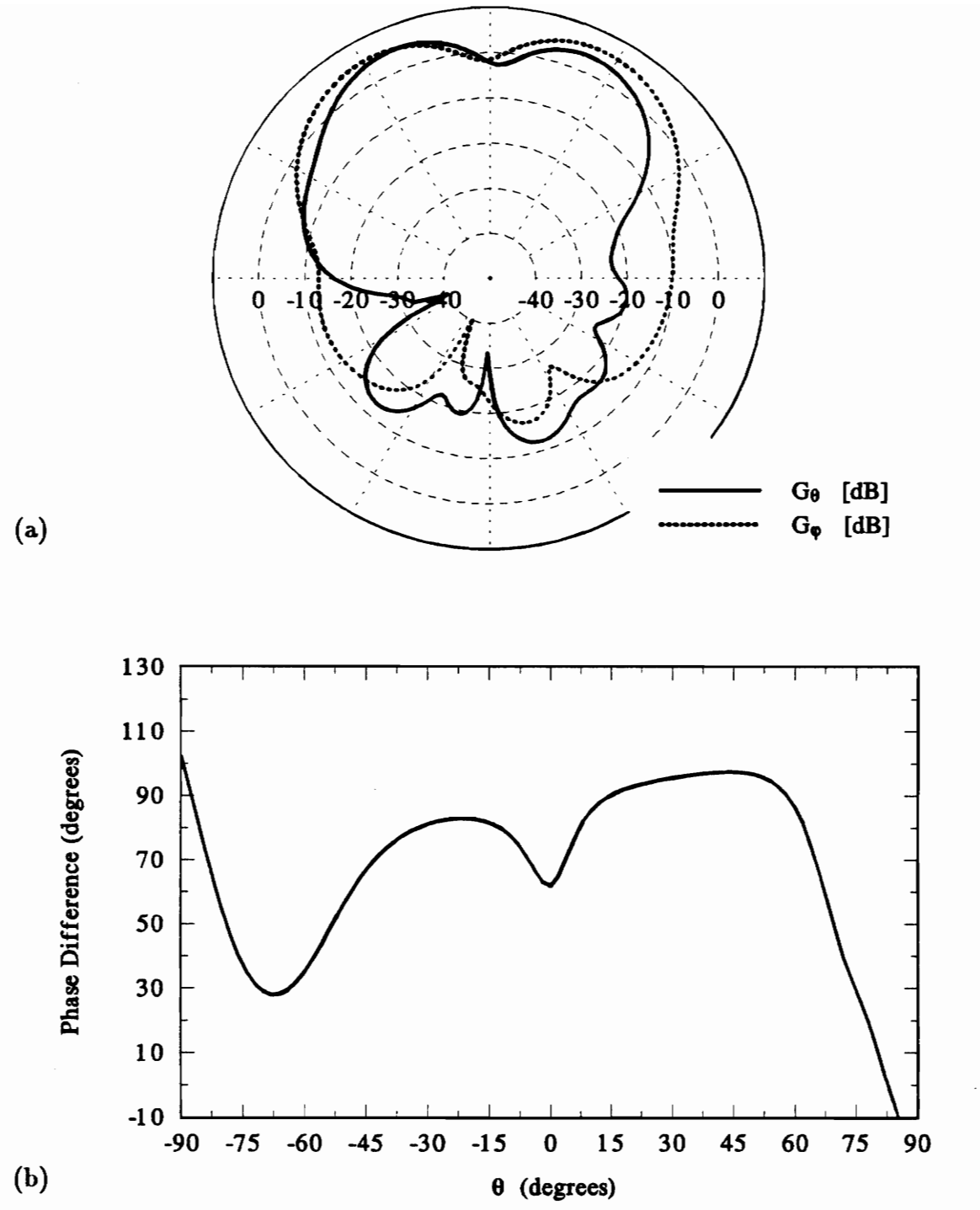

Figure C-11. Computed far-field pattern in the x-z plane of a 7-turn spherical helical antenna with a circumference of 2.231 λ. (a) Gain of E_θ and E_ϕ with respect to an isotropic linearly-polarized antenna. (b) Phase difference between E_θ and E_ϕ.

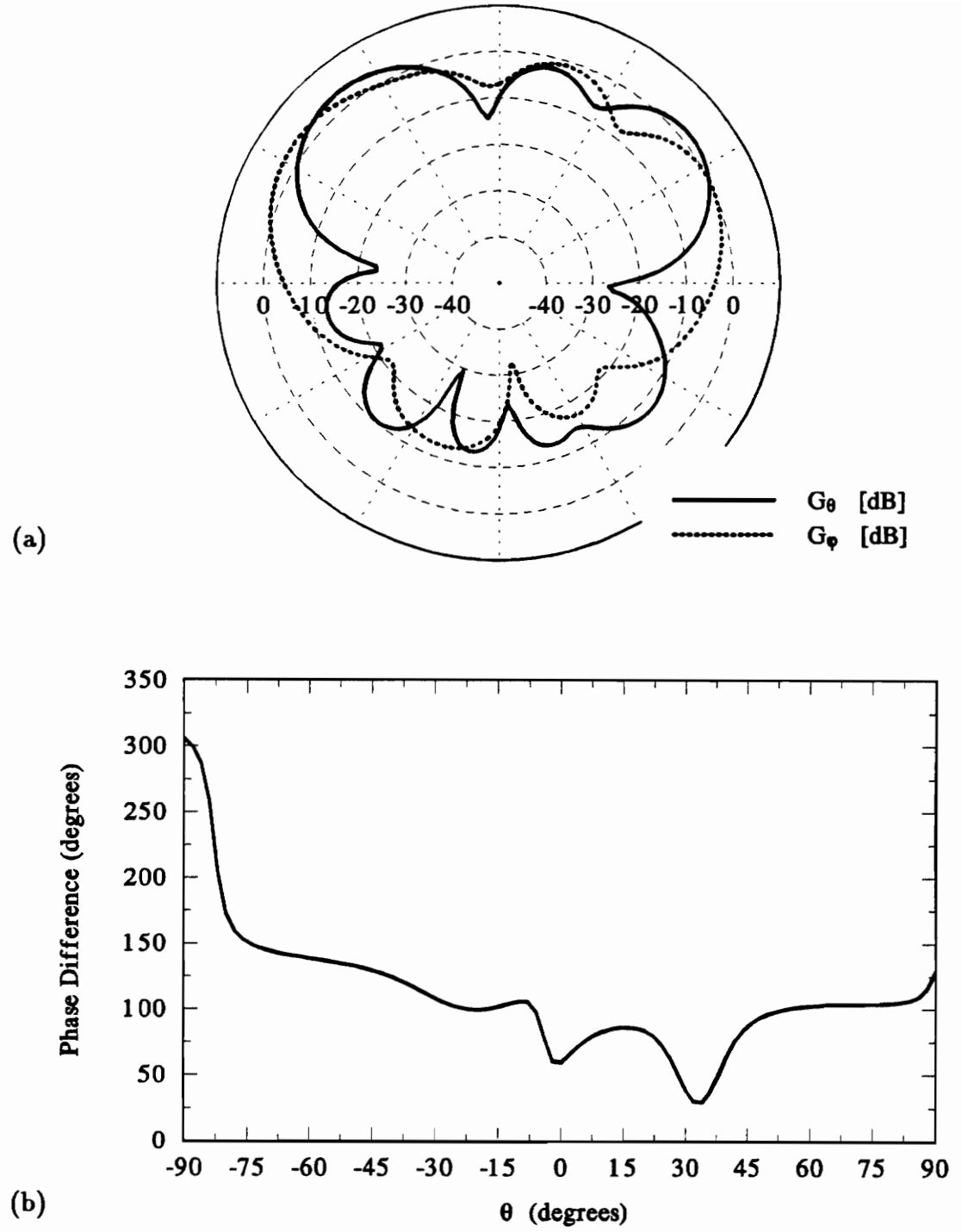

Figure C-12. Computed far-field pattern in the x-z plane of a 7-turn spherical helical antenna with a circumference of 2.385 λ. (a) Gain of E_θ and E_ϕ with respect to an isotropic linearly-polarized antenna. (b) Phase difference between E_θ and E_ϕ.

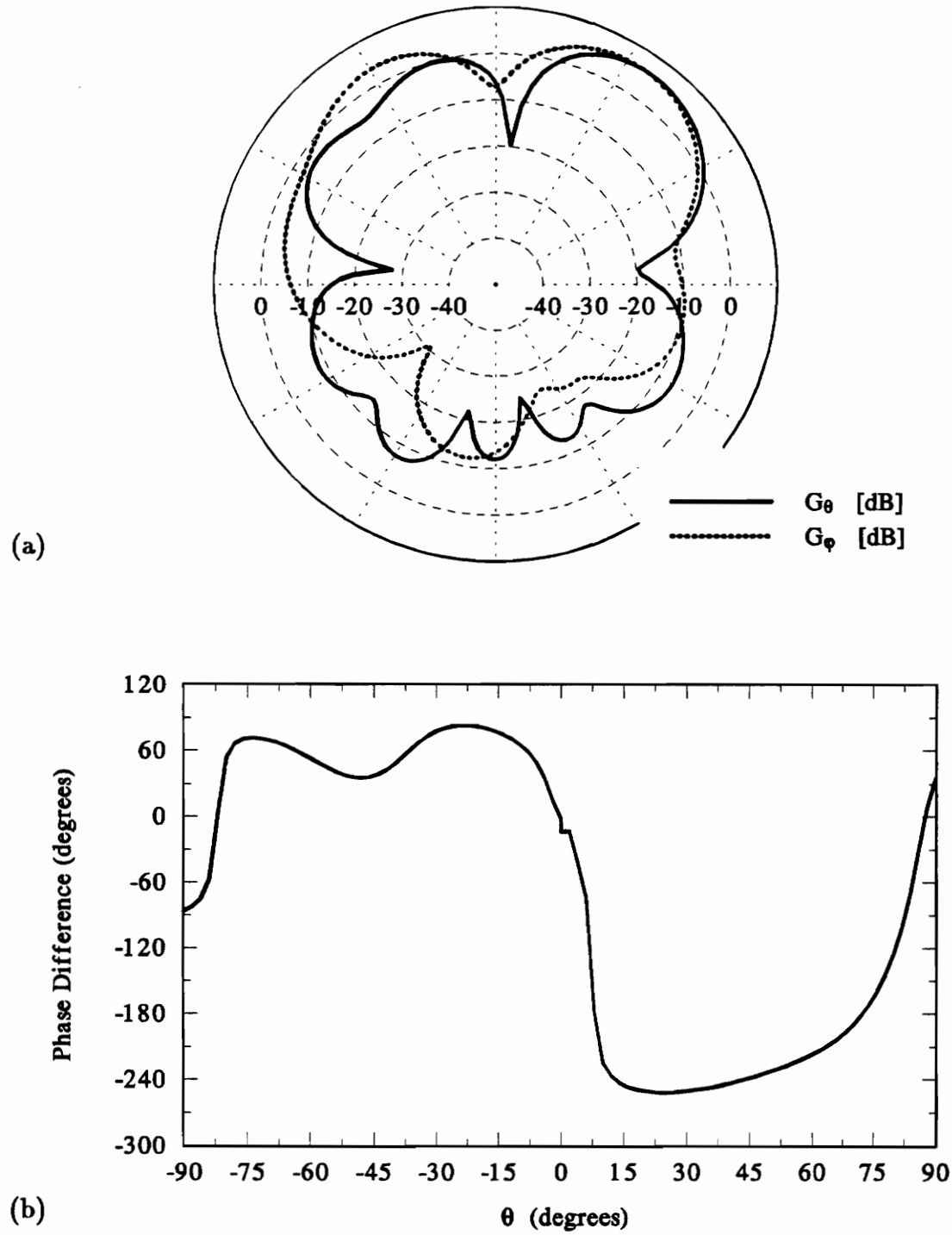

Figure C-13. Computed far-field pattern in the x-z plane of a 7-turn spherical helical antenna with a circumference of 2.538 λ. (a) Gain of E_θ and E_ϕ with respect to an isotropic linearly-polarized antenna. (b) Phase difference between E_θ and E_ϕ.

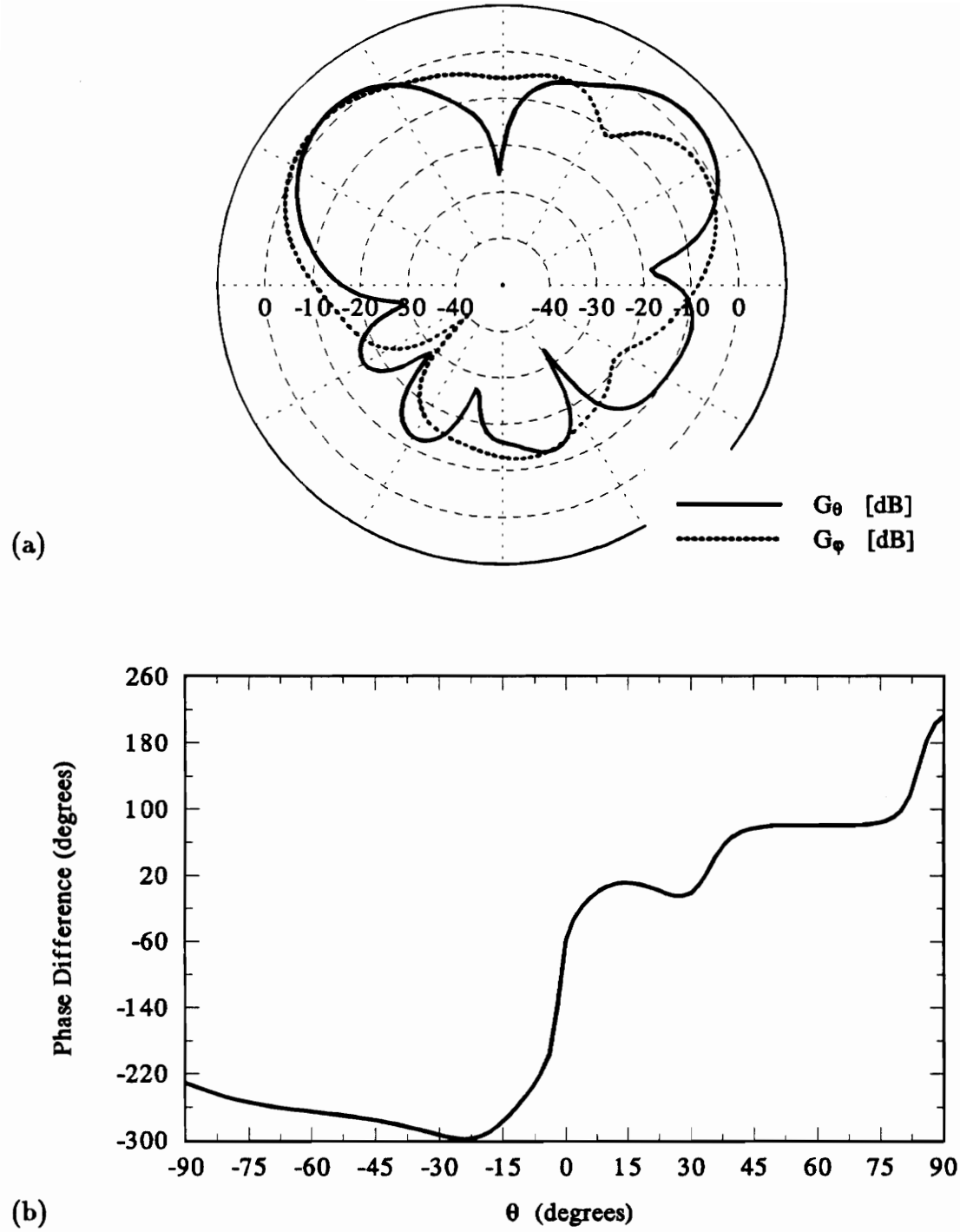

Figure C-14. Computed far-field pattern in the x-z plane of a 7-turn spherical helical antenna with a circumference of 2.692 λ. (a) Gain of E_θ and E_ϕ with respect to an isotropic linearly-polarized antenna. (b) Phase difference between E_θ and E_ϕ.

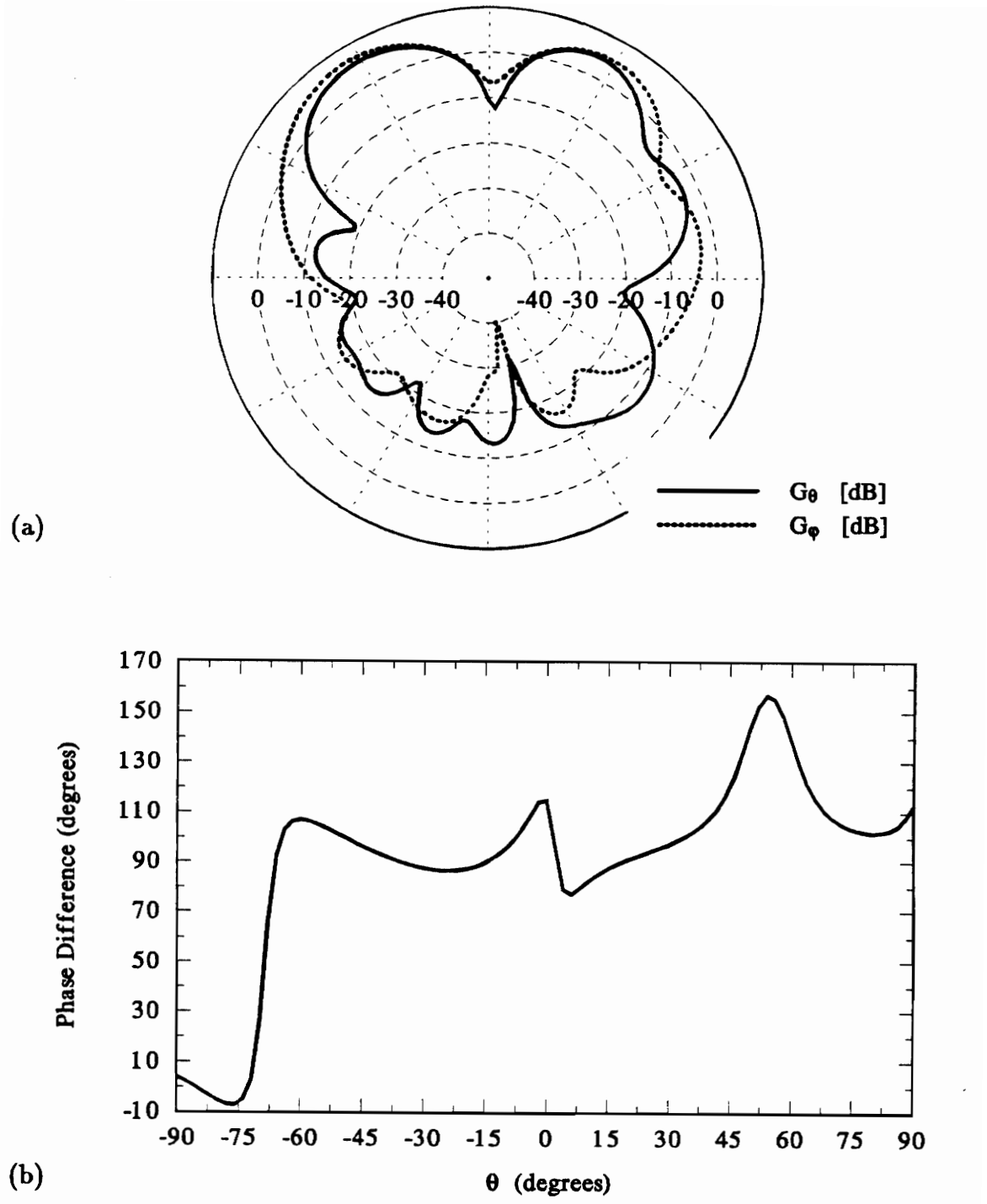

Figure C-15. Computed far-field pattern in the x-z plane of a 7-turn spherical helical antenna with a circumference of 2.846 λ. (a) Gain of E_θ and E_ϕ with respect to an isotropic linearly-polarized antenna. (b) Phase difference between E_θ and E_ϕ.

Appendix D. Measured Far-Field Patterns of a Spherical Helix

Far-field measurements are presented for a 7-turn spherical helix corresponding to the numerical results presented in Appendix C. The magnitudes in dB of both electric-field components, i.e. $20\ log\left(\left|E_{\theta,\phi}\right|\right)$, are plotted in the x-z plane for spherical circumferences between 0.67 λ and 2.85 λ. The measurements were taken at frequencies between 1 GHz and 4 GHz which is different from the frequencies used for numerical calculations (1.8 GHz to 7.4 GHz) since the spherical helix was constructed with a larger sphere than that used with ESP. The measurements were coordinated such that they occurred at the same normalized circumferences as those in Appendix C. The results are discussed in Section 5.2.

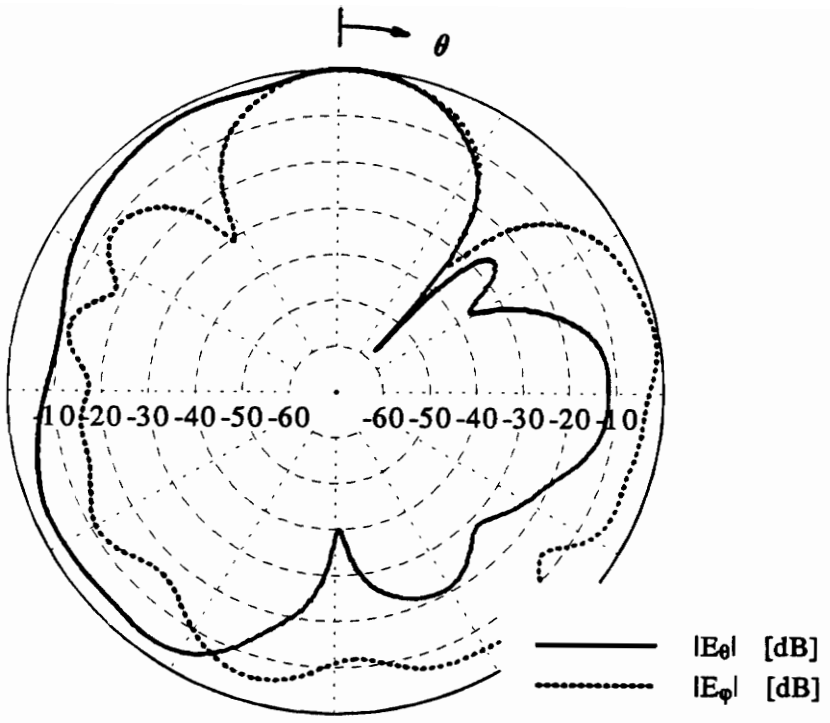

Figure D-1. Measured far-field pattern of a 7-turn spherical helical antenna with a circumference of 0.692 λ.

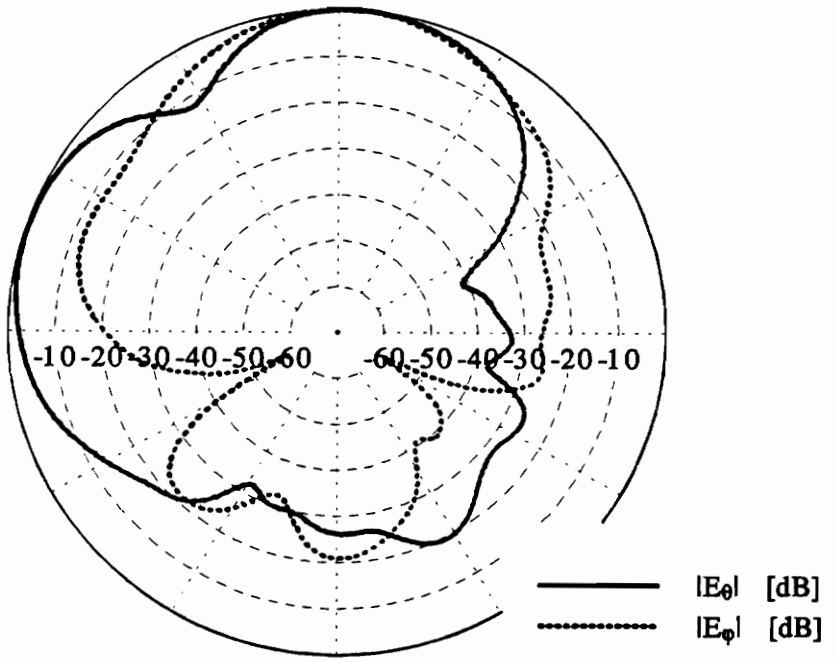

Figure D-2. Measured far-field pattern of a 7-turn spherical helical antenna with a circumference of 0.846 λ.

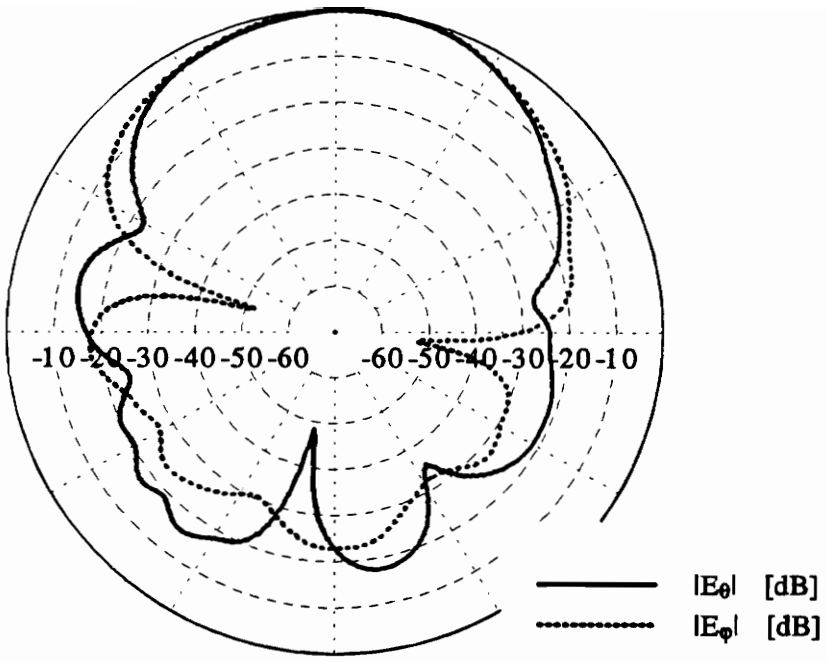

Figure D-3. Measured far-field pattern of a 7-turn spherical helical antenna with a circumference of 1.0 λ.

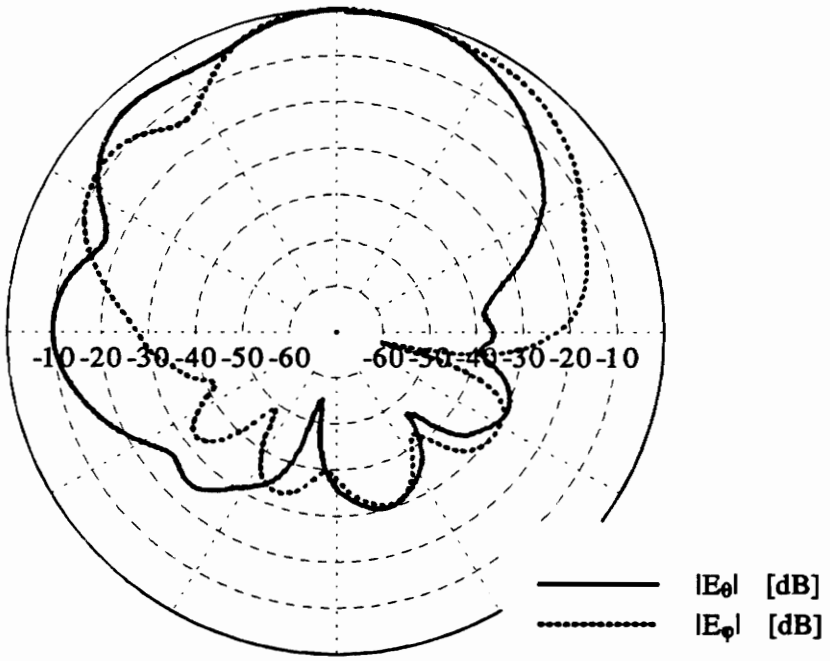

Figure D-4. Measured far-field pattern of a 7-turn spherical helical antenna with a circumference of 1.154 λ.

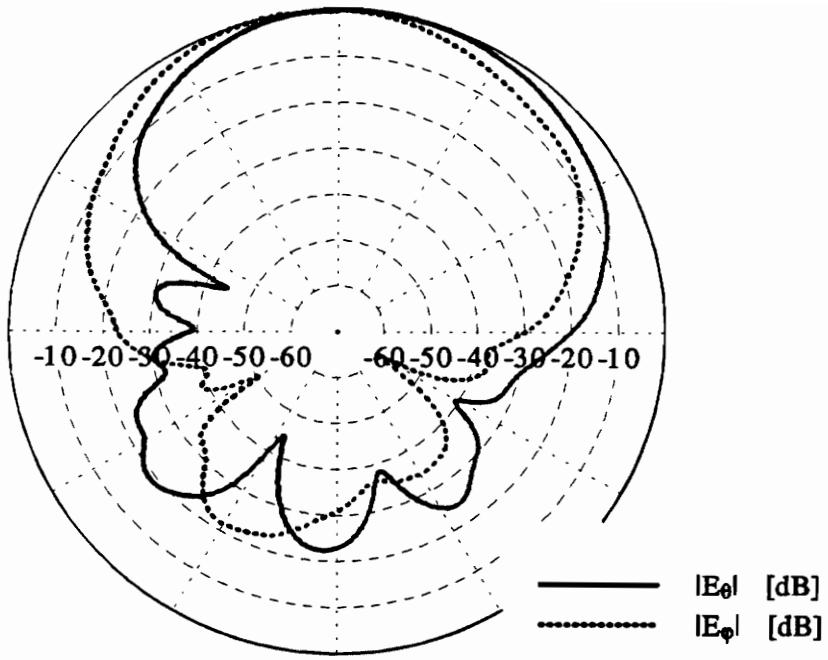

Figure D-5. Measured far-field pattern of a 7-turn spherical helical antenna with a circumference of 1.308 λ.

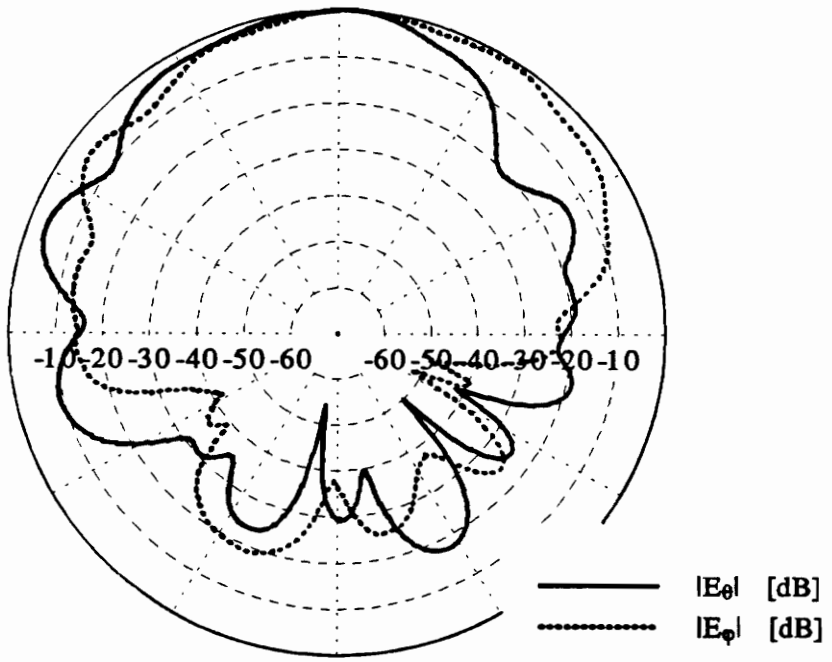

Figure D-6. Measured far-field pattern of a 7-turn spherical helical antenna with a circumference of 1.462 λ.

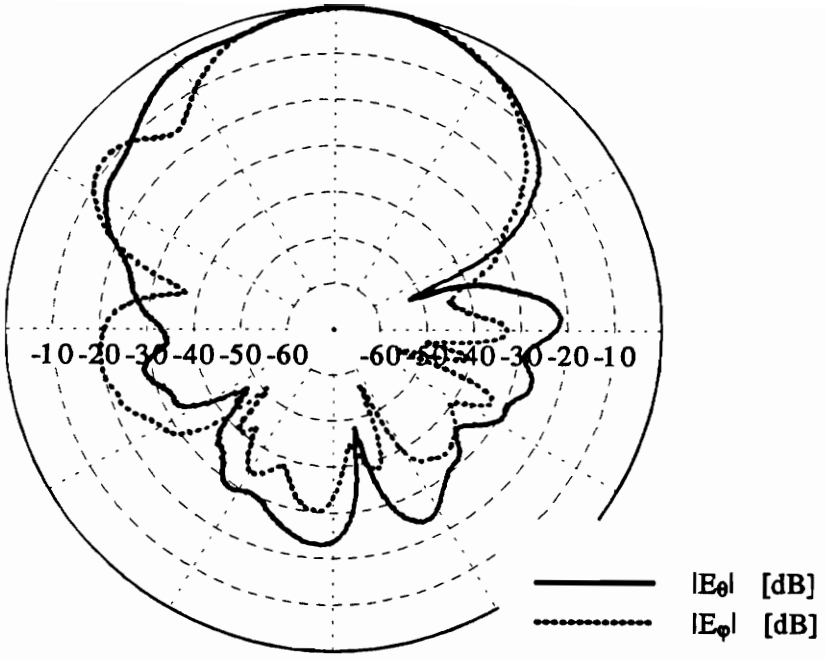

Figure D-7. Measured far-field pattern of a 7-turn spherical helical antenna with a circumference of 1.615 λ.

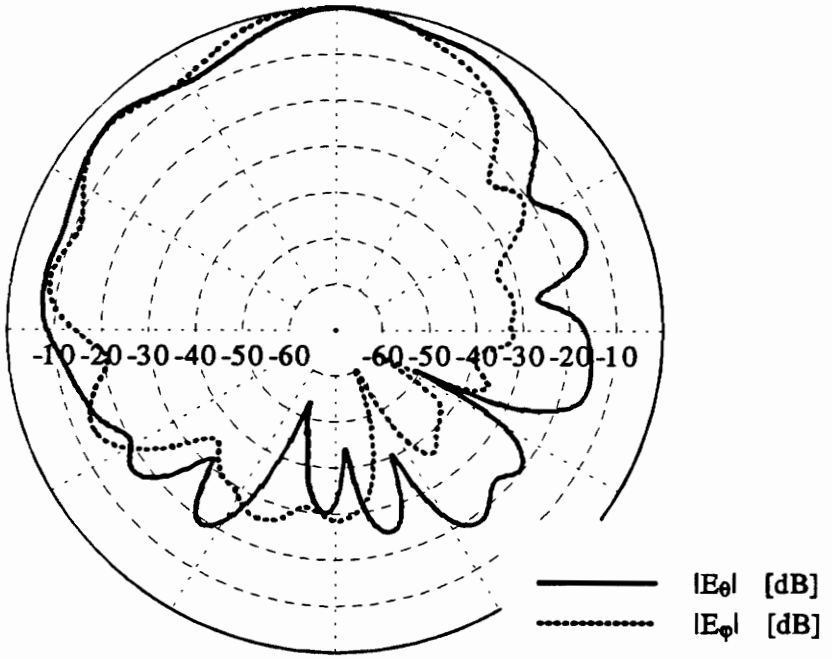

Figure D-8. Measured far-field pattern of a 7-turn spherical helical antenna with a circumference of 1.769 λ.

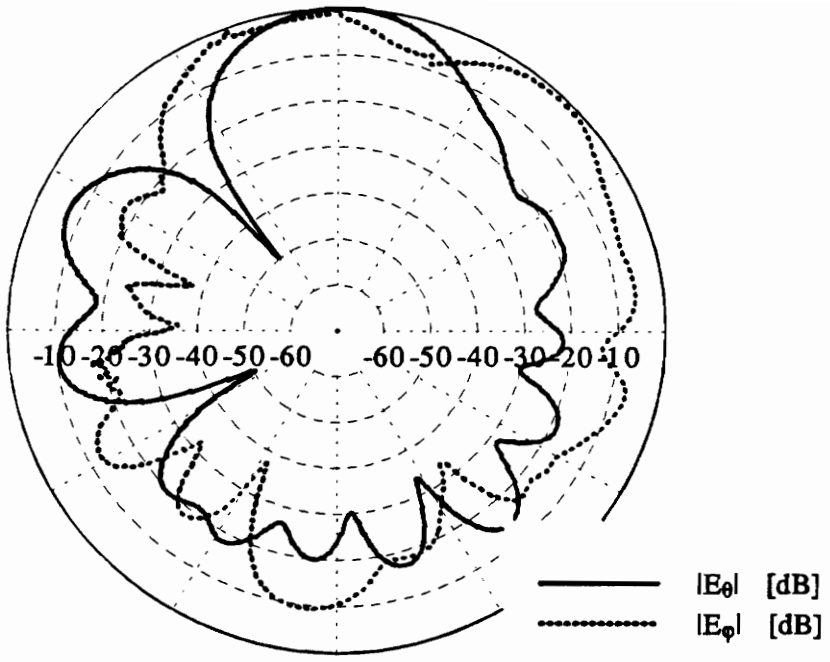

Figure D-9. Measured far-field pattern of a 7-turn spherical helical antenna with a circumference of 1.923 λ.

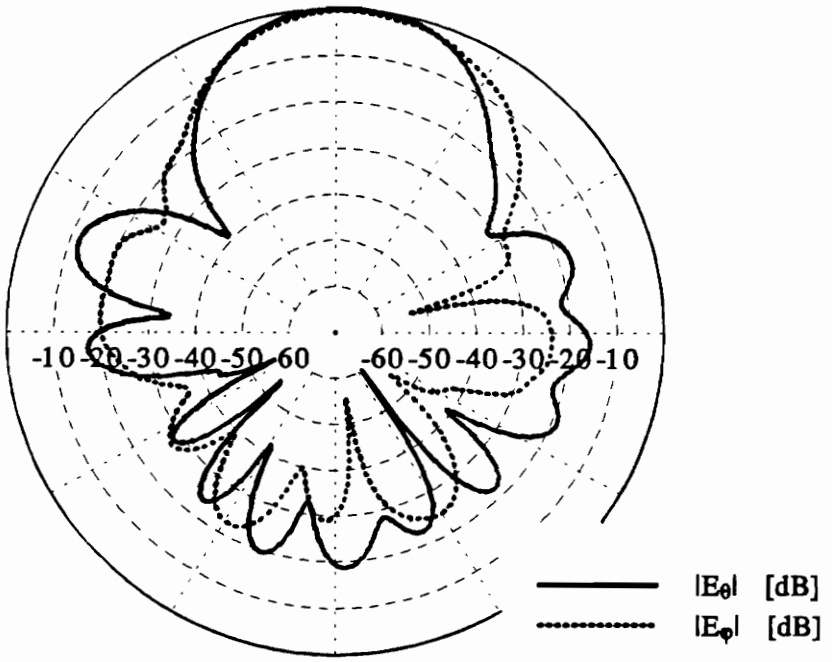

Figure D-10. Measured far-field pattern of a 7-turn spherical helical antenna with a circumference of 2.077 λ.

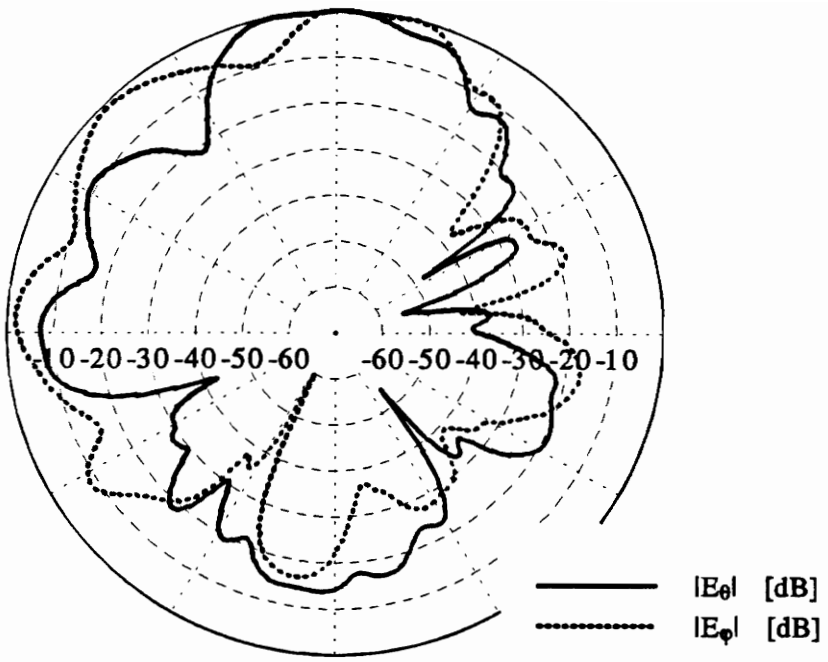

Figure D-11. Measured far-field pattern of a 7-turn spherical helical antenna with a circumference of 2.231 λ.

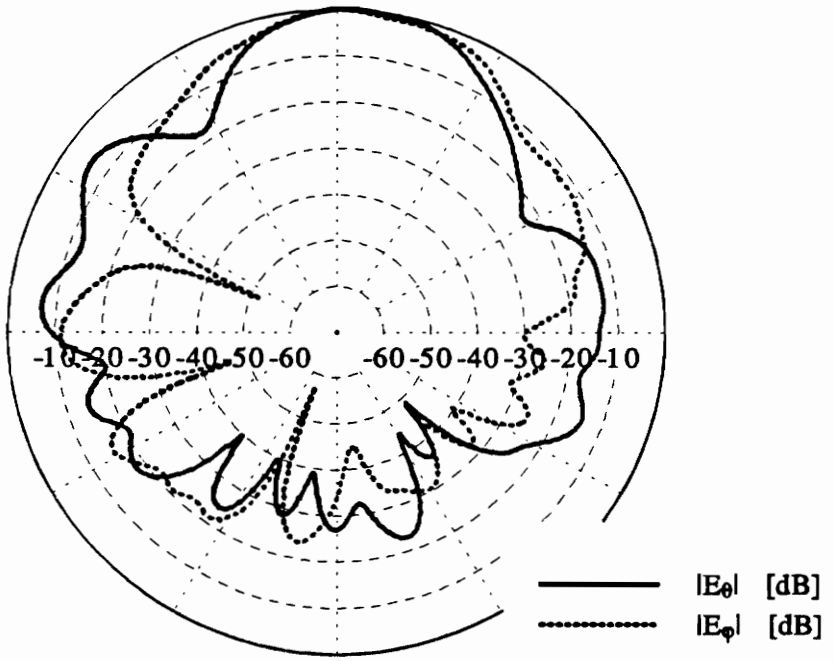

Figure D-12. Measured far-field pattern of a 7-turn spherical helical antenna with a circumference of 2.385 λ.

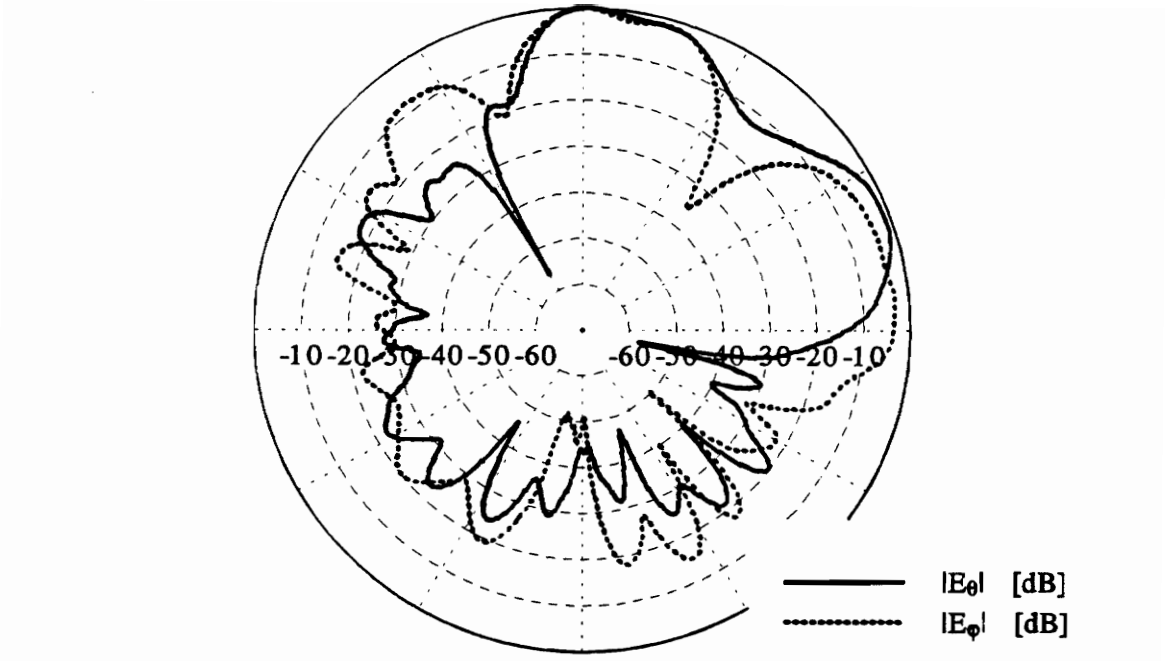

Figure D-13. Measured far-field pattern of a 7-turn spherical helical antenna with a circumference of 2.538 λ.

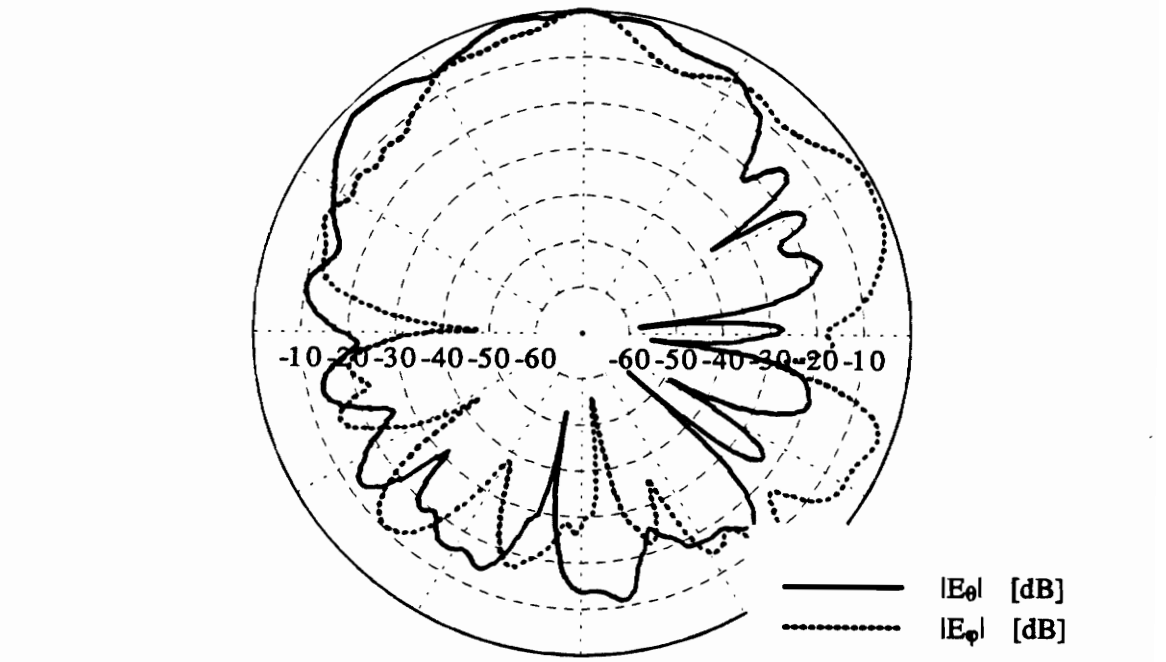

Figure D-14. Measured far-field pattern of a 7-turn spherical helical antenna with a circumference of 2.692 λ.

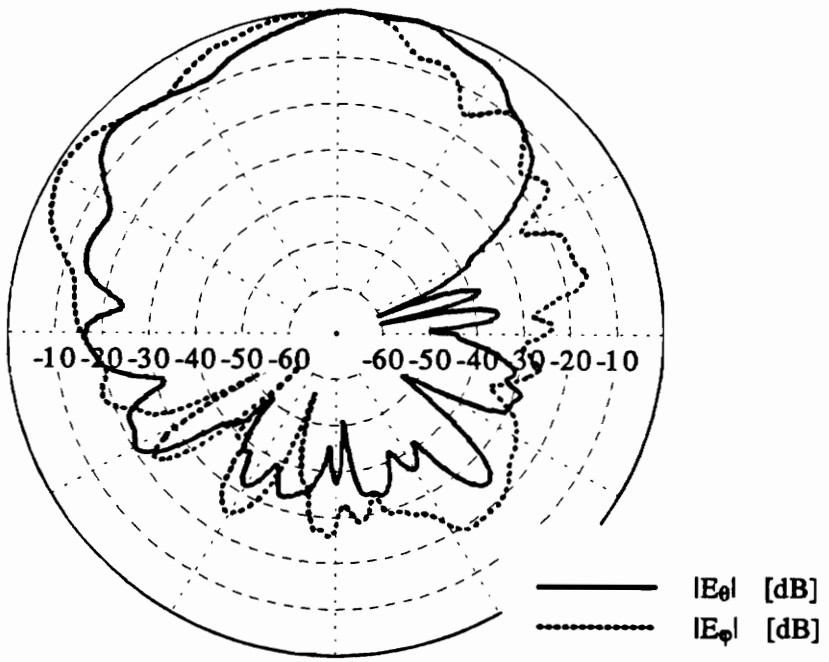

Figure D-15. Measured far-field pattern of a 7-turn spherical helical antenna with a circumference of 2.846 λ.

Vita

J. Christopher Cardoso was born to Mario T. and Margaret A. Cardoso on January 24, 1968 in Plainfield, New Jersey. He graduated from David Brearley Regional High School, Kenilworth, New Jersey, in 1986 and attended Virginia Polytechnic Institute and State University, where he received the Bachelor of Science degree in electrical engineering in May 1990 and the Master of Science degree in electrical engineering in September 1992. While at Virginia Tech, Mr. Cardoso worked as a graduate research assistant for the Satellite Communications Group and as a graduate teaching assistant. He now works for Hughes Aircraft Company in Reston, Virginia.

Chris Cardoso